A Unified Fundamental Equation for the Thermodynamic Properties of H_2O

Cite as: Journal of Physical and Chemical Reference Data **19**, 1233 (1990); https://doi.org/10.1063/1.555868
Submitted: 22 August 1989 . Published Online: 15 October 2009

Philip G. Hill

A Unified Fundamental Equation for the Thermodynamic Properties of H_2O

Philip G. Hill

Department of Mechanical Engineering, University of British Columbia, Vancouver, British Columbia, Canada V6T 1W5

Received August 22, 1989; revised manuscript received June 27, 1990

A new unified equation of state for H_2O is presented, which includes the revised and extended scaling equation of Levelt Sengers, Kamgar–Parsi, Balfour and Sengers, is continuous over all single phase states of H_2O from triple point pressure and temperature to 1000 MPa (or the melting line) and 1000 °C and provides accurate representation of existing thermodynamic data in that range. In addition it provides a smooth transition from singular critical region functions to the nonsingular far-field functions. This is demonstrated by the variations of isochoric specific heat, isothermal compressibility, speed of sound, specific heat ratio and coexistence line properties in the critical region.

Key words: critical point; equation of state; thermodynamic properties; water.

Contents

1. Introduction 1235
2. The Revised and Extended Scaling Equation 1235
3. The Unified Helmholtz Function 1235
4. Fitting Procedure 1236
5. Comparisons with Experimental Data 1237
   5.1. Saturation Properties 1238
   5.2. Densities 1243
   5.3. Pressures 1253
   5.4. Speed of Sound 1257
   5.5. Isopiestic Specific Heats 1260
   5.6. Isochoric Specific Heats 1263
   5.7. Throttling and Viral Coefficients 1263
   5.8. Virial Coefficients 1266
6. The Critical Region Transition 1266
7. Conclusions 1269
8. Acknowledgments 1269
9. References 1269

List of Tables

1. Correlation data 1237
2. Evaluation data 1238

List of Figures

1. Saturation pressure: 0–100 °C 1239
2. Saturation pressure: 100–350 °C 1239
3. Saturation pressure: 350–375 °C 1239
4. Liquid saturation density: 0–100 °C 1239
5. Liquid saturation density: 100–350 °C 1239
6. Liquid saturation density: 100–350 °C 1239
7. Liquid saturation density: 350–375 °C 1240
8. Vapor saturation density: 0–100 °C 1240
9. Vapor saturation density: 100–350 °C 1240
10. Vapor saturation density: 350–375 °C 1240
11. Liquid saturation enthalpy: 0–100 °C 1241
12. Liquid saturation enthalpy: 100–350 °C 1241
13. Liquid saturation enthalpy: 100–350 °C 1241
14. Liquid saturation enthalpy: 350–375 °C 1241
15. Vapor saturation enthalpy: 0–100 °C 1241
16. Vapor saturation enthalpy: 100–350 °C 1241
17. Vapor saturation enthalpy: 350–375 °C 1242
18. Saturation vapor enthalpy–difference–temperature–difference ratio: 0–150 °C 1242
19. Saturation function α 0–100 °C 1242
20. Saturation function α 100–350 °C 1243
21. Saturation function α 0–100 °C 1243
22. Saturation function α 0–250 °C 1243
23. Saturation function α 100–350 °C 1244
24. Liquid density maximum -5 to $+5$ °C 1244
25. Liquid density: 0 °C 1244
26. Liquid density: 20 °C 1244
27. Liquid density: 50 °C 1244
28. Liquid density: 100 °C 1244
29. Liquid density: 150 °C 1245
30. Liquid density: 200 °C 1245
31. Liquid density: 250 °C 1245
32. Liquid density: 300 °C 1245
33. Liquid density: 340 °C 1245
34. Liquid density: 350 °C 1246
35. Liquid density: 360 °C 1246
36. Liquid density: 370 °C 1246
37. Liquid density: 373.5 °C 1246
38. Liquid density: 374 °C 1246
39. Liquid density: 375 °C 1246

40. Liquid density: 374–375 °C 1247
41. Critical region density: 378–380 °C 1247
42. Density: 400 °C 1247
43. Density: 450 °C 1247
44. Density: 500 °C 1247
45. Density: 700 °C 1248
46. Density: 850 °C 1248
47. Vapor density: 150 °C 1248
48. Vapor density: 175 °C 1248
49. Vapor density: 200 °C 1248
50. Vapor density: 225 °C 1248
51. Vapor density: 250 °C 1249
52. Vapor density: 275 °C 1249
53. Vapor density: 300 °C 1249
54. Vapor density: 325 °C 1249
55. Vapor density: 340 °C 1249
56. Vapor density: 350 °C 1249
57. Vapor density: 360 °C 1250
58. Vapor density: 370 °C 1250
59. Vapor density: 373.5 °C 1250
60. Vapor density: 374 °C 1250
61. Vapor density: 375 °C 1250
62. Liquid density: 50 °C 1251
63. Liquid density: 100 °C 1251
64. Liquid density: 150 °C 1251
65. Liquid density: 200 °C 1251
66. Density: 400 °C 1251
67. Density at high pressures: 50–150 °C 1252
68. Density at high pressures: 200–600 °C 1252
69. Density at high pressures: 400 °C 1252
70. Density at high pressures: 600 °C 1252
71. Density at high pressures: 800 °C 1252
72. Supercooled liquid density at 0.1 MPa and − 30 to + 20 °C 1253
73. Liquid density at 0.1 MPa and 0–100 °C 1253
74. Superheated vapor at 0.1 MPa and 100–250 °C . 1253
75. Supersaturated vapor density: 178.1 °C 1253
76. Supersaturated vapor density: 200.2 °C 1253
77. Supersaturated vapor density: 248.13 °C 1253
78. Supersaturated vapor density: 298.16 °C 1254
79. Pressure: 374 °C 1254
80. Pressure: 375 °C 1254
81. Pressure: 380 °C 1254
82. Pressure: 400 °C 1255
83. Ultra high pressure 25 °C 1255
84. Ultra high pressure 75 °C 1255
85. Ultra high pressure 125 °C 1255
86. Ultra high pressure 175 °C (448–15 K) 1256
87. Ultra high pressure 500 °C (773.15 K) 1256
88. Ultra high pressure 1000 °C (1273.15 K) 1256
89. Ultra high pressure: Hugoniot curve 1256
90. Walsh and Rice (1958) estimate of $\left(\frac{\partial v}{\partial T}\right)_P$. Broken and full lines indicate their interpolations and extrapolations, respectively 1257
91. Speed of sound, supercooled liquid states: 0.1 MPa 1257
92. Speed of sound, liquid: 0.1 MPa 1257
93. Speed of sound, vapor: 0.1 MPa superheat 1258
94. Speed of sound, supercooled liquid states: 0.1 MPa 1258
95. Speed of sound, liquid: 0.1–100 MPa 1258
96. Speed of sound, supercooled liquid states: − 20 to + 20 °C 1258
97. Speed of sound, liquid: 100–400 °C 1258
98. Speed of sound, liquid: 0.1–1000 (P/MPa) 1259
99. Speed of sound, supercritical states: 375–500 °C 1259
100. Speed of sound, vapor: 150–330 °C 1259
101. Speed of sound, metastable liquid states; 150–300 °C 1260
102. Isopiestic specific heat C_p supercooled liquid states: 0.1 MPa 1260
103. Isopiestic specific heat C_p, liquid: 0.1 MPa 1260
104. Isopiestic specific heat C_p, liquid: 30–100 MPa . 1261
105. Liquid Isopiestic specific heat C_p, liquid: 20–50 MPa 1261
106. Isopiestic specific heat C_p, supercooled liquid: 0.1–400 MPa 1261
107. Isopiestic specific heat C_p, vapor: 12–22 MPa . 1262
108. Isopiestic specific heat C_p, vapor: 2–20 MPa ... 1262
109. Isopiestic specific heat C_p: 30–100 MPa 1262
110. Isopiestic specific heat C_p: 22–27 MPa 1262
111. Isopiestic specific heat C_p: 23–24 MPa 1263
112. Isochoric specific heat C_v: 0.3238 Kg dm^{-3} 1263
113. Isochoric specific heat C_v: 0.3103 kg dm^{-3} 1263
114. Isochoric specific heat C_v: vapor isochores kg dm^{-3} 1264
115. Isopiestic specific heat C_v, supercooled 0.1–400 MPa 1264
116. Joule–Thomson coefficient, vapor: 128–300 °C 1264
117. Joule–Thomson coefficient, vapor: 350–800 °C 1265
118. Isothermal throttling coefficient, vapor: 70–140 °C 1265
119. Isothermal throttling coefficient vapor: 350–400 °C 1265
120. Isentropic temperature–pressure derivative: 0–80 °C 1265
121. Isentropic temperature–pressure derivative: 295–495 K 1266
122. Second virial coefficient: 50–100 °C 1266
123. Second virial coefficient: 100–200 °C 1266
124. Second virial coefficient: 200–300 °C 1267
125. Third virial coefficient: 200–350 °C 1267
126. Blending function F, critical region 1267
127. Isochoric specific heat C_v, critical region 1267
128. Isochoric specific heat C_v, critical region 1268
129. Inverse isothermal compressibility $[\rho(\partial P/\partial\rho)]$, critical region 1268
130. Inverse isothermal compressibility $[\rho(\partial P/\partial\rho)]$, critical region 1268
131. Speed of sound, critical region 1268
132. Speed of sound, critical region 1269

1. Introduction

One of the first methods for uniting a scaled equation of state, valid only near the critical point, with a nonsingular equation representing states not in the critical region was devised by Chapela and Rowlinson (1974) for carbon dioxide [and used by Angus, Armstrong, and de Reuck (1976) in preparing their CO_2 tables]. The method could be represented as a linear combination of the pressure P_s produced by the simple scaling equation of Schofield and the pressure P_A produced by a nonsingular equation valid for states of CO_2 not near the critical point, i.e.,

$$P = P_S + f(P_A - P_S).$$

In this equation f, the "switching function", is a function of "distance" from the critical point such that f and all its derivatives are zero at the critical point. Away from the critical point (but sufficiently close that the scaling equation is still approximately valid) f approaches one, and its derivatives approach zero. The equation not being in fundamental form, numerical integration is required to produce derived properties; as shown by Angus, Armstrong, and de Reuck, this entails elaborate procedures in the critical region and close to the saturation boundary.

After it became clear that simple scaling is valid only in a region very close to the critical point, e.g., within $(T - T_C)/T_C = 10^{-3}$, [see for example Levelt Sengers (1981)], Levelt Sengers, Kamgar-Parsi, Balfour and Sengers (1983) used "revised and extended" scaling theory to produce an equation of state for H_2O showing excellent agreement with thermodynamic data in the region within $\pm$ 25% of the critical density and to about 50 °C above the critical point.

Woolley (1983) studied the feasibility of combining a scaling equation for H_2O [due to Murphy, Sengers and Levelt Sengers (1975)] with a nonsingular state equation [due to Pollak (1975)] to obtain a combined, continuously valid Helmholtz function. Woolley demonstrated that, whatever the switching function chosen, it is impossible for the combined Helmholtz free energy and its first two derivatives to be intermediate in value between those of the scaled and nonsingular functions. Only if, in the region of switching, the behavior of the two functions is essentially identical can a satisfactory transition be obtained.

The equation of state described herein is a unified Helmholtz function which is in exact agreement with the revised and extended scaling equation of Levelt Sengers, Kamgar-Parsi, Balfour and Sengers (1983) at the critical point and which includes a new "far-field" scaling equation providing a smooth transition through the critical region. The smoothness of that transition is demonstrated by the behavior of second derivative quantities in the critical region. The accuracy of the equation is shown by comparisons between the equation and thermodynamic data over a wide range of conditions.

2. The Revised and Extended Scaling Equation

Levelt Sengers, Kamgar-Parsi, Balfour and Sengers (1983) have formulated their fundamental equation in terms of a potential function

$$\overline{P} = \overline{P}(\bar{\mu}, \overline{T}),$$

in which

$$\overline{P} = \frac{PT_c}{P_c T}$$

$$\bar{\mu} = \frac{\mu \rho_c T_c}{P_c T},$$

and

$$\overline{T} = -\frac{T_c}{T},$$

and in which P is the pressure, μ the chemical potential, T the temperature, ρ the density and the subscript c denotes the critical state.

This fundamental relationship can be expressed in the equivalent form of a dimensionless Helmholtz function.

$$\bar{\psi}_n = \bar{\psi}_n(\bar{\rho}, \overline{T}), \tag{1}$$

in which $\bar{\psi} = \psi/RT$, ψ being the Helmholtz free energy and R the gas constant and $\bar{\rho} = \rho/\rho_c$, $\overline{T}$ being the same as given above. The subscript n denotes "near" the critical point.

The function $\bar{\psi}_n$ appearing in the rest of this paper is exactly equivalent to the $\overline{P}$ function given by Sengers *et al.* except for small adjustments in $\bar{\mu}_c$ (new value $-$ 11.2317), $\bar{\mu}_1$ (new value $-$ 22.6407) and $\bar{\mu}_2$ (new value $-$ 17.7876), and for the addition of the arbitrary function.

$$\Delta\bar{\psi}_n = C_{001} + C_{002}\Delta\overline{T},$$

in which $\Delta\overline{T} = 1 + \overline{T}$, $C_{001} = -0.000\,034\,631\,815$ and $C_{002} = -0.000\,030\,378\,112$. These constants are adjusted to guarantee zero values of energy and entropy for the triple point liquid state. The values of R, ρ_c, and T_c are the same as for the Sengers *et al.* formulation.

3. The Unified Helmholtz Function

The Helmholtz function is

$$\bar{\psi} = \bar{\psi}_f + F(\bar{\psi}_n - \bar{\psi}_f), \tag{2}$$

in which $\bar{\psi}_f = \bar{\psi}_f(\bar{\rho}, \overline{T})$ is the "far-field" function ($\bar{\psi}_f = \psi_f/RT$) and the function $F(\bar{\rho}, \overline{T})$ is unity at the critical point, where all its derivatives are zero; it descends to zero inside the region of validity of $\bar{\psi}_n$ and is zero everywhere outside the critical region.

Its definition is

$$F = 1 - \exp(-1/Z), \tag{3}$$

in which

$$Z = \exp[(\zeta/\delta)^4] - 1$$

and

$$\zeta = \sqrt{(\Delta\bar{\rho}/\Delta\bar{\rho}_0)^2 + (\Delta\overline{T}/\Delta\overline{T}_0)^2}$$

with

$$\delta = 1.028\,667, \quad \Delta\bar{\rho}_0 = 0.23, \quad \Delta\overline{T}_0 = 0.05.$$

The derivatives of F are given in Appendix E.

The far-field equation is in the form

$$\bar{\psi}_f = \ln\bar{\rho} + \bar{\psi}_0 + \bar{\psi}_1(\bar{\rho}, \overline{T}), \tag{4}$$

in which the first two terms pertain to the ideal gas and $\bar{\psi}_0$ is defined in Appendix A.

The function $\bar{\psi}_1(\bar{\rho},\bar{T})$ may be written

$$\bar{\psi}_1 = W_1 + EW_2 + GW_3 + HW_4,$$

in which

$$W_1 = \sum_{i=1}^{N_{R1}} \sum_{j=1}^{N_{T1}} A_1(i,j) R_1(i) T_1(j)$$

$$W_2 = \sum_{i=1}^{N_{R2}} \sum_{j=1}^{N_{T2}} A_2(i,j) R_2(i) T_1(j)$$

$$W_3 = \sum_{i=1}^{N_{R3}} \sum_{j=1}^{N_{T3}} A_3(i,j) R_3(i) T_2(j)$$

$$W_4 = \sum_{i=1}^{N_{R4}} \sum_{j=1}^{N_{T4}} A_4(i,j) R_4(i) T_1(j),$$

and

$$R_1(i) = (1-E)(\bar{\rho})^{i-2}$$

except that $R_1(2) = (1-E)\ln\bar{\rho} - \bar{\rho}^2 \ln\bar{\rho} + \bar{\rho}^2/2$.

$$R_2(i) = (\bar{\rho})^i$$

$$R_3(i) = (\bar{\rho})^{i+1}$$

$$R_4(i) = R_1(i)$$

and

$$T_1(j) = (\bar{T})^{j-1}$$

$$T_2(j) = (\bar{T})^{j+1}.$$

The coefficients, E, G, and H are defined as follows:

$$E = \exp(-\bar{\rho}^2)$$

$$G = \exp(-\alpha\Delta\bar{T} - \beta\Delta\bar{\rho} - \gamma\Delta\bar{T}^2 - \delta\Delta\bar{\rho}^2)$$

$$H = \exp[-\nu(\bar{T}+3)],$$

in which $\alpha = 80, \beta = 1, \gamma = 130, \delta = 12, \nu = 4$.

For computational precision the term $1-E = 1-\exp(-\bar{\rho}^2)$ should be replaced by $\bar{\rho}^2$ for $\bar{\rho} < 0.2\times10^{-4}$.

The indices of summation are

$$N_{R1} = 7 \quad N_{T1} = 7$$

$$N_{R2} = 7 \quad N_{T2} = 12$$

$$N_{R3} = 5 \quad N_{T3} = 5$$

$$N_{R4} = 5 \quad N_{T4} = 10.$$

The coefficients $A_1(i,j)$, $A_2(i,j)$, $A_3(i,j)$, $A_4(i,j)$ are given in Appendix B. Unless otherwise stated each coefficient has zero value.

Dimensionless variables and their derivatives are given in Appendix C. Appendices D and E provide the derivatives of functions needed for computation.

4. Fitting Procedure

The fitting procedure consisted of a weighted linear least-squares minimization which incorporated the Wagner (1977) selective multiple regression procedure. The coefficients of the nonlinear terms were adjusted one at a time while finding optimum values.

Table 1 shows the data used directly or indirectly in the linear fitting procedure. These data have been discussed by Hill and MacMillan (1988). An extended discussion of the process of assessing the experimental uncertainties in density and enthalpy has been provided by Sato, Uematsu, Watanabe, Saul and Wagner (1985).

The saturation properties deduced from the data of Osborne, Stimson and Ginnings (1933, 1937, 1939) Stimson (1969), Guildner (1976), Kell, McLaurin and Whalley (1985) and Kell (1977) were used indirectly in the fitting process by using the Saul and Wagner (1987) equations to represent these data with thermodynamic consistency. Values of saturation liquid and vapor densities and enthalpies were fitted at 10 degree intervals between the triple point and 370° and at 1° intervals close to the critical point. The data were weighted according to the tolerances assigned by Saul and Wagner.

Pressure data with wide ranges of density and temperature were selected from the data of Kell, McLaurin and Whalley (1975, 1985), Kell and Whalley (1977, 1978), Rivkin and Akhundov (1963, 1966), Vukalovich, Zubarev and Aleksandrov (1961, 1962), Hilbert (1979), Maier and Frank (1966) and Koster and Frank (1969). With exceptions for particular data sets, weighting factors were assigned corresponding to tolerances on relative pressure of

$$\frac{\delta P}{P} = \left(\frac{\delta\rho}{\rho}\right)\frac{\rho}{P}\left(\frac{\partial P}{\partial\rho}\right)_T,$$

in which $\delta\rho/\rho$ is the relative density tolerance identified in Table 1 for the PVT data, and the pressure-density derivative is an estimate obtained from a preliminary version of the Helmholtz function. The minimum relative density tolerance in the critical region (where the inverse isothermal compressibility is vanishingly small) was set at 0.0005.

For the low pressure vapor states, the Joule–Thomson data $(\partial T/\partial P)_h$ extrapolated to zero pressure were used to control the behavior of the second virial coefficient.

For the liquid states below the triple point temperature, a few values of the isochoric specific heat and a few values of the isothermal compressibility were used to control the property behavior in that region.

The two-phase equilibrium condition was introduced into the fitting procedure by requiring, at 10° intervals between the triple point and 370 °C (and 1° intervals close to the critical point), the equality of $(\psi + Pv)$ for liquid and vapor saturation states at the same temperature.

Special measures were needed to provide smoothness in the derivatives of the Helmholtz function in their variation from the singular critical region function near the critical point to the nonsingular far-field functions. It is apparent from the work of Woolley (1983) that the only way to obtain satisfactory smoothness in the transition from one function to another is that there be some finite range of states in which the two functions are essentially identical. With this in mind the far-field functions $\bar{\psi}_f$, $\bar{u}_f$, $\bar{\rho}_f$ and $(\partial\bar{P}/\partial\bar{\rho})_f$ were fitted to the corresponding values $\bar{\psi}_n$, $\bar{u}_n$, $\bar{P}_n$ and $(\partial\bar{P}/\partial\bar{\rho})_n$ obtained from the revised and extended scaling functions. The region in which these "data" were fitted was within $\pm$ 25% of the critical density and within 50 °C above and 2–3 °C below the critical temperature. The weighting factors used in the fit

TABLE 1. Correlation data.

Reference	Property	Region	Range T/°C	P/MPa	$(\delta\rho/\rho)_{tot}$
Osborne *et al.* (1933)	P_{sat}		100–t_{crit}		
Stimson (1969)	P_{sat}		25–100		
Guildner *et al.* (1976)	P_{sat}		0–01		
Kell *et al.* (1977)	v_f		0–150		
Kell *et al.* (1985)	v_f		150–350		
Osborne *et al.* (1937)	v_f		350–t_{crit}		
	h_f, v_f, h_g		100–t_{crit}		
Osborne *et al.* (1939)	h_f, v_f, h_g		0–100		
Kell *et al.* (1975)	PvT	liq	0–150	0–100	0.000 04
Kell *et al.* (1978)	PvT	liq	150–350	P_{sat}–100	0.000 1
Kell *et al.* (1985)	PvT	liq	150–350	P_{sat}–100	0.000 1
	PvT	vap	250–350	2.7–P_{sat}	0.001
	PvT	supercrit	375–500	2.7–100	0.000 1
Kell *et al.* (1989)	PvT	vap	150–275	0.2–P_{sat}	0.001
Rivkin *et al.* (1966)	PvT	critical			0.000 15
Rivkin *et al.* (1963)	PvT	critical region			0.000 15
Vukalovich *et al.* (1961)	PvT	supercrit	450–650	5–120	0.001
Vukalovich *et al.* (1962)	PvT	supercrit	700–900	5–120	0.001
Grindley *et al.* (1971)	PvT	high press	25–150	100–800	0.000 3
Hilbert (1979)	PvT	high press	150–600	100–400	0.001
Maier *et al.* (1968)	PvT	high press	200–850	100–600	0.002
Koster *et al.* (1969)	PvT	high press	0–600	600–1000	0.002
Ertle (1980)	μ_{jo}		150–750		

were the sums of terms proportional to the derivatives of the blending function F which appear in Appendix C: $\partial F/\partial\bar{\rho}$, $\partial^2 F/\partial\bar{\rho}^2$, $\partial F/\partial\bar{T}$, $\partial^2 F/\partial\bar{T}^2$.

Taking the isochoric specific heat as an example, we have

$$\bar{C}_V = \bar{C}_{Vf} + F(\bar{C}_{vn} - \bar{C}_{vf}) + 2\bar{T}\frac{\partial F}{\partial \bar{T}}(\bar{u}_n - \bar{u}_f) - \bar{T}^2\frac{\partial^2 F}{\partial \bar{T}^2}(\bar{\psi}_n - \bar{\psi}_f).$$

The transition between $\bar{C}_{vn}$ and $\bar{C}_{vf}$ can only be acceptably smooth if the third and fourth terms on the right-hand side are negligibly small compared to the first two. For this reason the weighting factor for the fit $\bar{\psi}_f = \bar{\psi}_n$ needs to have a term proportional to $\partial^2 F/\partial\bar{T}^2$ which is very large in a very narrow band of states around the critical point. The weighting factor for this fit also needs a term proportional to $\partial^2 F/\partial\bar{\rho}^2$.

The objective function for the fit can be written

$$D = \sum_{j=1}^{N}\sum_{i=1}^{n_j} Q_i (P_{obs} - P_{calc})_i^2,$$

in which P_i denotes any property at state i, N is the number of kinds of data used in the fit (pressure, enthalpy, free energy, isochoric specific heat, isothermal compressibility, internal energy) and n_j is the number of data used in each kind of fit. Numerous trials were required to obtain appropriate adjustments of weighting factors and data representation, as well as in adjustments of the nonlinear coefficients of the functions defined in Appendix E.

No constraints were imposed on the fit except for adjustments of arbitrary constants to make the entropy and internal energy values zero at the triple point liquid states.

5. Comparisons with Experimental Data

In what follows, comparisons are made both with the "correlation" data of Table 1, which can be accommodated within a linear fit, and also with the "evaluation" data of Table 2. The latter include numerous data on speed of sound, isobaric specific heat and throttling coefficients as well as pressure and other data not used in the fitting process. Table 2 refers to a large body of data which provide an independent check of the accuracy, as well as the thermodynamic consistency, of the unified formulation. Unless otherwise indicated, the base for comparison is the unified equation described in Sec. 3.

TABLE 2. Evaluation data.

Reference	Property	Region	Range T/°C	P/MPa
Gildseth *et al.* (1972)	PvT	liq	0.8 0.1	
Grigorev *et al.* (1974)	PvT	liq	20–360	16–80
Zubarev *et al.* (1977)	PvT	supercrit	400–600	0–200
Aleksandrov *et al.* (1974)	PvT	critical	340–380	3–100
Hanafusa *et al.* (1983)	PvT	critical	370–380	21–40
	P_{sat}	critical	370–373.5	
Del Grosso *et al.* (1972)	a	liq	0–95	0.1
Aleksandrov *et al.* (1976)	a	liq	− 3–374	0.1–70
Aleksandrov *et al.* (1979)	a	liq	− 7–150	5–100
Aleksandrov *et al.* (1980)	a	liq	200–400	50–100
Erokhin *et al.* (1980)	a	supercrit	374–500	0–50
Novikov *et al.* (1968)	a	vap	150–330	0–P_{sat}
Holton *et al.* (1968)	a	liq	0–80	0.1–1000
Petitet *et al.* (1985)	a	supercrit	200–700	50–300
Petitet *et al.* (1983)	a	liq	− 20–20	0.1–460
Evstefeev *et al.* (1979)	a	liq (meta)	150–300	0.1–10
Sirota *et al.* (1962)	C_v	liq	300–370	12–22
		supercrit	375–500	22–27
Sirota *et al.* (1956)	C_p	vap	200–375	2–12
Sirota *et al.* (1962)	C_p	vap	350–375	6–20
Sirota *et al.* (1959)	C_p	supercrit	12–500	2.5–49
Sirota *et al.* (1960)	C_p	supercrit	450–600	30–50
Sirota *et al.* (1963)	C_p	supercrit	340–600	60–80
Sirota *et al.* (1966)	C_p	supercrit	220–700	40–100
Sirota *et al.* (1970)	C_v	supercrit	− 2–35	29–98
Angell *et al.* (1982)	C_p	liq(meta)	− 40–10	0.1
Baehr *et al.* (1975)	C_v	liq, vap	280–t_{crit}	
		supercrit	t_{crit}–420	
Ertle *et al.* (1980)	$(\partial T/\partial p)_h$	vap	155–800	0.5
LeFevre *et al.* (1975)	virial	vap	0–1250	
Wormald (1964)	$(\partial h/\partial p)_T$	vap	40–140	
Osborne *et al.* (1939)	α,β,γ		0–100	P_{sat}
Osborne *et al.* (1937)	α,β,γ		100–374	P_{sat}
Rogener *et al.* (1980)	$(\partial t/\partial p)_s$	liq	3–100	0–80
Aleksandrov *et al.* (1981)	ρ_{max}	liq	− 3–4	− 1–30

5.1. Saturation Properties

Figures 1–3 show comparisons of the saturation pressures determined from the present formulation with experimental data and with the saturation property formulations of Saul and Wagner (1987) for H_2O, as well as the tolerances on the vapor pressure established by the International Association for the Properties of Steam (IAPS) and given by Wagner and Sengers (1986). The unified formulation agrees with the Saul and Wagner formulation within about a part in 10 000 over the entire range and the discrepancies are within the IAPS tolerances. At 273.16 K the computed vapor pressure falls within 0.002 Pa of the determination of Guildner, Johnston, and Jones (1976) whose uncertainty estimate was 0.01 Pa. Figure 2 also shows close agreement between the unified equation and the Saul and Wagner formulation. Here the IAPS tolerance can be viewed with respect to the scatter in the Kell, McLaurin, and Whalley data, which were the principal source for the Saul and Wagner formulation in this temperature range. Figure 3 shows very close agreement between the saturation pressure obtained from the unified equation, and that derived from the revised and extended scaling equation very close to the critical point.

Figures 4–7 show the saturated liquid density differences between the Saul and Wagner values and those of the unified equation. Below 100 °C the two are in close agreement. In the range 250–350 °C the differences shown by Fig. 5, though well within the tolerances, are considerable. In Figs. 5–23, the caption Wagner, Sengers Tolerance (1986) refers to the tolerance published by those authors and accepted by the International Association for the Properties of Steam (IAP). Figure 6 shows the large discrepancy in this region between the Osborne measurements of the liquid density and the Kell measurements which are closely represented by the Saul and Wagner formulation. Figure 7 displays close agreement between the unified formulation and the revised and extended scaling equation of Levelt Sengers *et al.*, whose validity range extends only a few degrees (though shown over an 80° range) below the critical. Again, the Osborne data show considerable scatter.

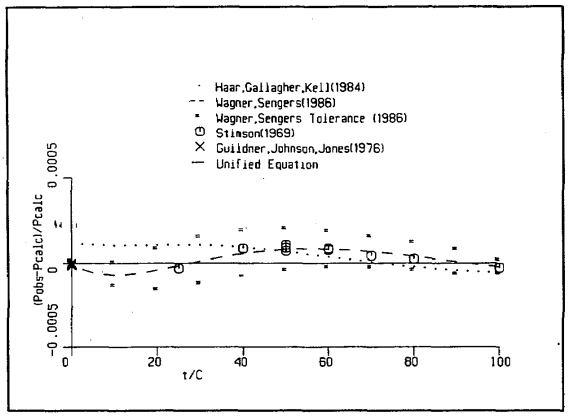

FIG. 1. Saturation pressure: 0–100 °C.

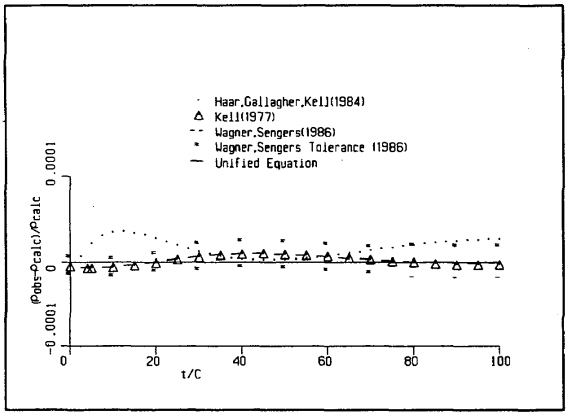

FIG. 4. Liquid saturation density: 0–100 °C.

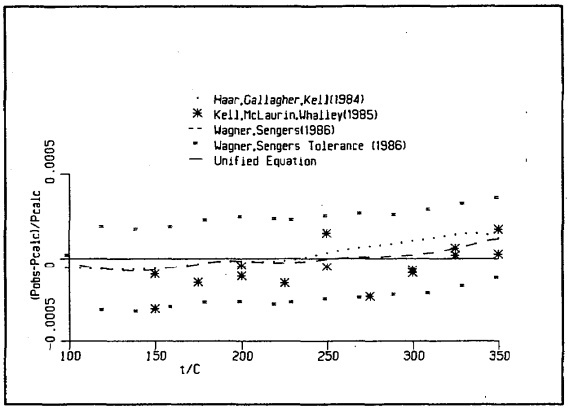

FIG. 2. Saturation pressure: 100–350 °C.

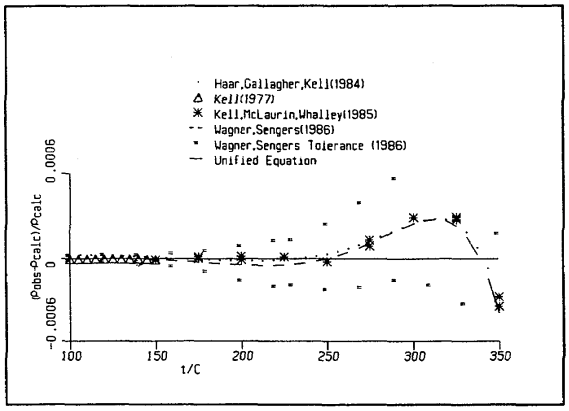

FIG. 5. Liquid saturation density: 100–350 °C.

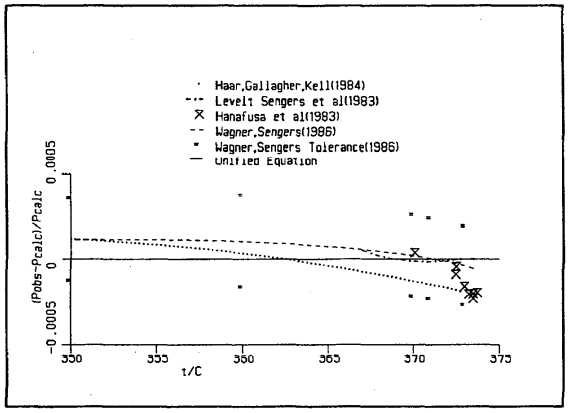

FIG. 3. Saturation pressure: 350–375 °C.

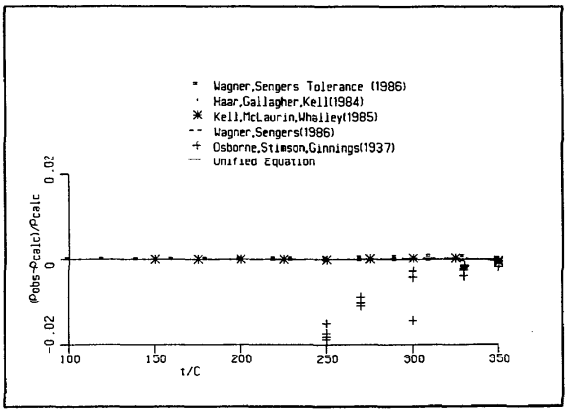

FIG. 6. Liquid saturation density: 100–350 °C.

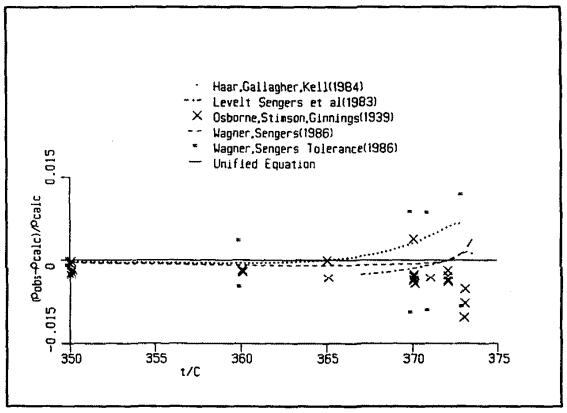

FIG. 7. Liquid saturation density: 350–375 °C.

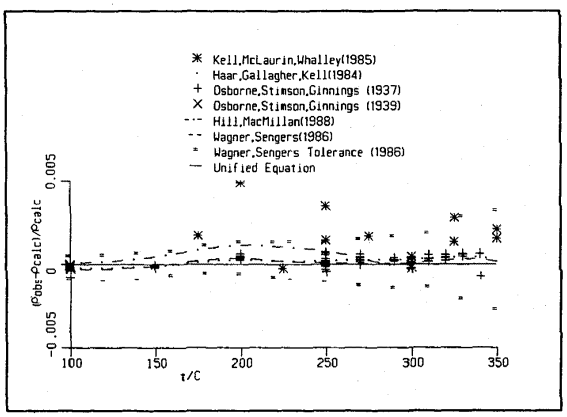

FIG. 9. Vapor saturation density: 100–350 °C.

The critical temperature value used in the unified equation 647.067 K is necessarily the same as the value used in the scaling equation of Levelt Sengers *et al.* (1983). It is not the same as the value established by Levelt Sengers, Straub, Watanabe and Hill (1985) *viz.* 647.14 ± 0.1 K though within the stated tolerance for the latter.

Figures 8–10 show comparisons of the saturation vapor density calculated from the unified equation with the Osborne experimental determinations and with the Saul and Wagner formulation. Relative to experimental uncertainty and to the IAPS tolerances provided by Wagner and Sengers, the agreement, well within one part in 1000 everywhere except very near the critical temperature, indicates that the unified equation represents the saturated vapor density well within experimental uncertainty.

Figures 11–14 show the differences between values of the saturated liquid enthalpy calculated from the unified equation and the Saul and Wagner formulation in relation to the IAPS tolerances. The differences appear to be well within experimental uncertainty. Figure 13 shows the scatter in the Osborne data relative to the Saul and Wagner formulation which will be discussed further subsequently. Figure 14 shows close agreement with the revised and extended scaling equation within the temperature range of validity.

A corresponding comparison of the saturation vapor enthalpies over the whole temperature range is displayed in Figs. 15–17. The scatter in the Osborne determination is in the range ± 2 J/g up to about 350 °C, above which the uncertainty increases considerably. However, the unified equation appears to agree with the Saul and Wagner formulation very closely over the entire range. The equation of Hill and MacMillan (1988) is an extended virial-type equation valid up to about 300 °C.

Since the Saul and Wagner formulation has been used in this work as the best available thermodynamically consistent formulation of the saturation properties of H_2O, it is in order to consider its validity. Figure 18 shows the variation with temperature, in the first 50 °C above the triple point, of the zero pressure specific heat C_{po} (calculated from the unified equation) and estimates of the temperature derivative of the

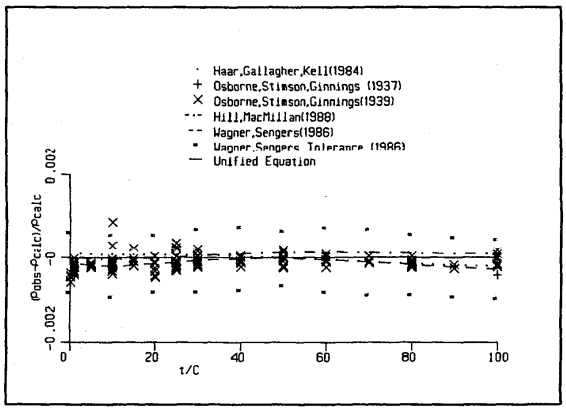

FIG. 8. Vapor saturation density: 0–100 °C.

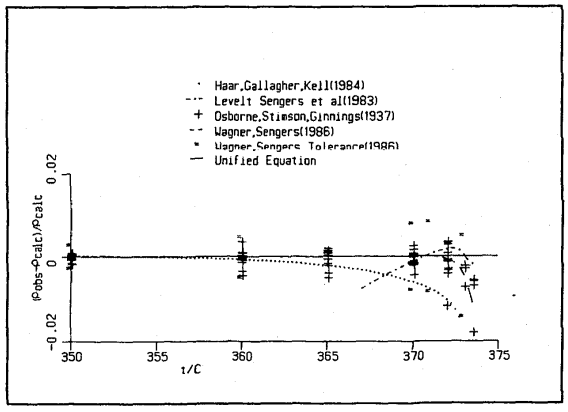

FIG. 10. Vapor saturation density: 350–375 °C.

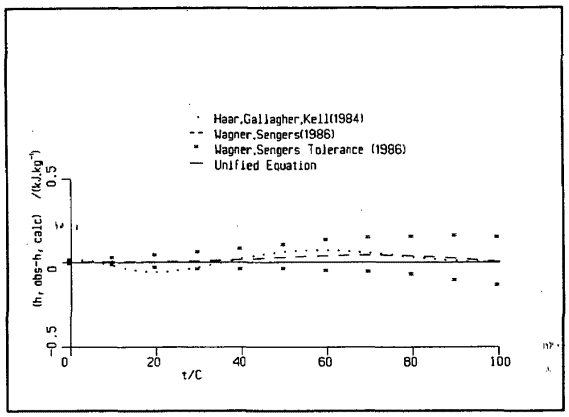

FIG. 11. Liquid saturation enthalpy: 0–100 °C.

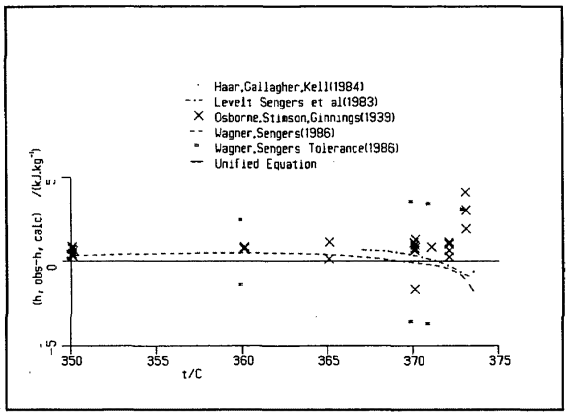

FIG. 14. Liquid saturation enthalpy: 350–375 °C.

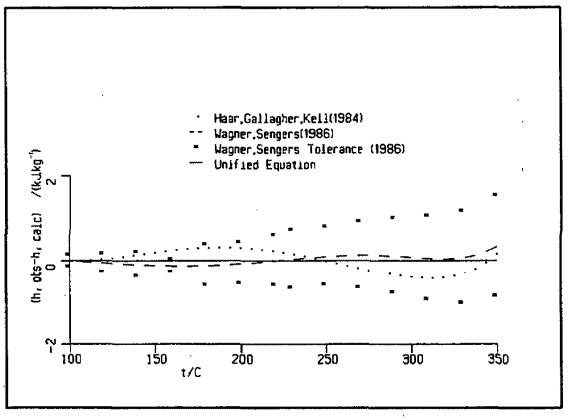

FIG. 12. Liquid saturation enthalpy: 100–350 °C.

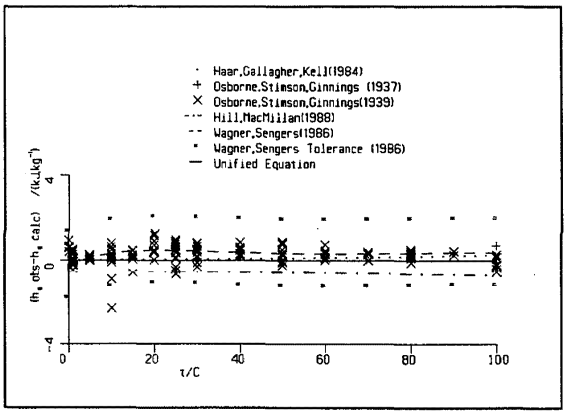

FIG. 15. Vapor saturation enthalpy: 0–100 °C.

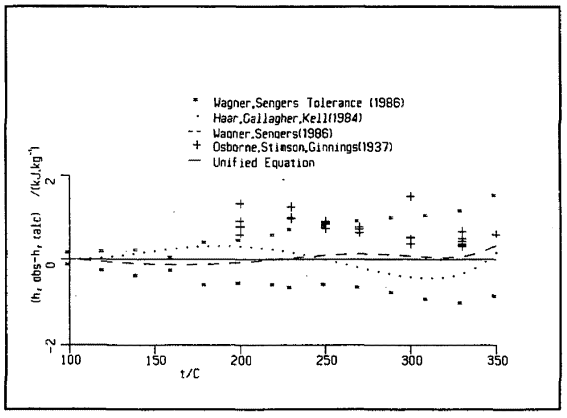

FIG. 13. Liquid saturation enthalpy: 100–350 °C.

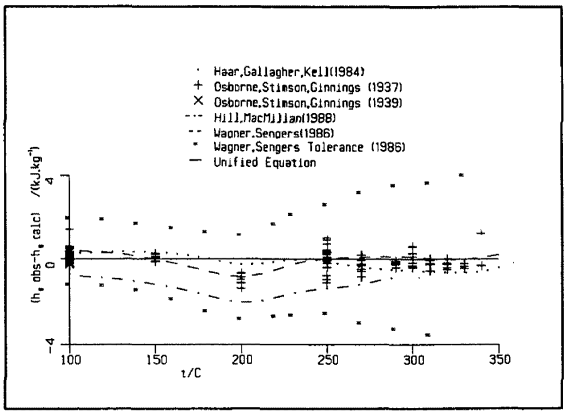

FIG. 16. Vapor saturation enthalpy: 100–350 °C.

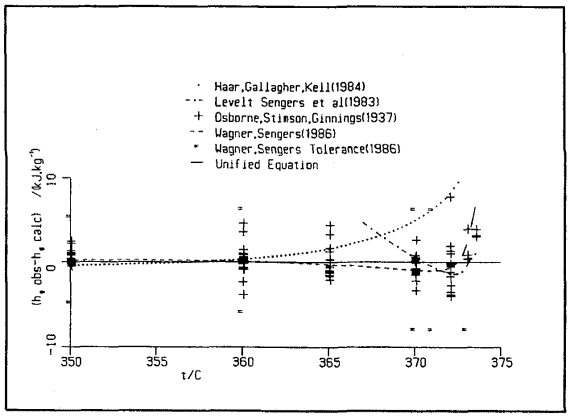

FIG. 17. Vapor saturation enthalpy: 350–375 °C.

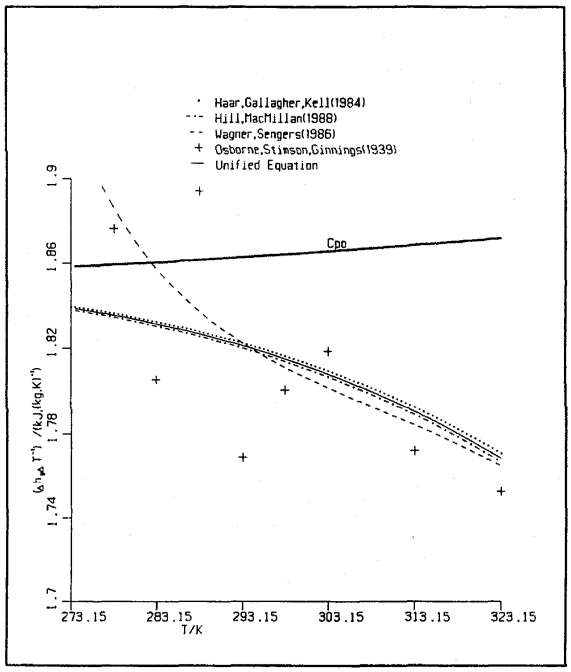

FIG. 18. Saturation vapor enthalpy–difference–temperature–difference ratio: 0–150 °C.

saturated vapor enthalpy h_g. (The values of $\Delta h_g/\Delta T$ were computed for 10° temperature increments). As shown, the unified equation and that of Haar, Gallagher and Kell provide values of $\Delta h_g/\Delta T$ which asymptotically approach the low temperature values of C_{po} (as they should since at low temperature the saturation vapor enthalpy becomes a function of temperature only). This is not true of the $\Delta h_g/\Delta T$ values calculated from the Saul and Wagner functions. It appears that, at least for the first 20–25 °C above the triple point, these functions need adjustment.

The saturation enthalpy values were determined by Osborne, Stimson and Ginnings from their experimental observations of the temperature T, saturation pressure P_{sat} and 3 quantities α, β, and γ for which the following conditions apply

$$\gamma = \frac{T}{\rho_g}\frac{dP_{\text{sat}}}{dT} = h_g - \alpha$$

$$\beta = \frac{T}{\rho_f}\frac{dP_{\text{sat}}}{dT} = h_f - \alpha,$$

so that the saturation vapor and liquid enthalpies are

$$h_g = \alpha + \frac{T}{\rho_g}\frac{dP_{\text{sat}}}{dT}$$

and

$$h_f = \alpha + \frac{T}{\rho_f}\frac{dP_{\text{sat}}}{dT}.$$

With the benefit of more recent data, Saul and Wagner were able to formulate an equation for $P_{\text{sat}}(T)$ which is more accurate than that of Osborne and at the same time to improve upon the estimates of ρ_f (see e.g., Fig. 6). Thus the values of γ and β are considered to be better established today than as the result of Osborne's work. However, the Osborne measurements of α (i.e., the ratio $\Delta\alpha/\Delta T$ over variable temperature increments ΔT) have not been superseded. Saul and Wagner have fitted a single function $\alpha(T)$, continuous between the triple and critical points, which represents these measurements within their experimental scatter. For the calorific values h_f and h_g, the best direct comparison of the unified equation of state with the Osborne measurements is a direct comparison with the experimental values $\Delta\alpha/\Delta T$. Figure 19 shows the differences between the Osborne determinations and those obtained from the unified equation for the same temperature increments and for the range 0–100 °C. Figure 20 shows the same for the range 100–350 °C. As may be seen, the scatter in the experimental uncertainty is much larger above 100 °C than below. Making a slight allowance for systematic error below 100 °C, it may be said that over the entire temperature range the unified equation

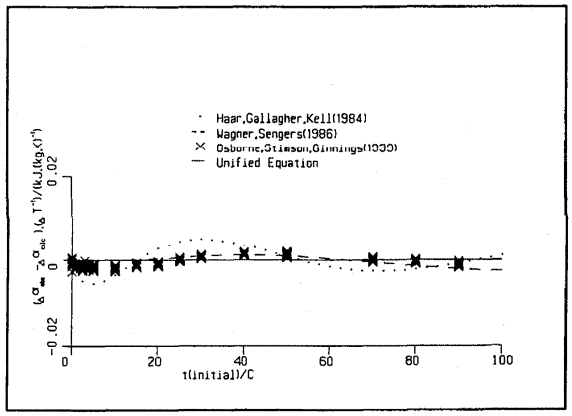

FIG. 19. Saturation function α 0–100 °C.

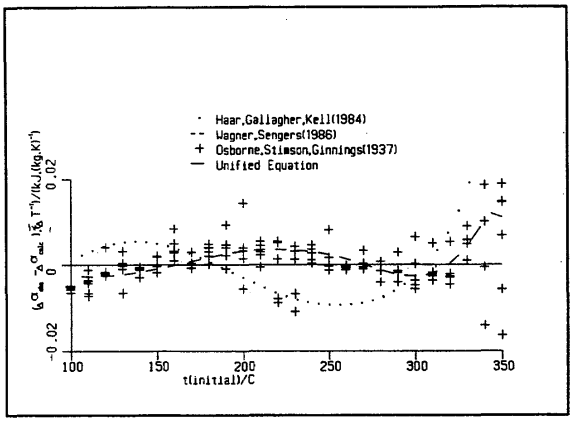

FIG. 20. Saturation function α 100–350 °C.

represents the Osborne data within the experimental data. Figures 21–23 show the direct comparison with the corresponding values obtained from the unified equation, the Wagner and Saul formulation and the equation of Haar, Gallagher and Kell.

In summary it appears that the unified equation represents all experimental determinations of the saturation properties of H_2O within their experimental uncertainty.

5.2. Densities

Figure 24 shows a comparison of the maximum density line obtained from the unified equation in relation to that obtained by Aleksandrov, Okhotin, and Orshova (1981). These authors determined the maximum density line by using an equation representing speed of sound data between 265 and 573 K and at pressures up to 100 MPa. The equation was used in an iterative numerical integration, along a series

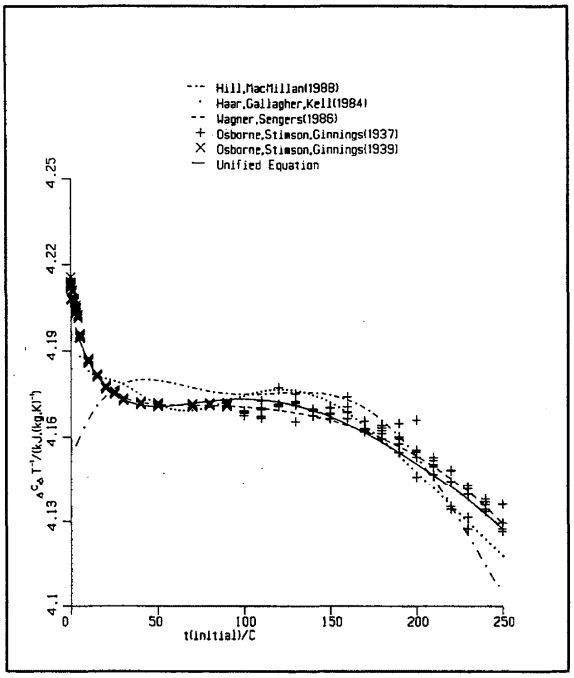

FIG. 22. Saturation function α 0–250 °C.

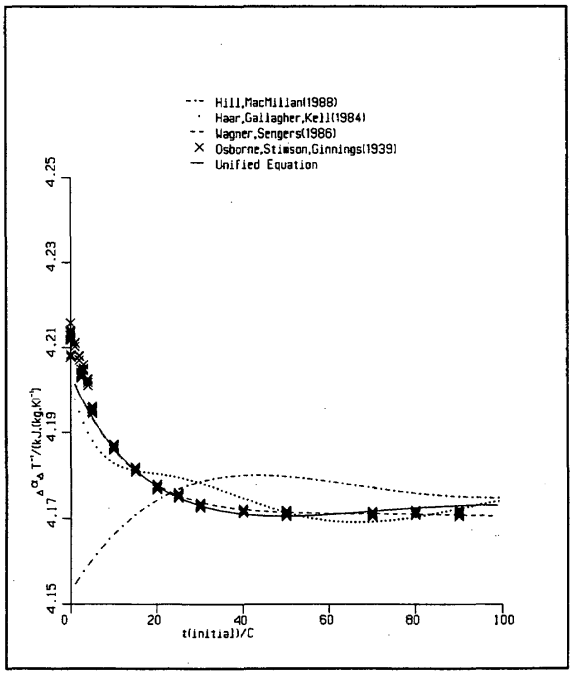

FIG. 21. Saturation function α 0–100 °C.

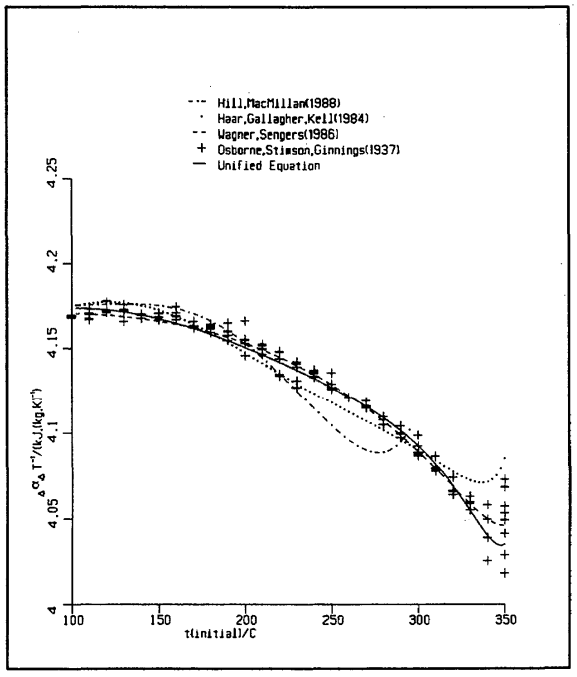

FIG. 23. Saturation function α 100–350 °C.

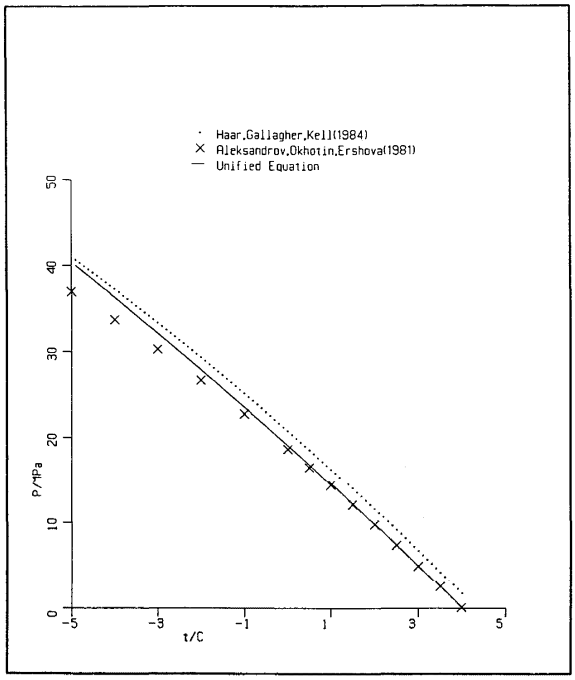

FIG. 24. Liquid density maximum -5 to $+5$ °C.

of isotherms starting from atmospheric pressure, to obtain densities from speed of sound.

Figures 25–28 show that over the temperature range 0–100 °C and in the pressure range up to 100 MPa, the densities obtained from the unified equation are within 20 or 30 ppm of the values measured by Kell and Whalley and quite closely confirmed by the determinations of Aleksandrov, Okhotin, and Ershova, using their speed of sound equation.

Figure 29 shows close agreement between 2 sets of Kell data which are within, say, 30 ppm of the values obtained from the unified equation. These data, which were measured to highest precision in the 0–150 °C range, are in disagree-

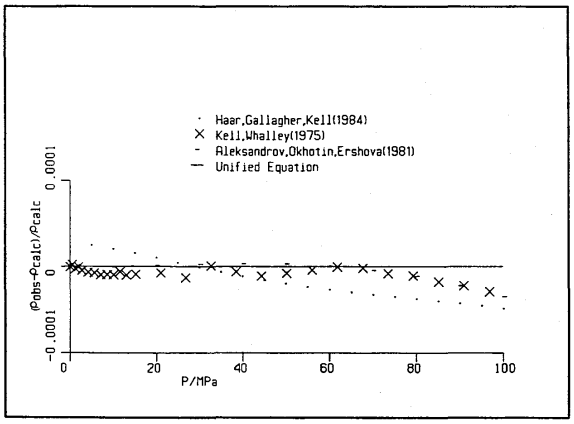

FIG. 26. Liquid density: 20 °C.

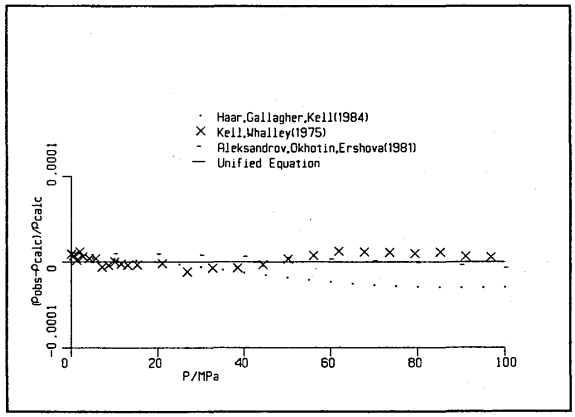

FIG. 27. Liquid density: 50 °C.

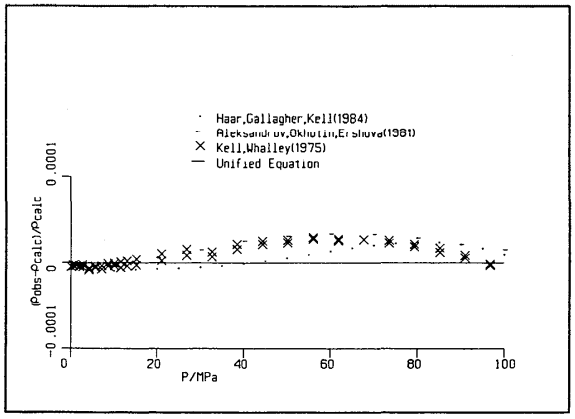

FIG. 25. Liquid density: 0 °C.

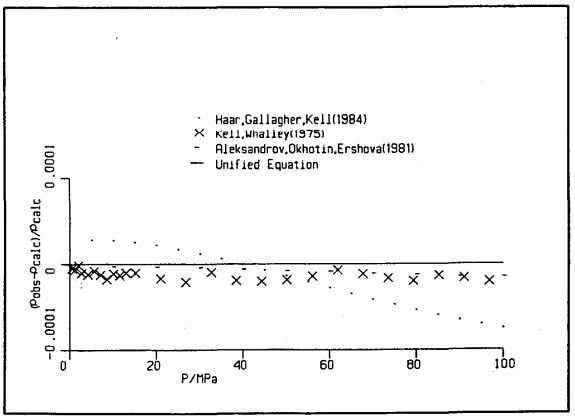

FIG. 28. Liquid density: 100 °C.

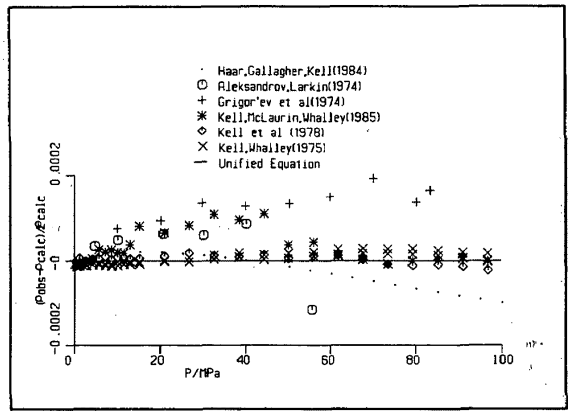

FIG. 29. Liquid density: 150 °C.

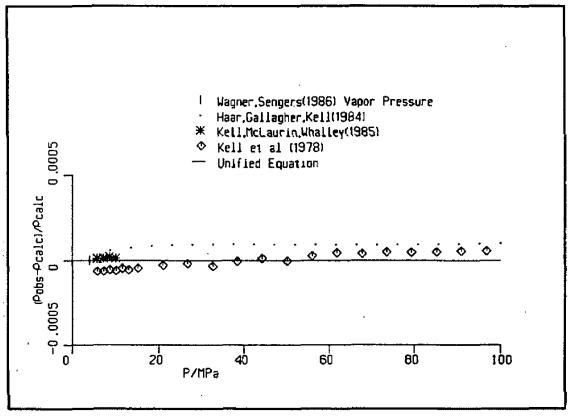

FIG. 31. Liquid density: 250 °C.

ment at the 150 °C isotherm with the 1985 150–500 °C measurements which might have been expected to be generally less precise than the lower temperature data. Figure 29 illustrates the need to select the best data for the correlation data base, rather than using whatever is available; the existence of data on other properties not used in the fit, e.g., speed of sound and specific heat, in the same region offers a warning if the wrong choice has been made.

Covering the range 200–300 °C and up to 100 MPa, Figs. 30–32 show close agreement of the unified equation with the Kell, McLaurin and Whalley 1978 data though not with the 1985 results.

The density difference between the unified equation and the Aleksandrov data shown in Figs. 33–36 needs to be viewed in relation to the differences between the Aleksandrov data and to what are believed to be the more accurate Kell data, as shown in Fig. 34.

Close to the critical temperature, the differences between measured liquid densities and values calculated from the unified equation are shown in Figs. 37–41. Very near the critical pressure (22.046 MPa) where $(\partial P/$

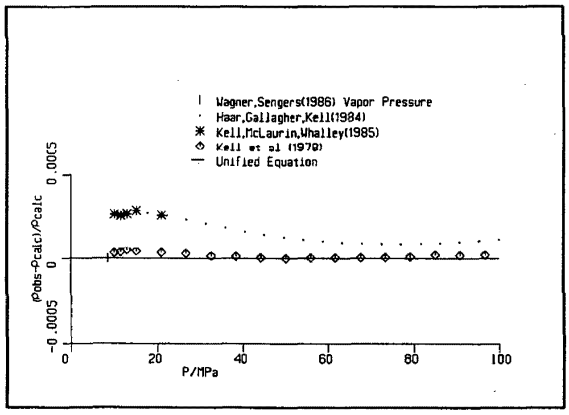

FIG. 32. Liquid density: 300 °C.

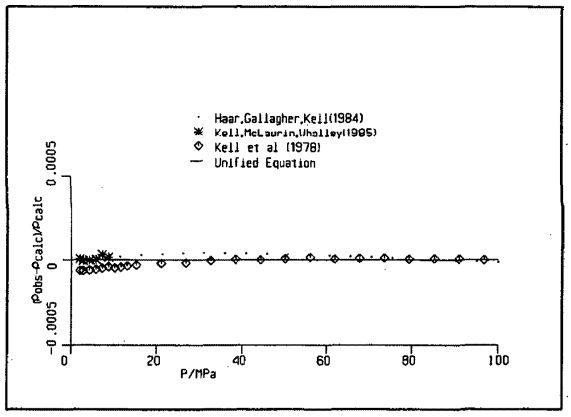

FIG. 30. Liquid density: 200 °C.

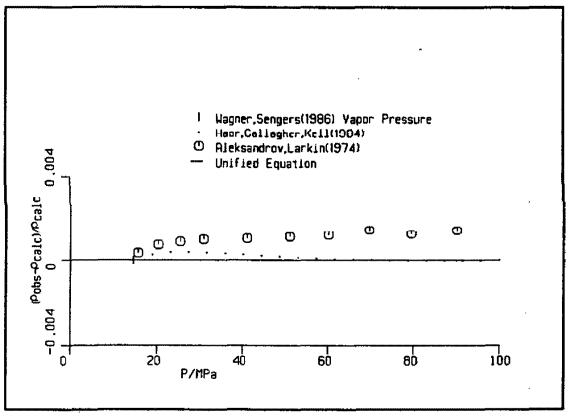

FIG. 33. Liquid density: 340 °C.

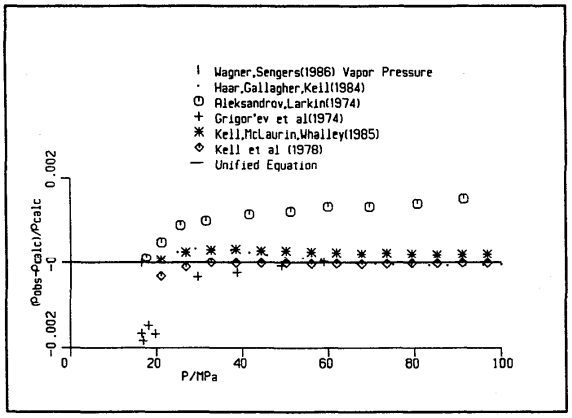

FIG. 34. Liquid density: 350 °C.

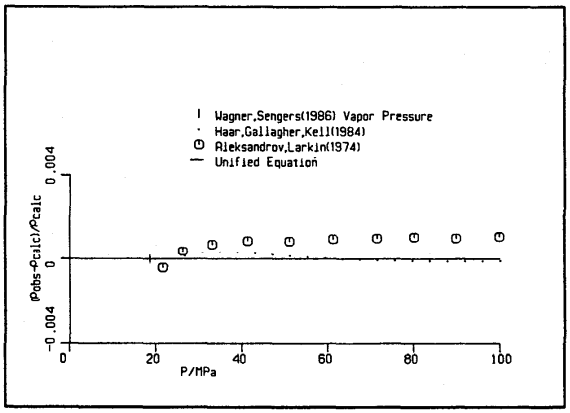

FIG. 35. Liquid density: 360 °C.

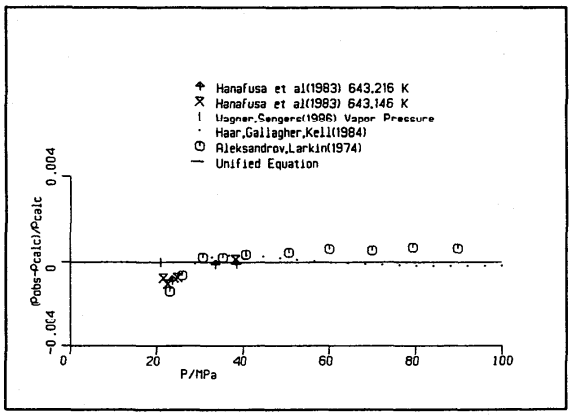

FIG. 36. Liquid density: 370 °C.

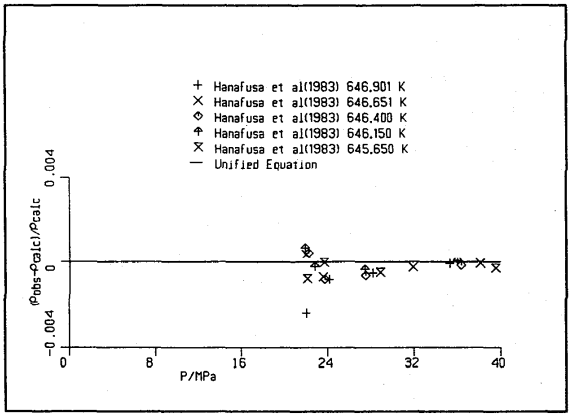

FIG. 37. Liquid density: 373.5 °C.

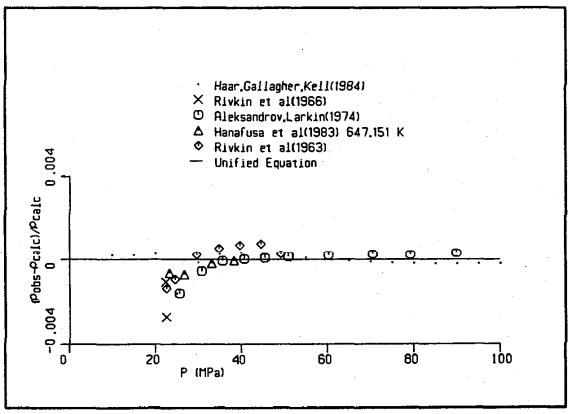

FIG. 38. Liquid density: 374 °C.

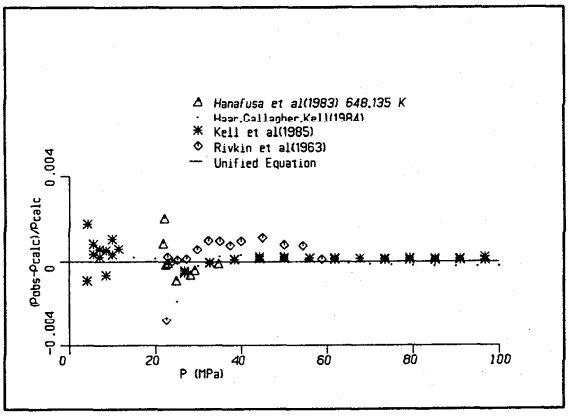

FIG. 39. Liquid density: 375 °C.

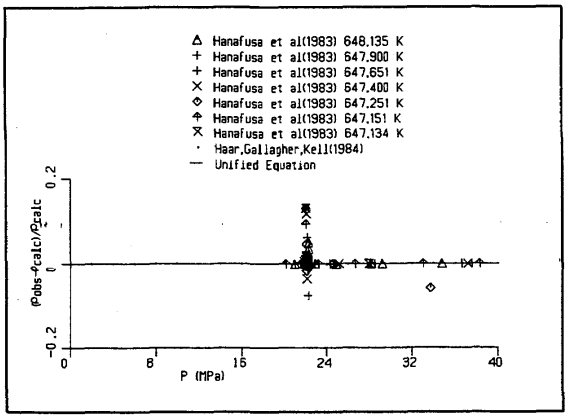

FIG. 40. Liquid density: 374–375 °C.

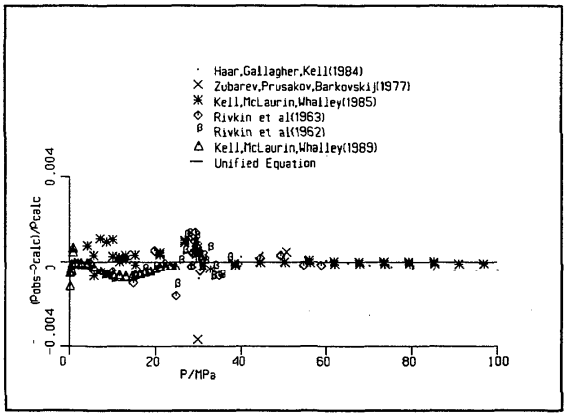

FIG. 42. Density: 400 °C.

$\partial\rho)_T \rightarrow 0$ a large density uncertainty necessarily results from any small inaccuracy in establishing the experimental pressure. The results of this are readily apparent in Figs. 40 and 41 which show the differences on a relatively large scale. Plotting density difference against pressure at the critical pressure compresses the width of the critical region so that the revised and extended equation is not shown in Figs. 37–48. A different view of the critical region (pressure differences as a function of density) will be dicussed in Sec. 5.3, along with a comparison with the scaling equation.

Figures 42–46 show the differences between experimental values of the density at supercritical temperatures and values obtained from the unified equation. In all cases the degree of agreement appears to be within the experimental uncertainty.

Figures 47–61 compare experimental data on vapor density with values calculated from the unified equation. At the lowest temperatures (150 and 175 °C), and to some ex-

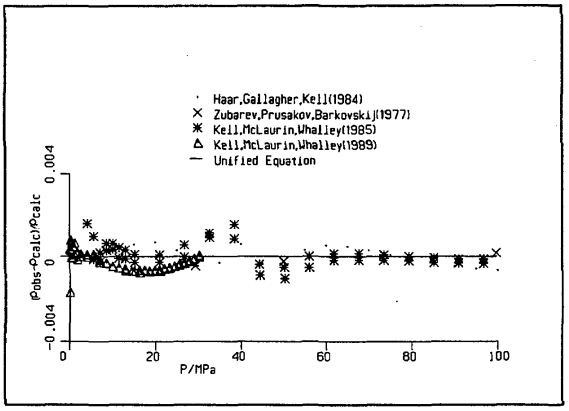

FIG. 43. Density: 450 °C.

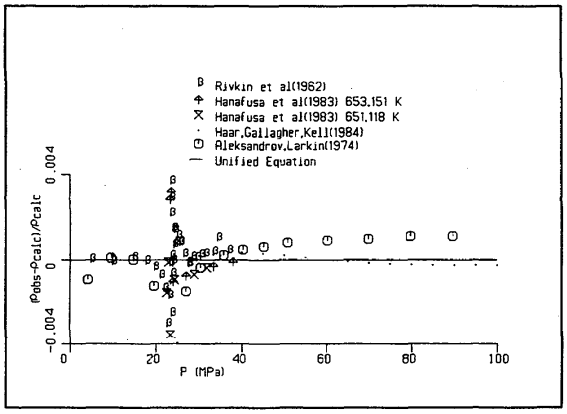

FIG. 41. Critical region density: 378–380 °C.

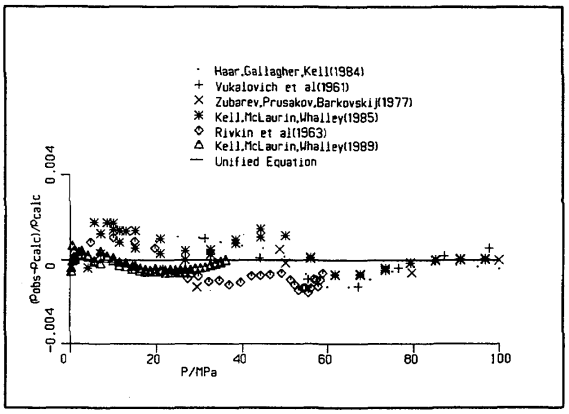

FIG. 44. Density: 500 °C.

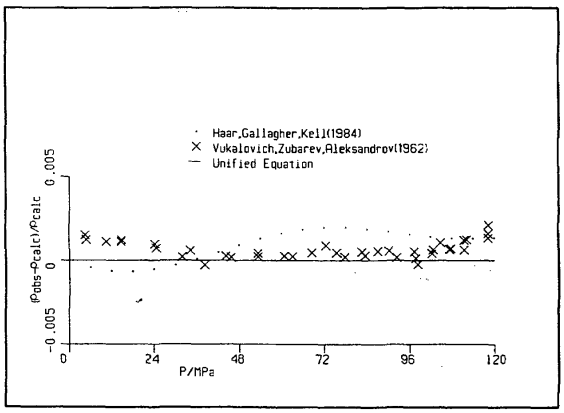

FIG. 45. Density: 700 °C.

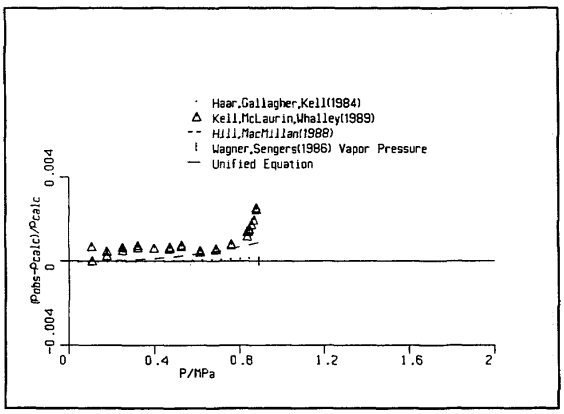

FIG. 48. Vapor density: 175 °C.

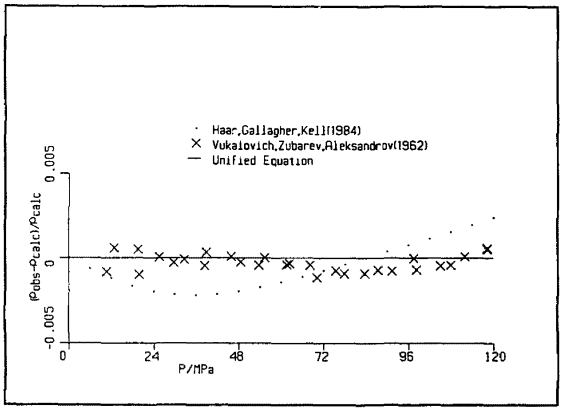

FIG. 46. Density: 850 °C.

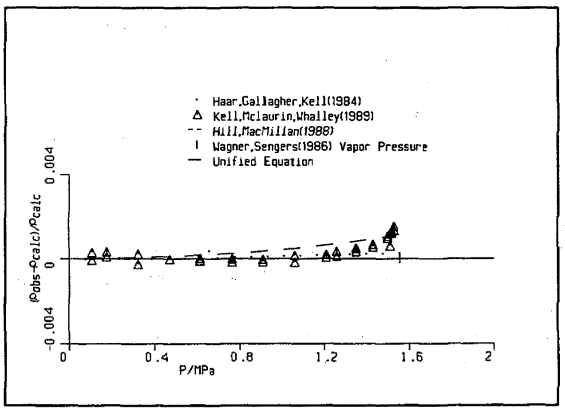

FIG. 49. Vapor density: 200 °C.

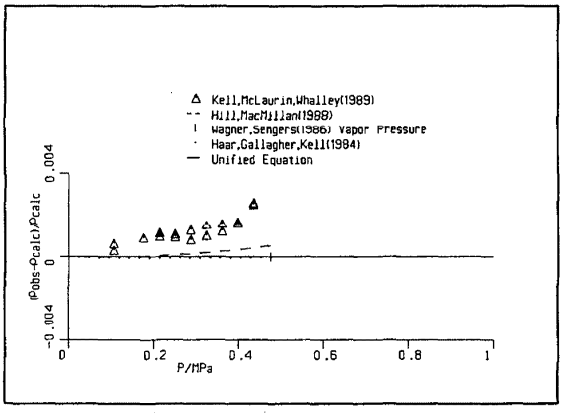

FIG. 47. Vapor density: 150 °C.

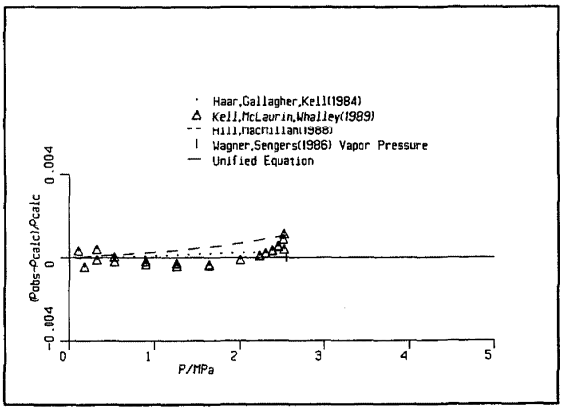

FIG. 50. Vapor density: 225 °C.

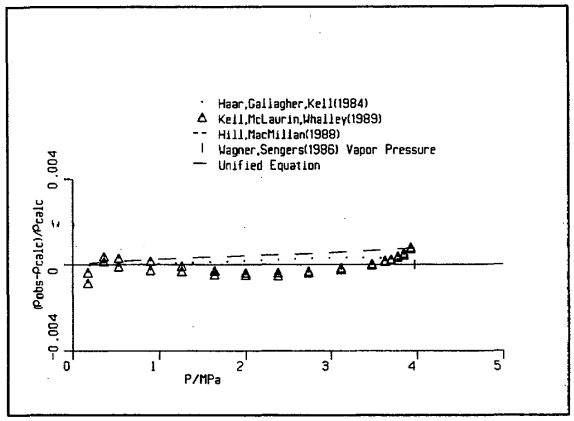

FIG. 51. Vapor density: 250 °C.

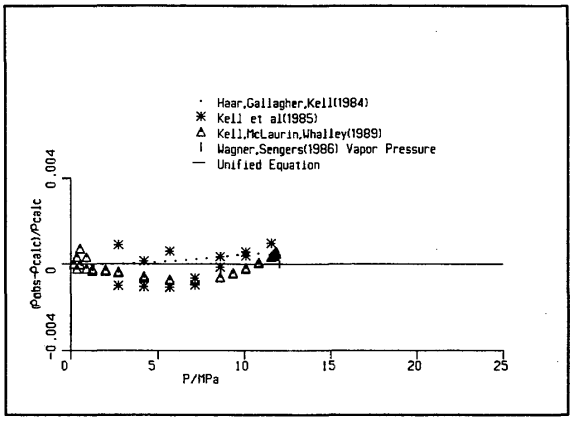

FIG. 54. Vapor density: 325 °C.

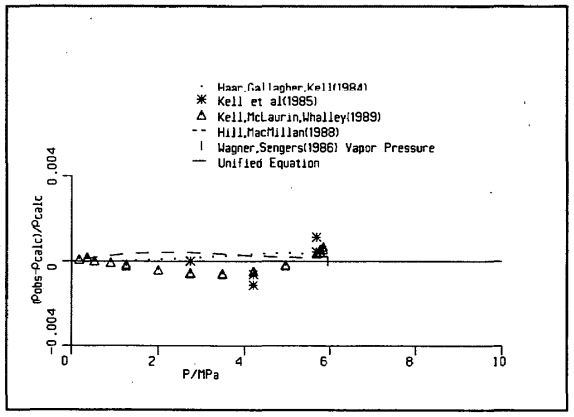

FIG. 52. Vapor density: 275 °C.

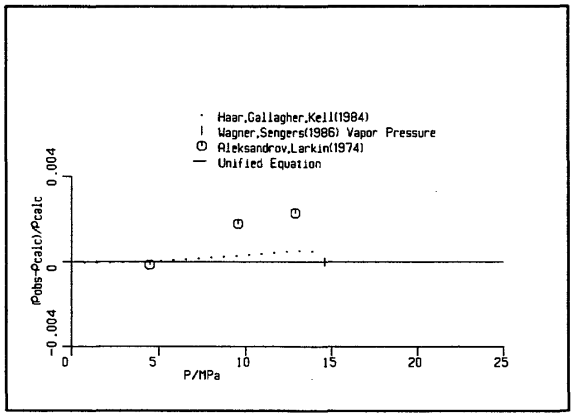

FIG. 55. Vapor density: 340 °C.

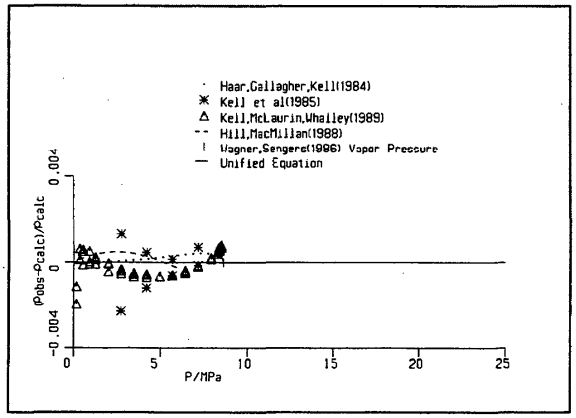

FIG. 53. Vapor density: 300 °C.

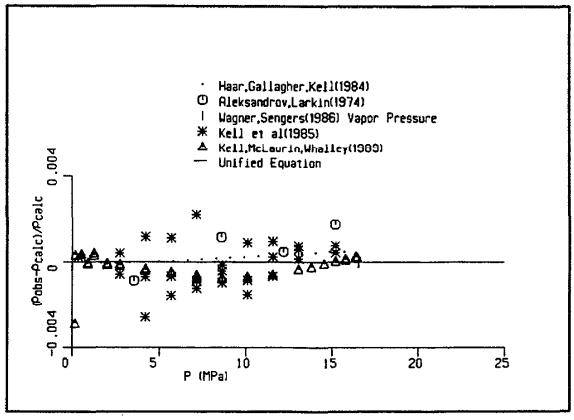

FIG. 56. Vapor density: 350 °C.

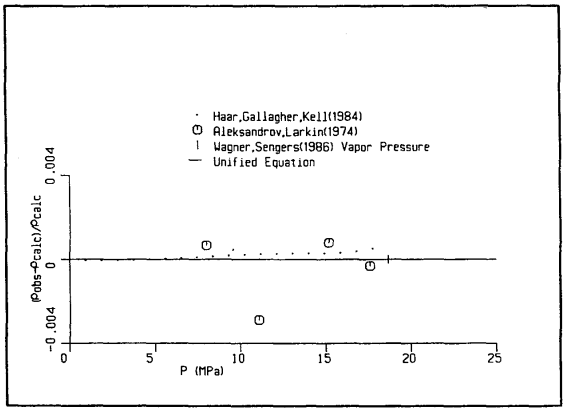

FIG. 57. Vapor density: 360 °C.

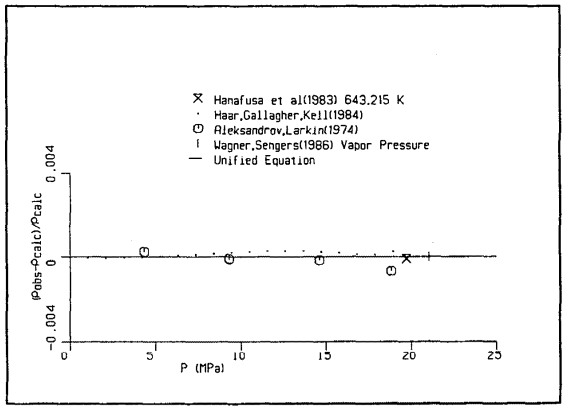

FIG. 58. Vapor density: 370 °C.

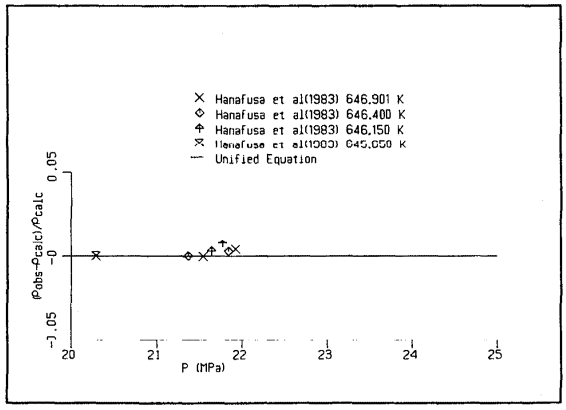

FIG. 59. Vapor density: 373.5 °C.

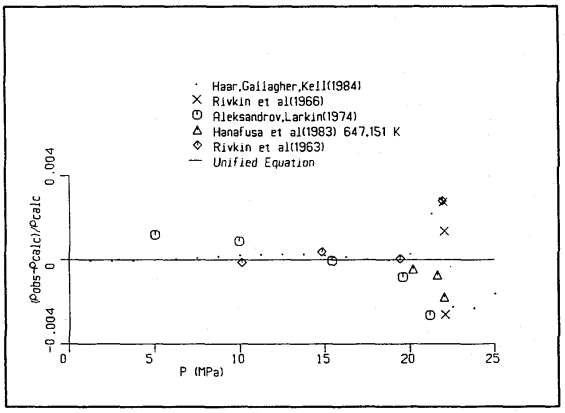

FIG. 60. Vapor density: 374 °C.

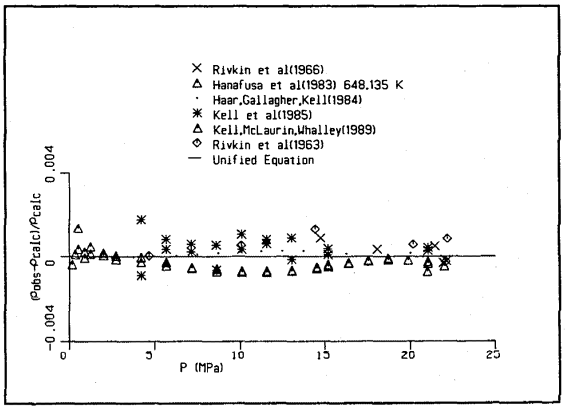

FIG. 61. Vapor density: 375 °C.

tent at higher temperatures, there are substantial discrepancies between data and equation values near the saturation line. The reason for this discrepancy at low temperature could be due to absorption or capillarity effects on the screw thread of the liquid injector so that, at a given pressure and temperature, the "observed" density tends to be higher than the density in the bulk of the vapor.

At the saturation line, even with the aid of the Osborne determinations, the uncertainty in the density of the vapor ranges between about 0.5 and 0.1% [see Wagner and Sengers (1986)]. With this in mind, and allowing for the experimental difficulty of deducing density from PvT measurements near the saturation line at low temperature, it may be said that the available data are well represented by the unified equation.

At 350 °C there are considerable discrepancies between the four experimental data sets displayed in Fig. 56. The unified equation is closely in accord with the mean of these data. Near the critical temperature also there are substantial experimental differences (see Figs. 60 and 61).

For the liquid states there are, in addition to the highly accurate measurements of Kell *et al.*, and Aleksandrov *et al.* which extend to about 100 MPa and have been displayed in Figs. 26 to 44, the high pressure data of Hilbert (1979), Grindley and Lind (1971), Maier and Frank (1966), Koster and Frank (1969) and Zubarev, Prousakov and Barkovski (1977). These generally are of lower accuracy than the Kell and Aleksandrov data sets and their degree of consistency with the latter data sets is shown in Figs. 62–66. In the pressure range up to 100 MPa, the Grindley and Lind densities appear to be too high by at least 100 ppm in the temperature ranges 50–150 °C. The Hilbert data, though not

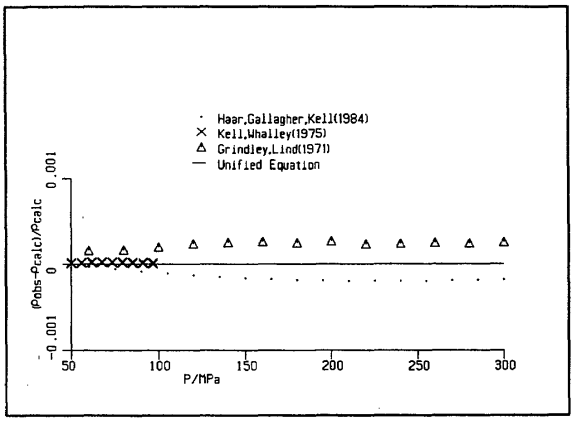

FIG. 64. Liquid density: 150 °C.

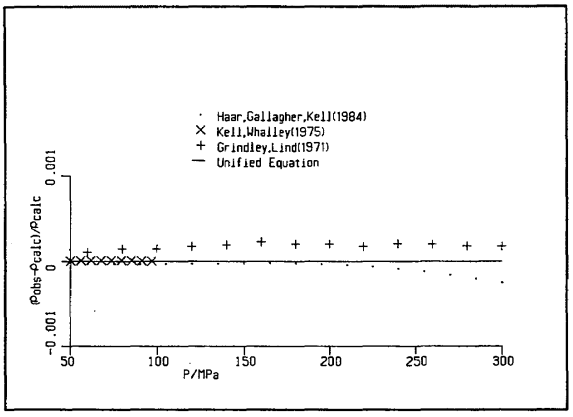

FIG. 62. Liquid density: 50 °C.

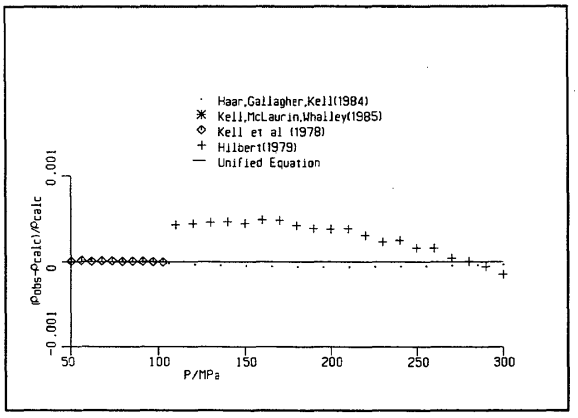

FIG. 65. Liquid density: 200 °C.

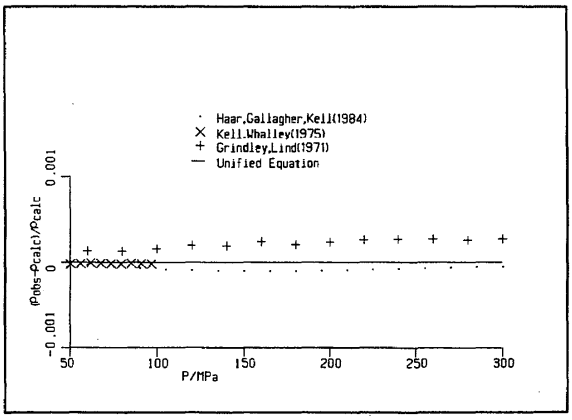

FIG. 63. Liquid density: 100 °C.

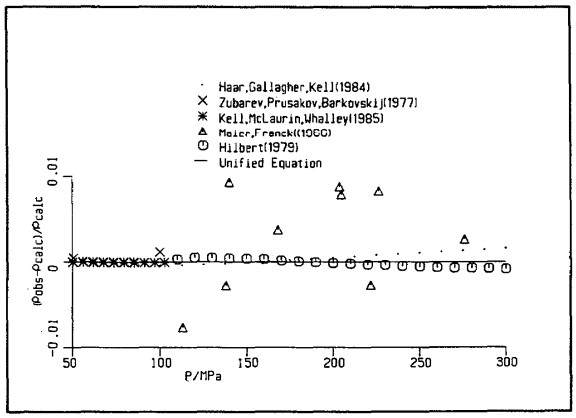

FIG. 66. Density: 400 °C.

overlapping, appear inconsistent with the Kell data in Fig. 65 at 200 °C, and only less so at 400 °C because of the factor of 10 change in the vertical scale. The Zubarov data exhibit considerable scatter. These comparisons in the regions of data overlap are helpful to keep in mind in viewing comparisons of the unified equation with the high pressure data shown in Figs. 67–71. In the high pressure region, principal reliance was placed upon the Hilbert (1979) data in formulating the unified equation.

Comparisons of experimental and calculated densities of water at one atmosphere pressure are shown in Figs. 72–74. Figure 72 concerns subcooled water to − 30 °C and indicates very close agreement with the extrapolation of Kell (1975). This degree of agreement, within 10 ppm, is also shown in Fig. 73, in the range 0–100 °C and in Fig. 74 (100–250 °C).

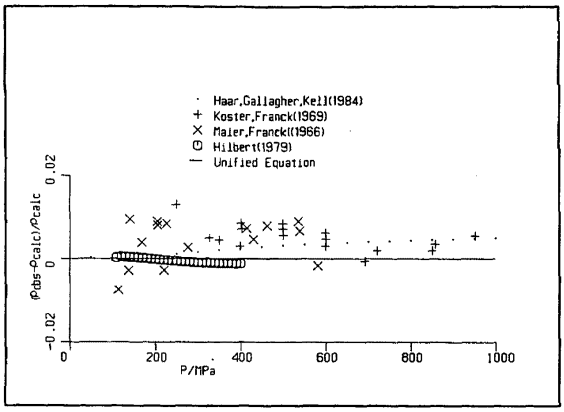

FIG. 69. Density at high pressures: 400 °C.

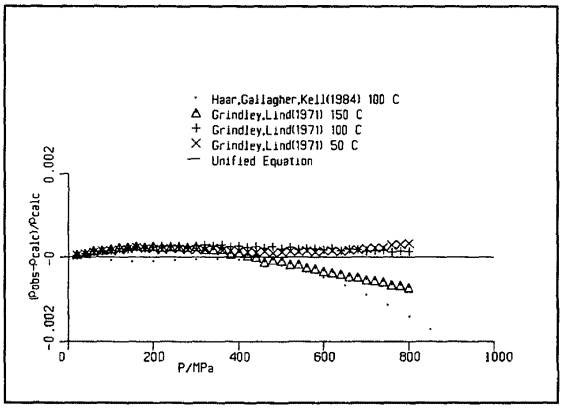

FIG. 67. Density at high pressures: 50–150 °C.

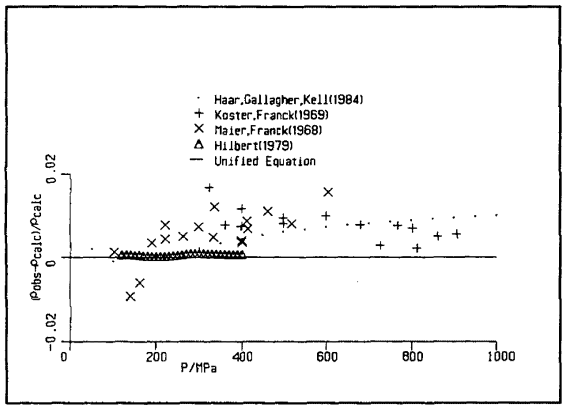

FIG. 70. Density at high pressures: 600 °C.

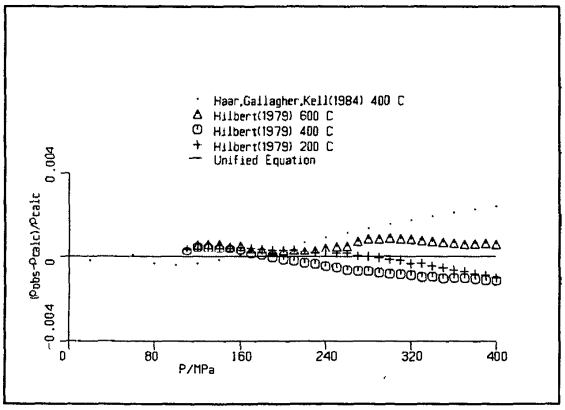

FIG. 68. Density at high pressures: 200–600 °C.

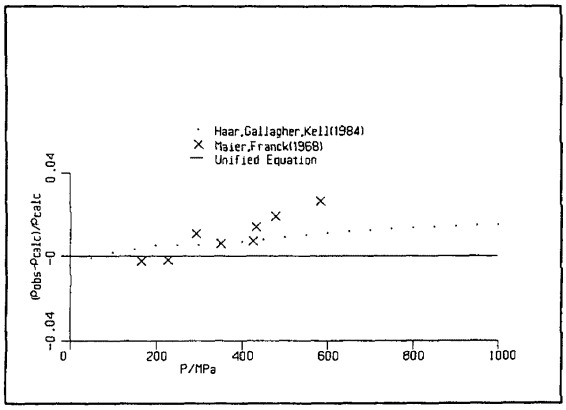

FIG. 71. Density at high pressures: 800 °C.

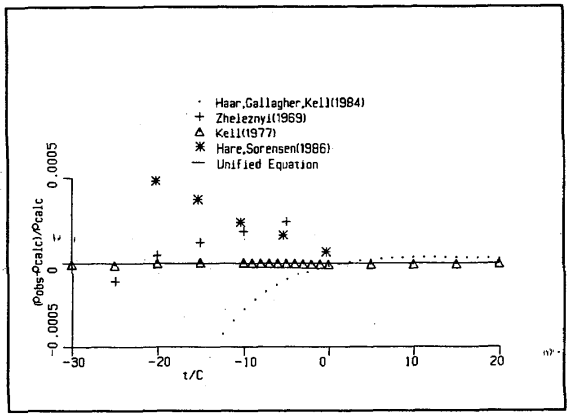

FIG. 72. Supercooled liquid density at 0.1 MPa and − 30 to + 20 °C.

Figures 75–78 contain the results of comparison of density data for the metastable states, with values calculated from the unified equation. The data of Chukanov and Skripov (1971) and Estefeev, Chukanov and Skripov (1977) for both super- and undersaturated vapor states in the range of temperature 178–300 °C are compared with the Kell vapor data discussed earlier by means of a common comparison with density values produced by the unified equation, except for pressures above 10 000 MPa at 175 °C, where the equation differs considerably from the Bridgeman data.

5.3. Pressures

As mentioned earlier, it is appropriate in the vicinity of the critical point where the pressure-density isotherms tend to have very small slope $(\partial P/\partial \rho)_T$, to compare experimental and calculated pressures at a given density. Figures 79

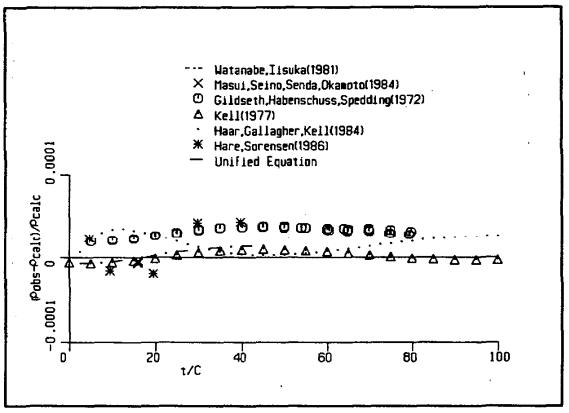

FIG. 73. Liquid density at 0.1 MPa and 0–100 °C.

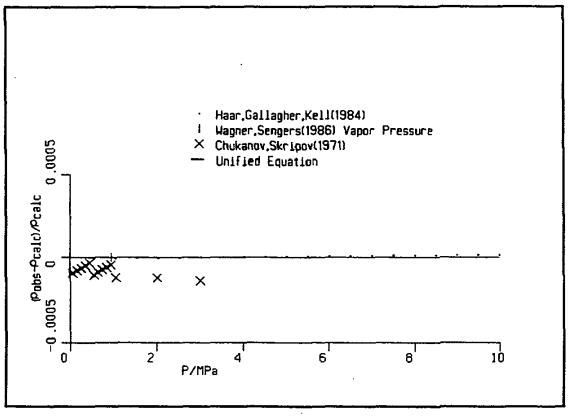

FIG. 75. Supersaturated vapor density: 178.1 °C.

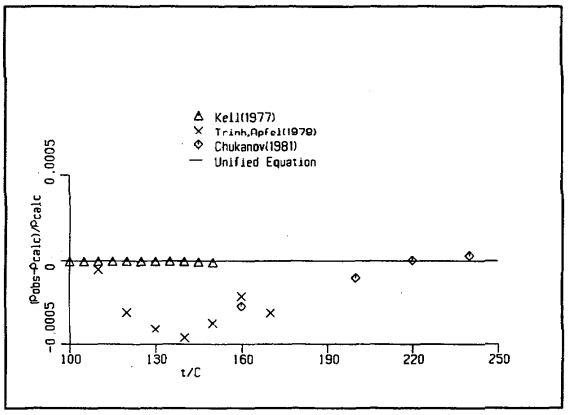

FIG. 74. Superheated vapor at 0.1 MPa and 100–250 °C.

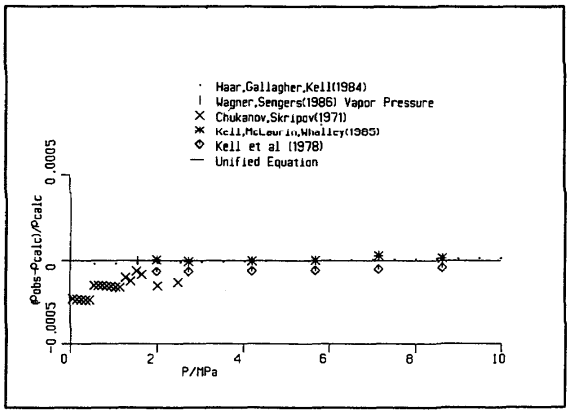

FIG. 76. Supersaturated vapor density: 200.2 °C.

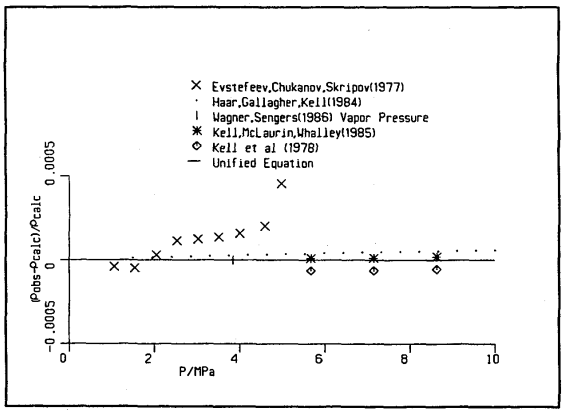

FIG. 77. Supersaturated vapor density: 248.13 °C.

and 80 refer to near-critical isotherms. Though Fig. 79 suggests a systematic difference between the experimental data and the unified equation, Fig. 80 shows considerable experimental uncertainty. At 380 °C the experimental data of Rivkin (1966) and Aleksandrov (1974), as well as the revised and extended scaling equation of Levelt Sengers *et al.*, (1983) are compared with the unified equation in Fig. 81. At densities less than 0.25 or greater than 0.4 kg/dm^3 the scaling equation is beginning to be out of range. At 400 °C (Fig. 82) the density range of validity of the scaling equation is considerably narrowed.

The high pressure data of Bridgeman (1947) have been compared with values calculated from the unified equation. Figures 83–88, for the temperature range 25–175 °C and pressures as high as 3500 MPa, show quite close agreement between the Bridgeman data, which were not used in the fit,

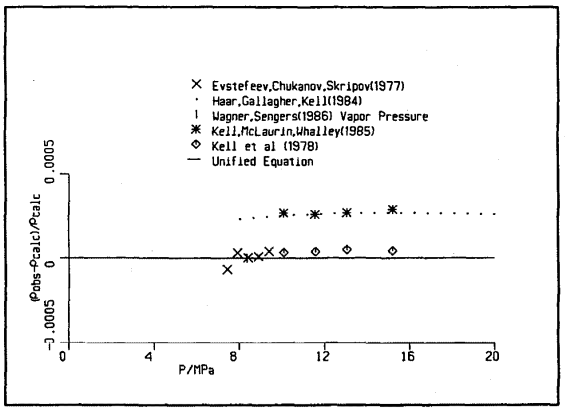

FIG. 78. Supersaturated vapor density: 298.16 °C.

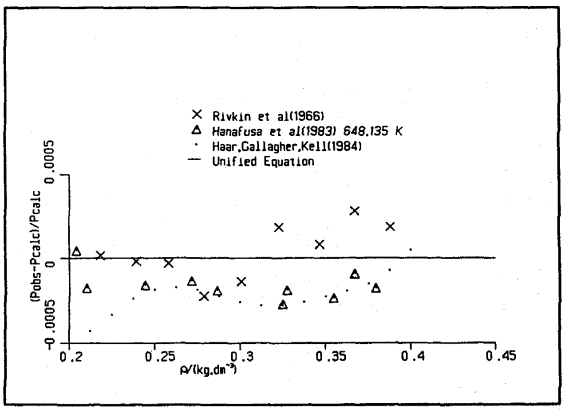

FIG. 80. Pressure: 375 °C.

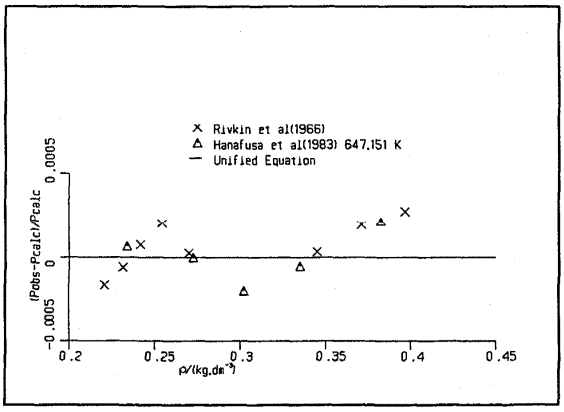

FIG. 79. Pressure: 374 °C.

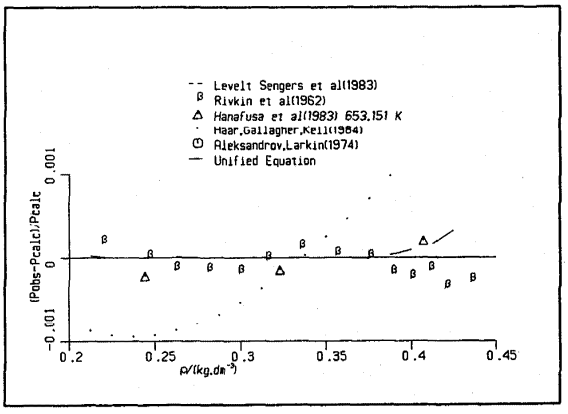

FIG. 81. Pressure: 380 °C.

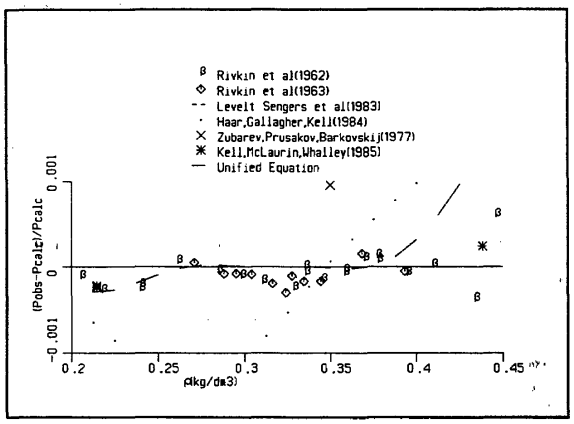

FIG. 82. Pressure: 400 °C.

and the unified equation, except for pressures above 10 000 MPa at 175 °C, where the equation differs considerably from the Bridgeman data.

The determinations of Walsh and Rice (1957), shown for ultra high pressures in Figs. 87–89, are not PvT measurements since the temperature was not measured. The values were derived from shock tube measurements which provided sets of pressure, volume and enthalpy values with the use of the Hugoniot relations and the assumption of a plane shock wave. Walsh and Rice inferred the temperature by use of the identity

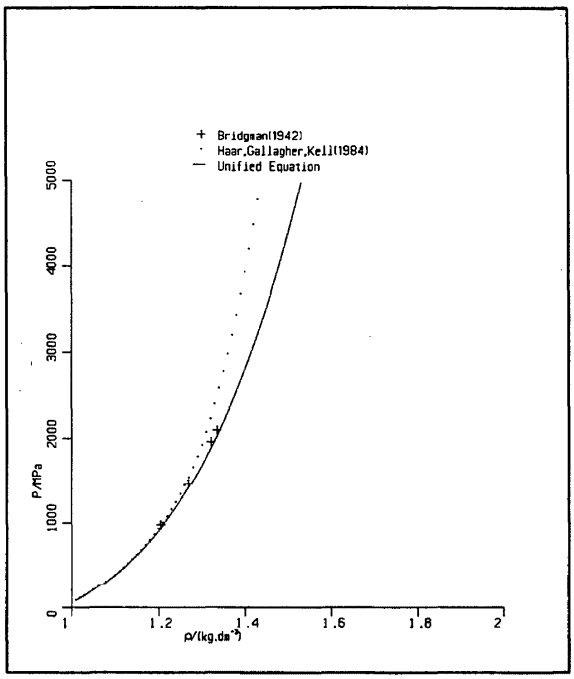

FIG. 84. Ultra high pressure 75 °C.

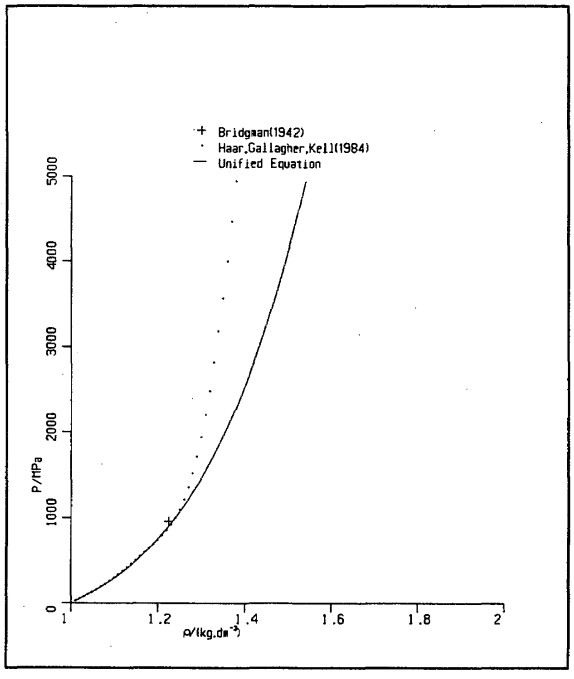

FIG. 83. Ultra high pressure 25 °C.

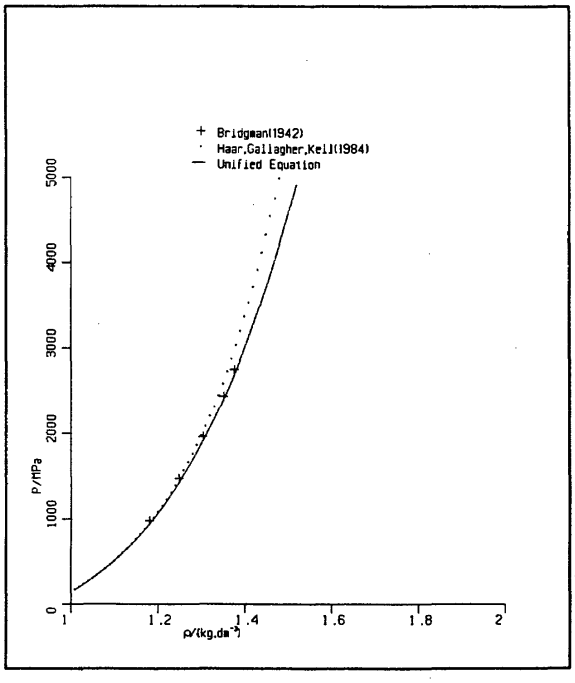

FIG. 85. Ultra high pressure 125 °C.

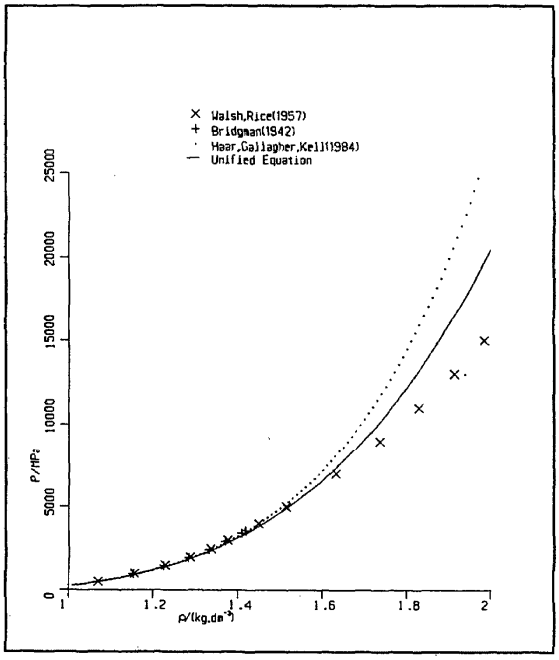

FIG. 86. Ultra high pressure 175 °C (448–15 K).

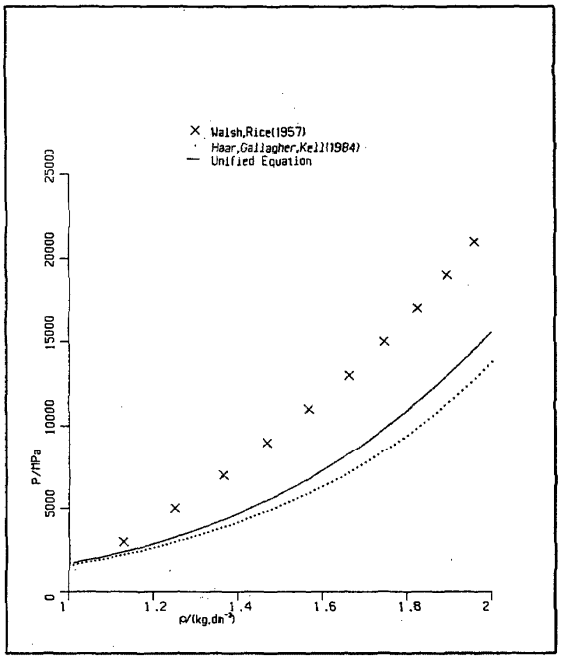

FIG. 88. Ultra high pressure 1000 °C (1273.15 K).

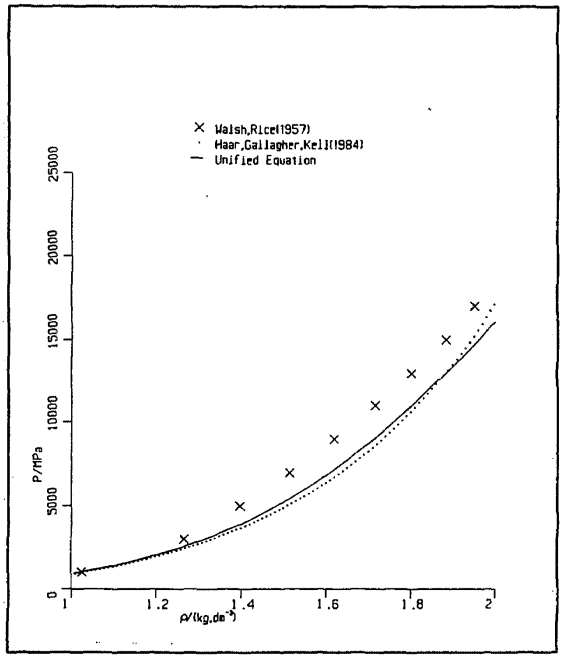

FIG. 87. Ultra high pressure 500 °C (773.15 K).

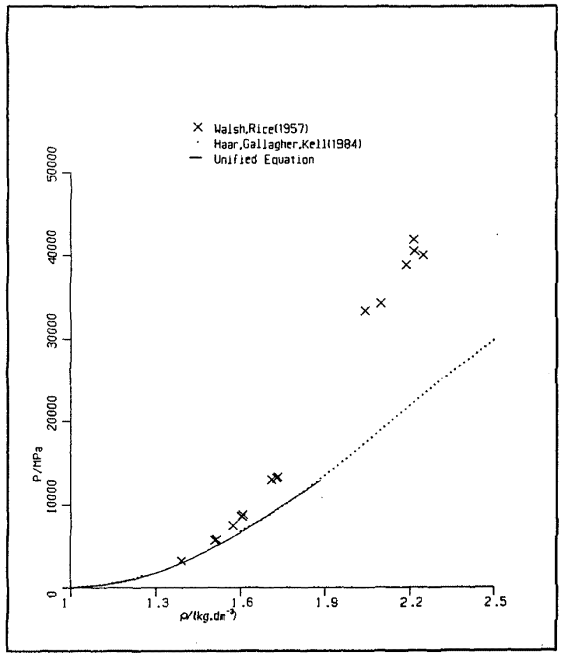

FIG. 89. Ultra high pressure: Hugoniot curve.

$$dT = \frac{1}{C_p}\left[dh - \left\{v - \left(\frac{\partial v}{\partial T}\right)_P\right\}dP\right],$$

to calculate the temperature variation along a process line connecting the series of states for which the values of P, v, and h are known. To do this it is necessary to use estimated values of specific heat C_p and the derivative $(\partial v/\partial T)_P$.

Rice and Walsh performed calculations up to 45 000 MPa and 3147 °C by assuming $(\partial v/\partial T)_P$ independent of temperature and having the same variation with pressure as on the Bridgeman 175 °C isotherm extrapolated as shown in Fig. 90. Thus the determinations of temperature for the Walsh and Rice results shown in Figs. 87–89 are quite uncertain. For still higher pressures (50–80 GPa) Lyzenga, Ahrens, Nellis, and Mitchell (1982) reported direct temperature measurements which suggest that the Walsh and Rice temperatures were a few hundred degrees too high. The Lysenga *et al.*, temperature measurements (3280–5270 K) lie well outside the temperature range of the unified equation.

5.4. Speed of Sound

Figures 91–95 show the results of comparison of abundant speed of sound data available at atmospheric pressure with values obtained from the unified equation. Figure 91 indicates that at lowest temperature, the discrepancy with the data of Petitet, Tufeu, and LeNeindre (1983) for 15 degrees of subcooling exceeds the claimed experimental uncertainty of 0.5%. Generally however, the Petitet *et al.* experimental data, which were not used in the formulation procedure, are in close accord with the unified equation. Figures 95 and 97 also indicate close agreement with the speed of sound data of Aleksandrov and Kochetov (1979) and Aleksandrov and Larkin (1976).

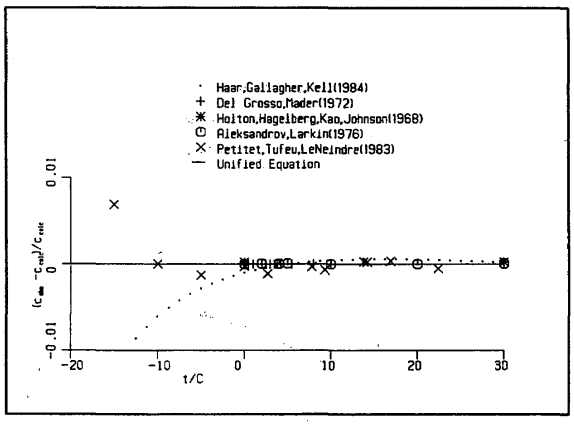

FIG. 91. Speed of sound, supercooled liquid states: 0.1 MPa.

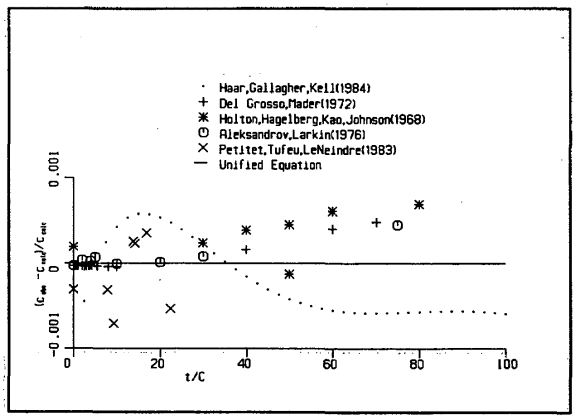

FIG. 92. Speed of sound, liquid: 0.1 MPa.

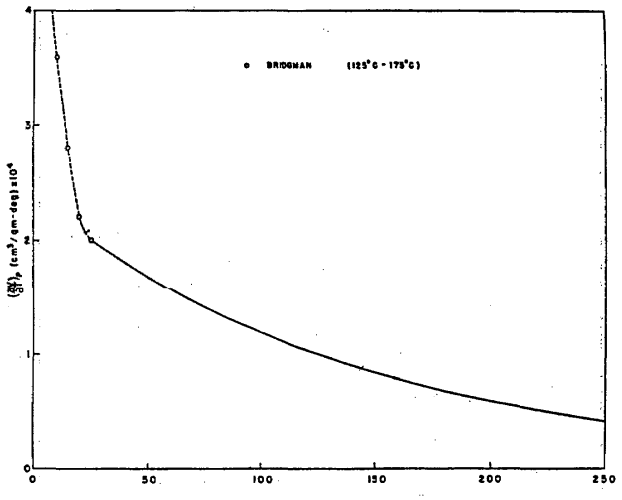

FIG. 90. Walsh and Rice (1958) estimate of $(\partial v/\partial T)_P$. Broken and full lines indicate their interpolations and extrapolations, respectively.

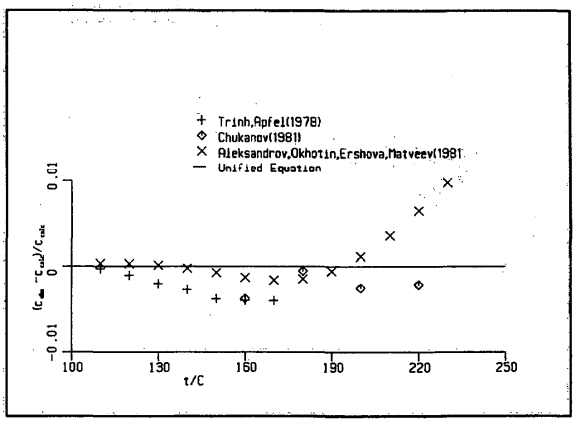

FIG. 93. Speed of sound, vapor: 0.1 MPa superheat.

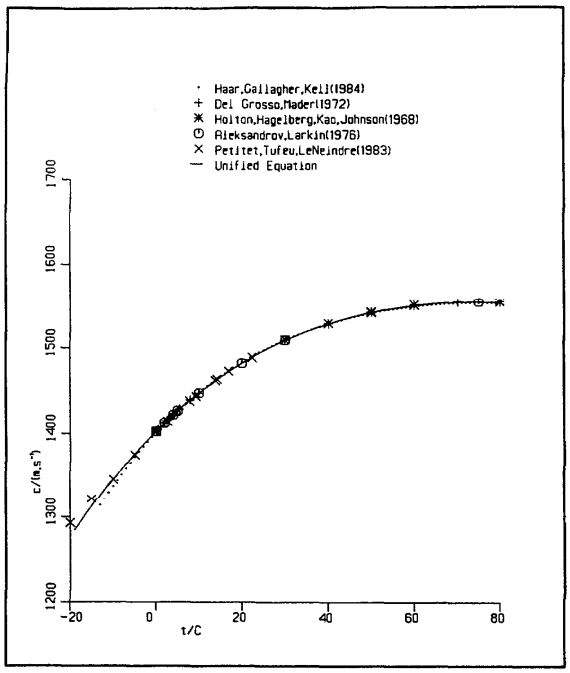

FIG. 94. Speed of sound, supercooled liquid states: 0.1 MPa.

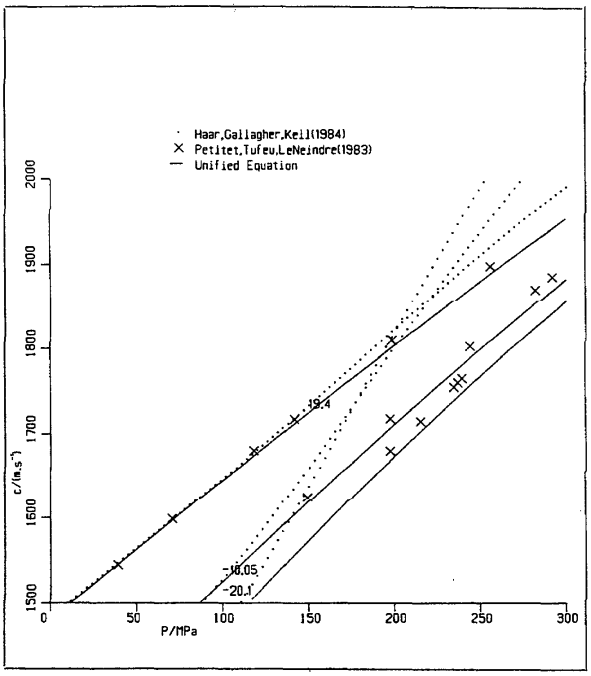

FIG. 96. Speed of sound, supercooled liquid states: − 20 to + 20 °C.

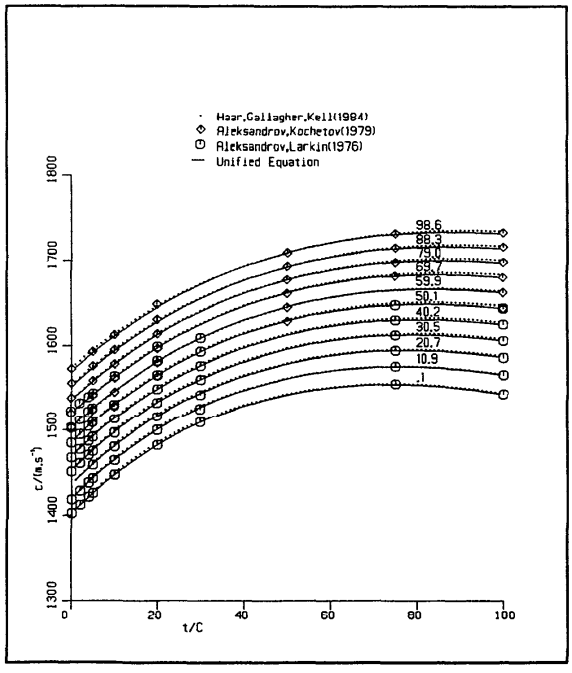

FIG. 95. Speed of sound, liquid: 0.1–100 MPa.

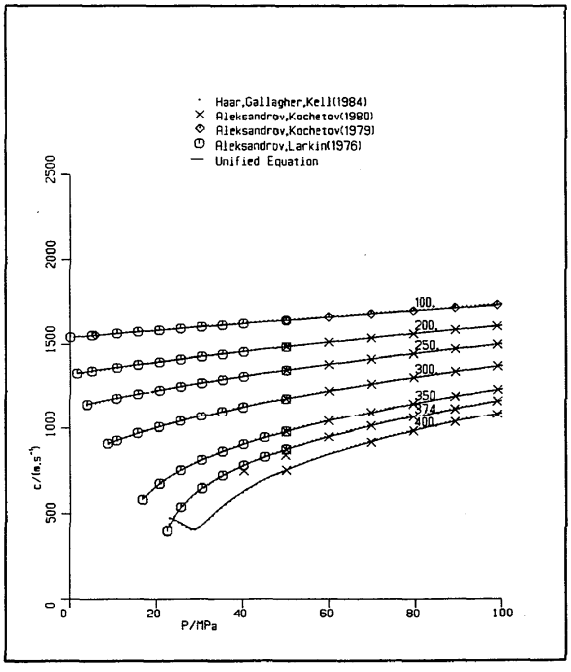

FIG. 97. Speed of sound, liquid: 100–400 °C.

Figure 96 compares the speed of sound data of Petitet *et al.*, at − 20.1, − 10.1, and + 19.4 °C over a wide range of pressure. Figure 97 shows that the values calculated from the unified equation are in good agreement with the Aleksandrov and Larkin (1976) and Aleksandrov and Kochetov (1979) (1980), data on the speed of sound for the pressure range 0–100 MPa and temperature range 100–400 °C. Figure 98 extends the pressure range of comparison to 980 MPa (at low temperature) and 600 or 650 °C for pressures below 300 MPa. Figure 99 compares the critical region speed of sound data of Erokhin, and Kalynov (1980) with values calculated from the unified equation.

Data on speeds of sound in vapor states between 150 °C and 330 °C and from low pressures up to saturation were measured by Novikov and Avdonin (1960) and are compared with values obtained from the unified equation in Fig. 100. Despite close agreement for vapor states, the equation characteristically produces saturation values 0.5% 1% higher than those inferred by Novikov and Avdonin for vapor saturation. Figure 101 indicates however, that crossing the saturation line at 150, 240, and 300 °C, the speed of sound data of Estefeev, Skripov, and Chukanov (1979) are in very close agreement with the values obtained from the unified equation.

Comparisons of both isopiestic specific heat and speed of sound data with the equation are particularly important

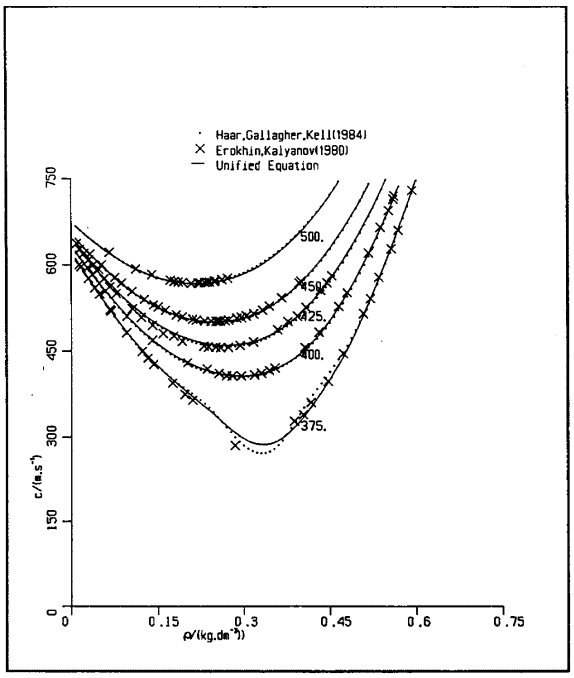

FIG. 99. Speed of sound, supercritical states. 375–500 °C.

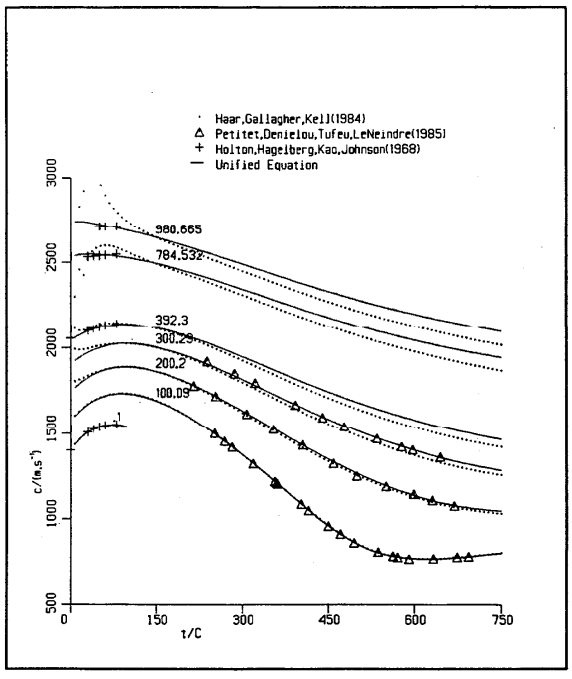

FIG. 98. Speed of sound, liquid: 0.1–1000 (P/MPa).

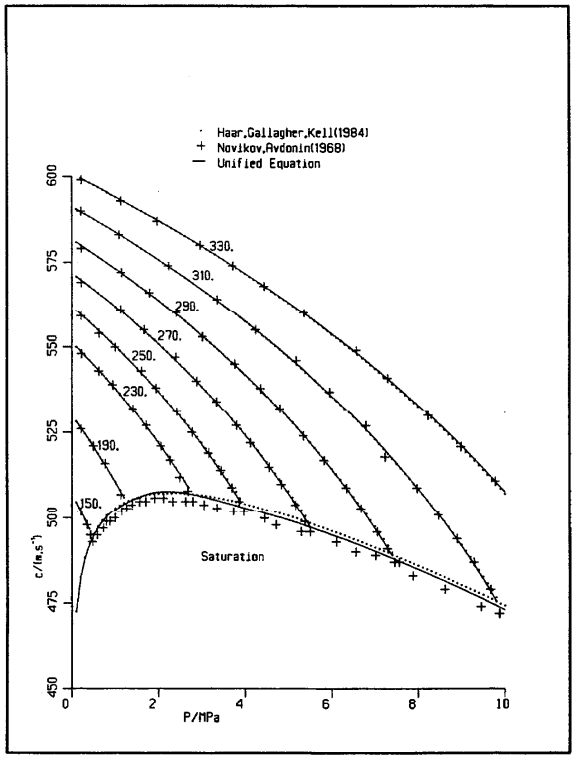

FIG. 100. Speed of sound, vapor: 150–330 °C.

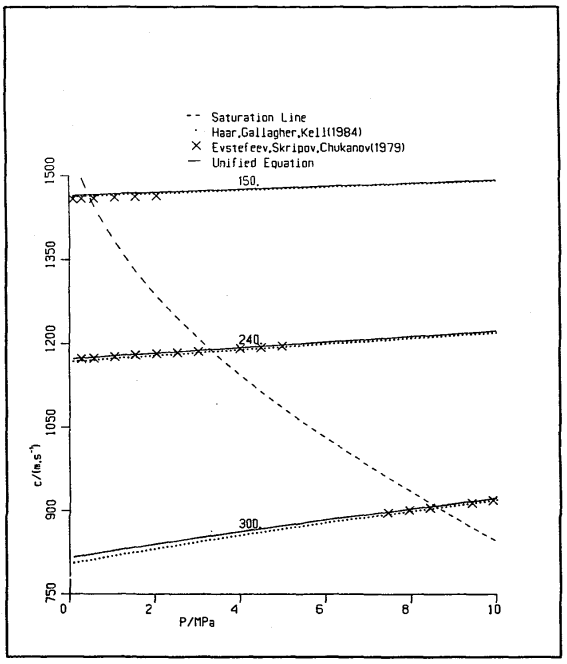

FIG. 101. Speed of sound, metastable liquid states; 150–300 °C.

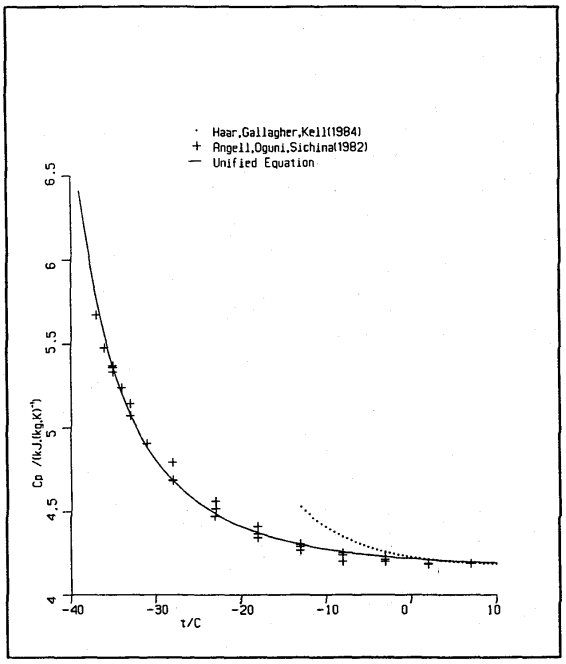

FIG. 102. Isopiestic specific heat C_p supercooled liquid states: 0.1 MPa.

since none of these data were used in the formulation process.

5.5. Isopiestic Specific Heats

Figures 102 and 103 show the one-atmospheric specific heat data of Angell, Oguni and Sichina (1982) for subcooled emulsions and illustrate the rapid increases in C_p as the temperature declines below 20 or 30 °C. The unified equation readily represents this behavior.

With an expanded vertical scale, Fig. 104 compares the C_p data of Sirota, Grishkov and Tomishko (1970) with values produced by the unified equation for temperatures between −3 °C and 45 °C and pressures up to 98 MPa. The degree of agreement, within 0.5%, is within what is believed to be the uncertainty of the data. Figures 105 and 106 show a similar degree of agreement between the data of Phillipi (1987) and the equation for pressures up to 30 MPa and for temperatures up to about 250 °C.

Over a range of pressure from 0.1 to 200 MPa and at low temperatures, Fig. 106 compares the determinations of Alexandrov, Okhotin, and Ershova (1981) with the unified equation. Also shown are the estimates of Terminassian, Pruzan, and Soulard (1981) who used measurements of heat liberation during isothermal compression to determine the isothermal compressibility and the isopiestic specific heat.

Typical comparisons with equation values of the exten-

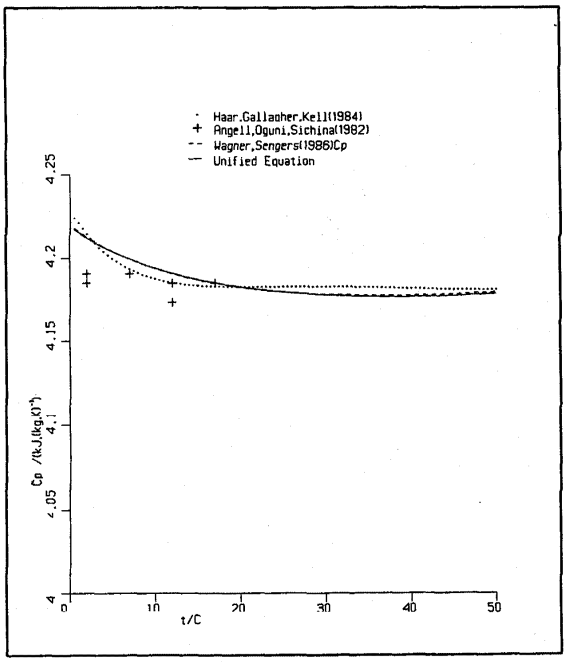

FIG. 103. Isopiestic specific heat C_p, liquid: 0.1 MPa.

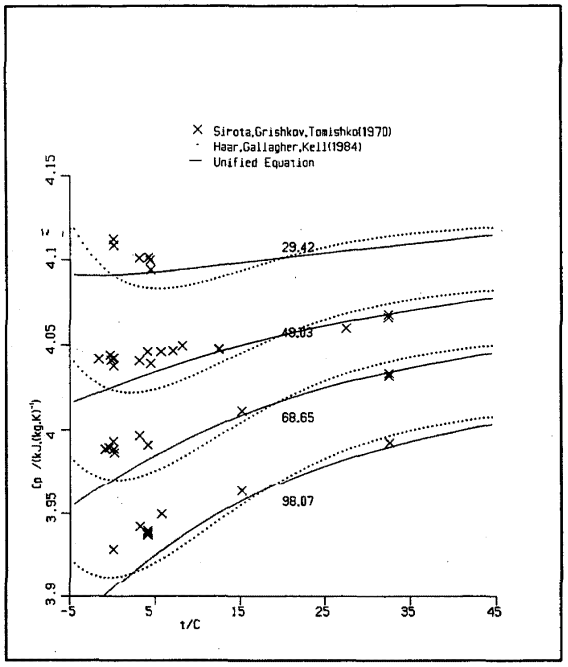

FIG. 104. Isopiestic specific heat C_p, liquid: 30–100 MPa.

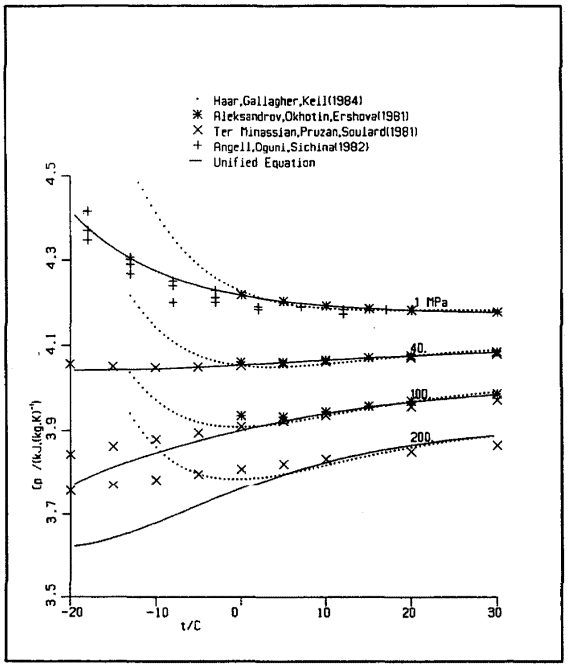

FIG. 106. Isopiestic specific heat C_p, supercooled liquid: 0.1–400 MPa.

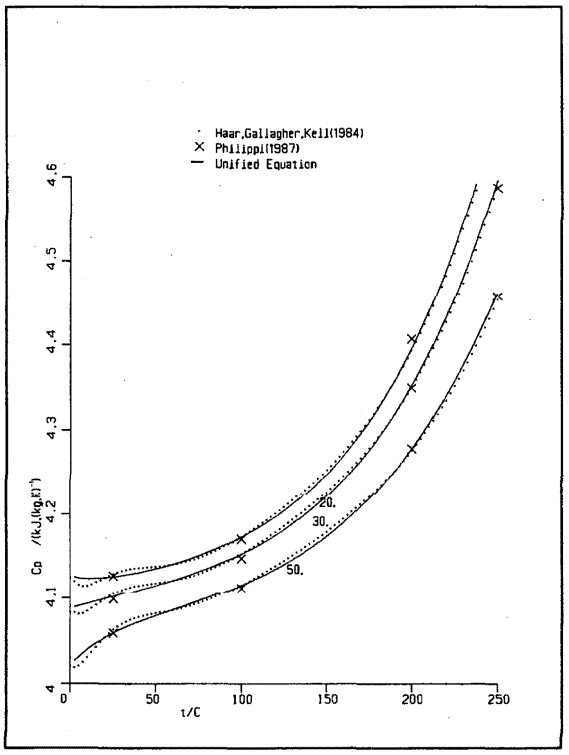

FIG. 105. Liquid Isopiestic specific heat C_p. liquid: 20–50 MPa.

sive specific heat data of Sirota and Timrot (1956), Sirota and Maltsev (1959), (1960), (1962), and (1966), Sirota, Maltsev and Grishkov (1963), and Sirota and Grishkov (1966) are shown in Figs. 107–110. Figures 107 and 108 show liquid and vapor isobars, respectively, approaching the saturation boundary with maximum pressures approaching the critical pressure so that the values of C_p rise steeply to large values. The unified equation very closely represents the experimental data.

Figures 109 and 110 show supercritical isobars of specific heat C_p over a wide range of density with several data sets. Close agreement may be observed though, as the critical point is closely approached with C_p values as high as 500 kJ/kg K, the data of Sirota and Maltsev (1962) appear to differ appreciably from the unified equation.

However, in this region the unified equation agrees very closely with the scaling equation of Levelt–Sengers *et al.* (1983) who closely examined the compatibility of C_p, PvT, and speed of sound data in the critical region. They concluded that differences of the magnitude shown in Fig. 110 would largely disappear if the experimental temperature had been about 0.05 degrees lower than indicated. In 1984, Sirota communicated to those authors his conclusion that the reported experimental temperatures had indeed been about 0.05 degrees too high.

Figure 111 shows the degree of agreement between the unified equation and the data of Phillipi (1987) in the critical region.

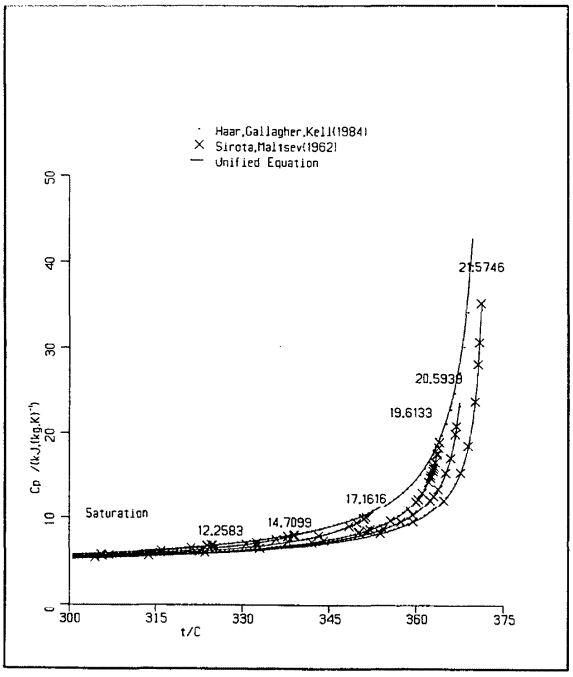

FIG. 107. Isopiestic specific heat C_p, vapor: 12–22 MPa.

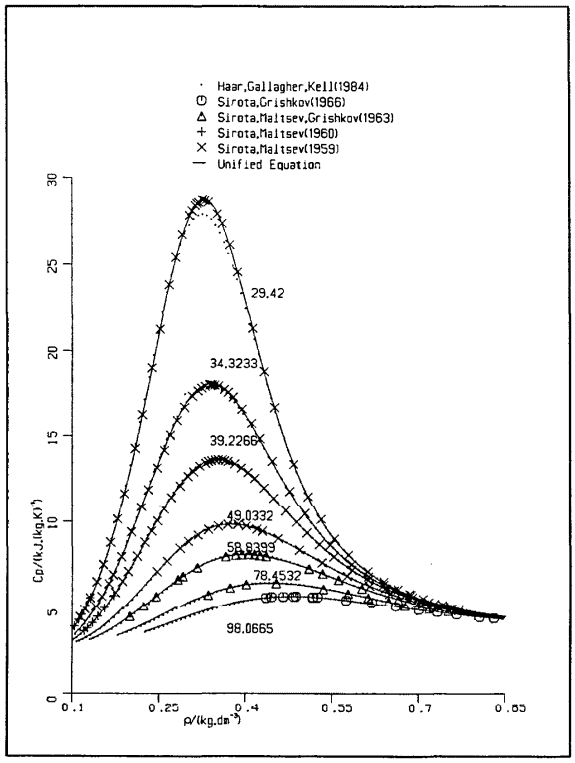

FIG. 109. Isopiestic specific heat C_p: 30–100 MPa.

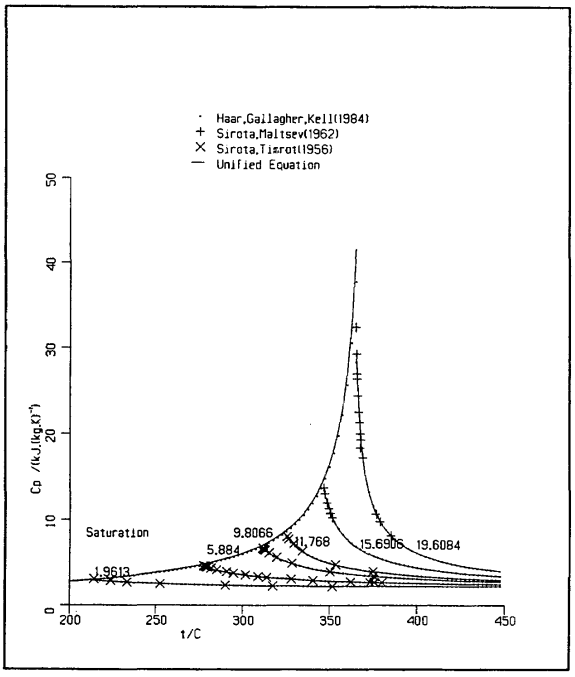

FIG. 108. Isopiestic specific heat C_p, vapor: 2–20 MPa.

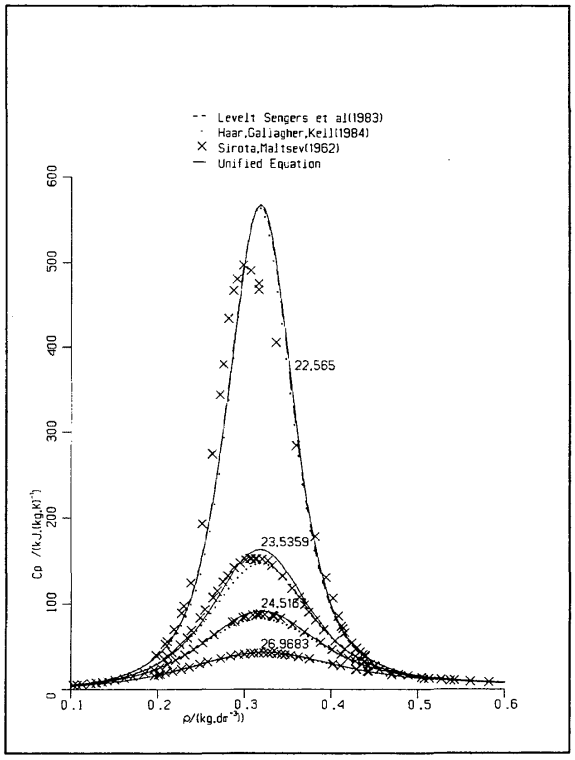

FIG. 110. Isopiestic specific heat C_p: 22–27 MPa.

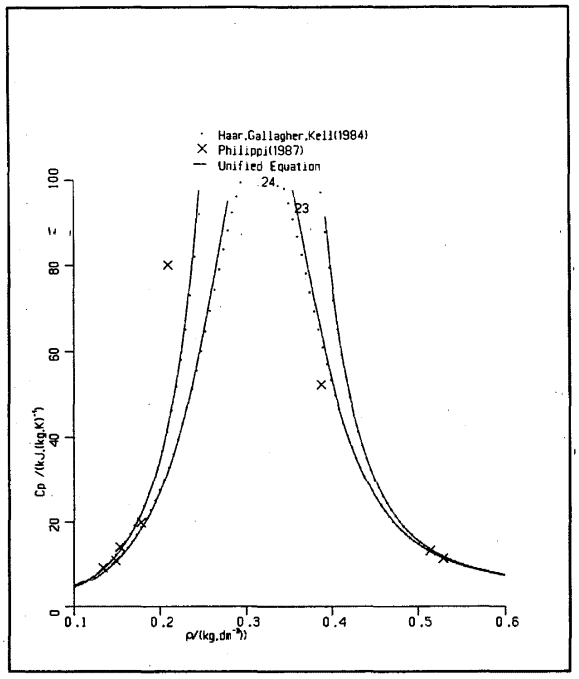

FIG. 111. Isopiestic specific heat C_p: 23–24 MPa.

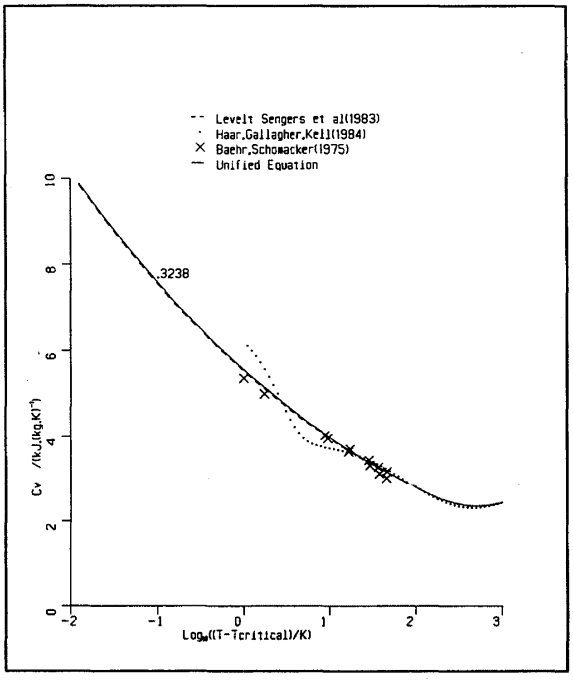

FIG. 112. Isochoric specific heat C_v: 0.3238 Kg dm^{-3}.

5.6. Isochoric Specific Heats

The variation of specific heat C_v with temperature along near-critical isochores is displayed by Figs. 112 and 113 using a log scale on temperature difference to reveal more clearly the behavior very close to the critical temperature. Shown are the data of Baehr and Schomacker (1975) in relation to the unified equation and the revised and extended scaling equation.

Figure 114 compares the isochoric specific heat data of Kerimov and Alieva (1975) with the unified equation for 3 vapor isochores over the temperature range from 250 to 500 °C.

In Fig. 115 the estimates of C_v of Aleksandrov, Okhotin, and Ershova (1981) are compared with values obtained from the unified equation over a range of pressure up to 100 MPa.

5.7. Throttling and Viral Coefficients

For the low pressure vapor, particularly at low temperature the steady flow isenthalpic and isothermal throttling data, $(\partial T/\partial P)_h$ and $(\partial h/\partial P)_T$, provide valuable information which does not require density measurement and directly indicates the difference between ideal and real gas behavior.

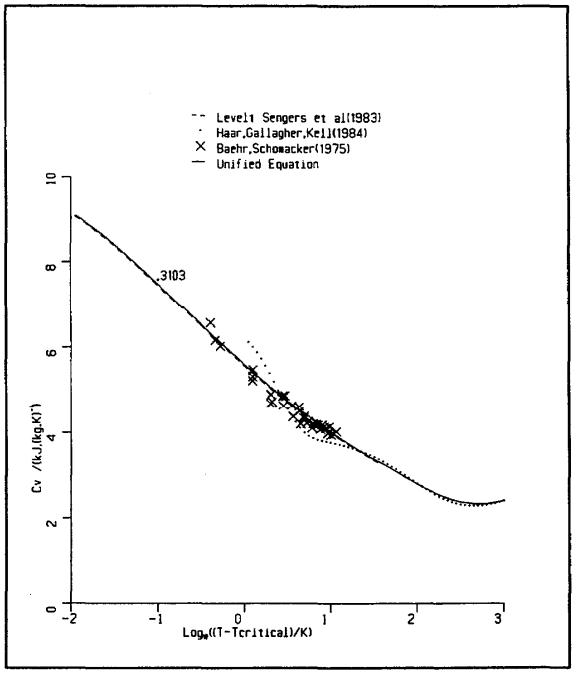

FIG. 113. Isochoric specific heat C_v: 0.3103 kg dm^{-3}.

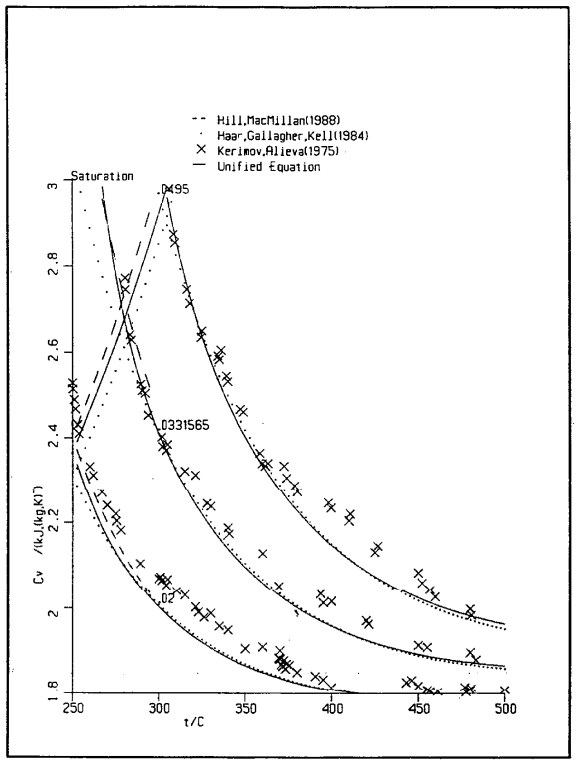

FIG. 114. Isochoric specific heat C_v: vapor isochores kg dm^{-3}.

Figures 116 and 117 show the behavior of the Joule–Thomson coefficient $(\partial T/\partial P)_h$ over a range of temperatures from 128 to 800 °C and from low pressures up to saturation values. The data of Ertle, Grigull, and Straub (1980) are in close agreement with the values obtained from the unified equation. At lower temperatures, down to 70 °C, Fig. 118 shows the data of Wormald (1964) on the variation of the isothermal throttling coefficient $(\partial h/\partial P)_T$ with pressure and temperature, in relation to the values obtained from the unified equation. Figure 119 shows a comparison between the $(\partial h/\partial P)_T$ data of Ertle *et al.*, and values from the unified equation at 350 and 400 °C.

Figure 120 shows close agreement between the measurements of the isentropic derivative $(\partial T/\partial P)_s$ of Rogener and Soll (1980) and the equation values for liquid states varying in temperature from 2.75 to 80 °C and in pressure up to 100 MPa. Figure 121 compares the data of Stasenko, Phillipov, and Blagenravov (1984) on the same coefficient for temperatures between 295 and 495 °C and for pressures up to 20 MPa.

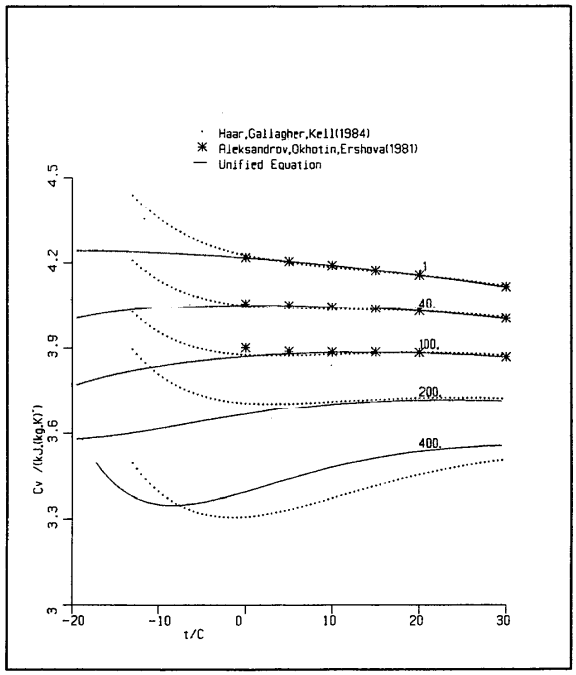

FIG. 115. Isopiestic specific heat C_v, supercooled 0.1–400 MPa.

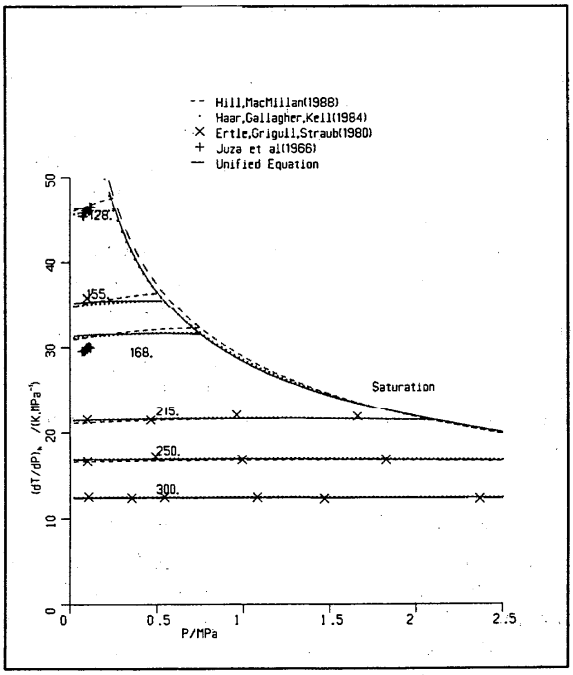

FIG. 116. Joule–Thomson coefficient, vapor: 128–300 °C.

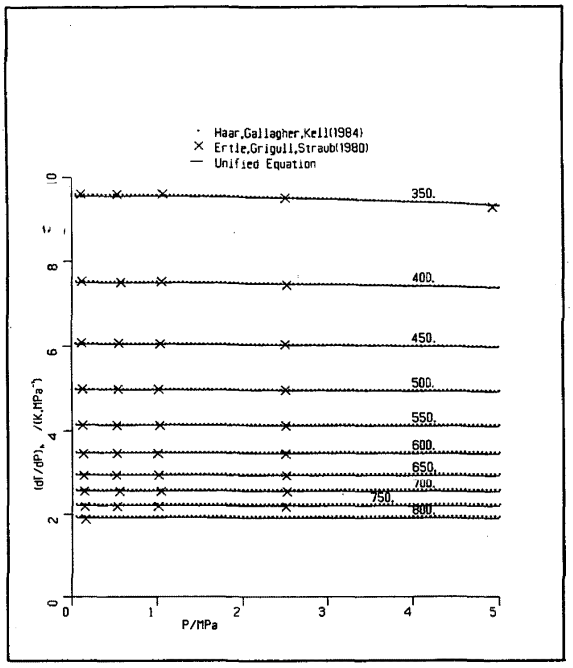

FIG. 117. Joule–Thomson coefficient, vapor: 350–800 °C.

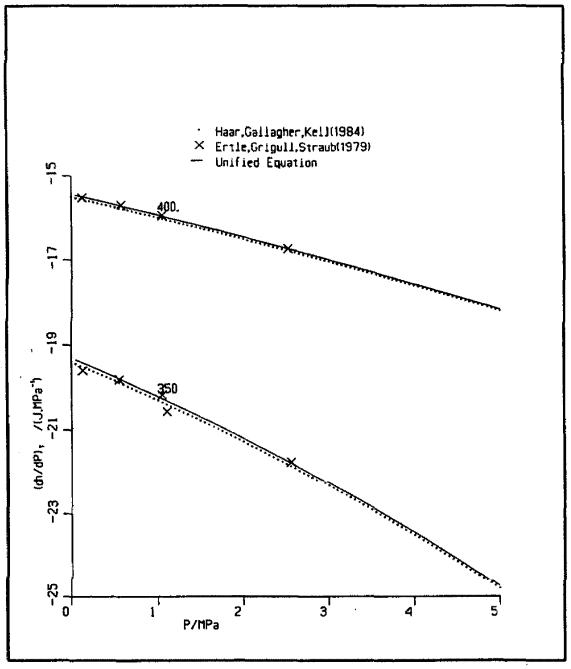

FIG. 119. Isothermal throttling coefficient vapor: 350–400 °C.

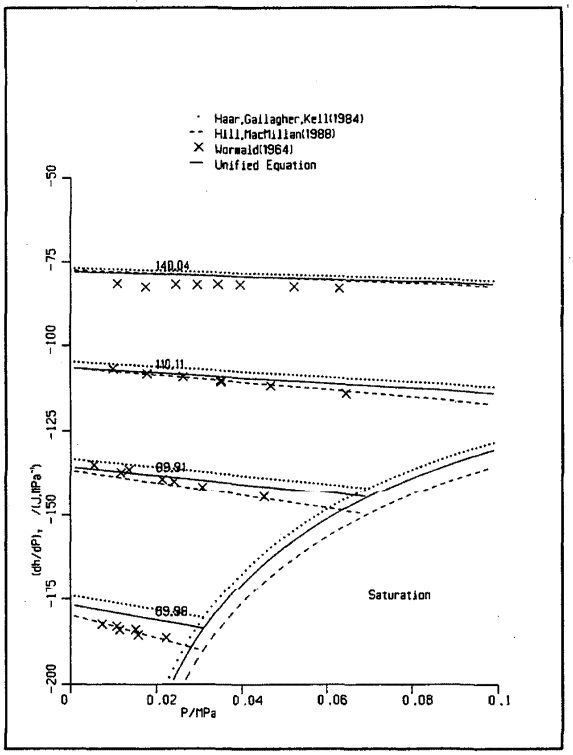

FIG. 118. Isothermal throttling coefficient, vapor: 70–140 °C.

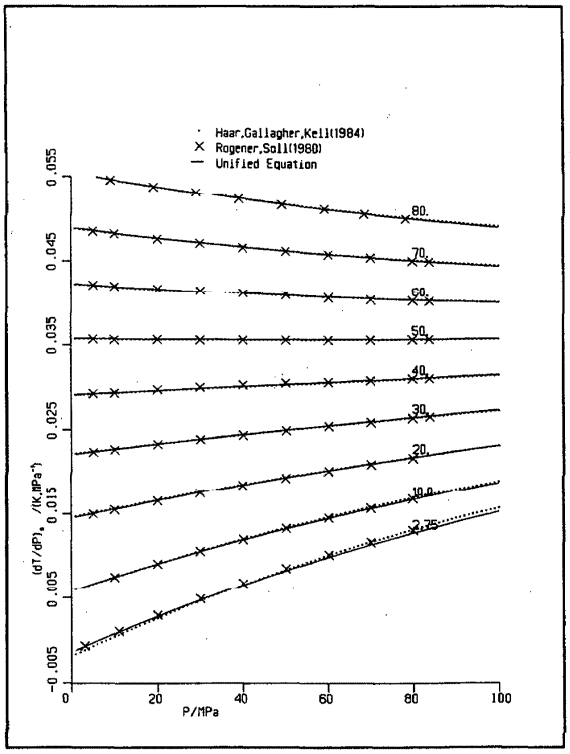

FIG. 120. Isentropic temperature–pressure derivative: 0–80 °C.

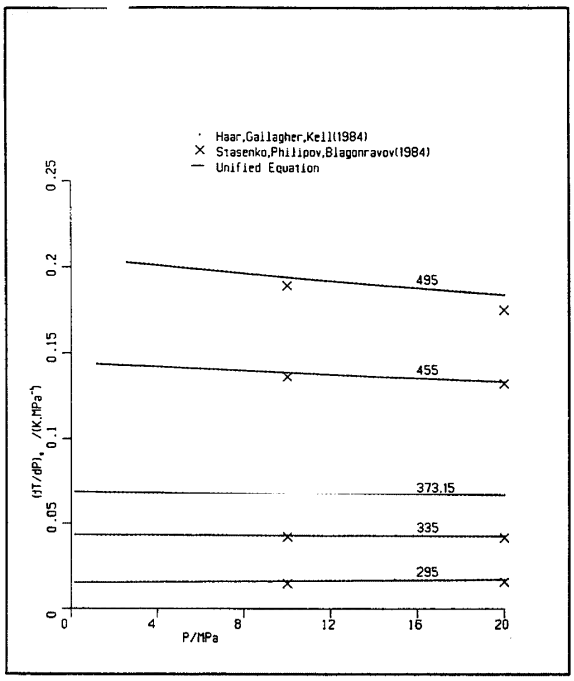

FIG. 121. Isentropic temperature–pressure derivative: 295–495 K.

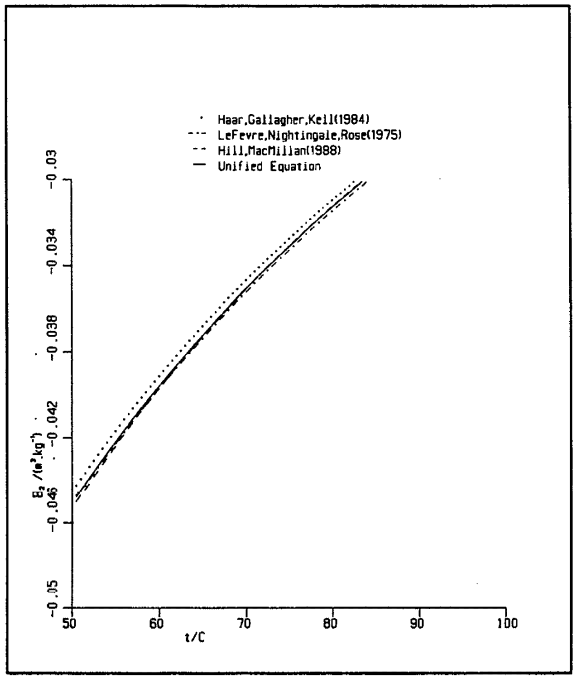

FIG. 122. Second virial coefficient: 50–100 °C.

5.8. Virial Coefficients

Figures 122–124 show a comparison of the second virial coefficient obtained from the unified equation of state with those obtained from the LeFevre, Nightingale and Rose (1975) formulation, and with the data of Kell, McLaurin, and Whalley (1989), which are less accurate at low temperatures. Figure 125 draws a corresponding comparison of experimental and calculated results for the third virial coefficients.

6. The Critical Region Transition

Figure 126 shows contours of the blending function $F(\Delta\rho,\Delta T)$ defined in Eq. (3). The contour $F = 0.5$ may be taken as the mid-point-of the transition between the analytic far field and the revised and extended scaling equations. Because of the structure of the F function, $F = 0$ means exact conformity with the scaling function, and F approaches 0 decisively within a short distance from the critical point e.g., and on the critical isochore at 50° above the critical temperature the value of F is about 0.023; at 75° above it is less than 10^{-8}, at 80 °C less than 10^{-9}.

To show the smoothness of the transition from the far field to the scaling functions, Figs. 127 and 128 show contours of isochoric specific heat in the critical region. Figure 128 shows specific heat contours very close to the critical

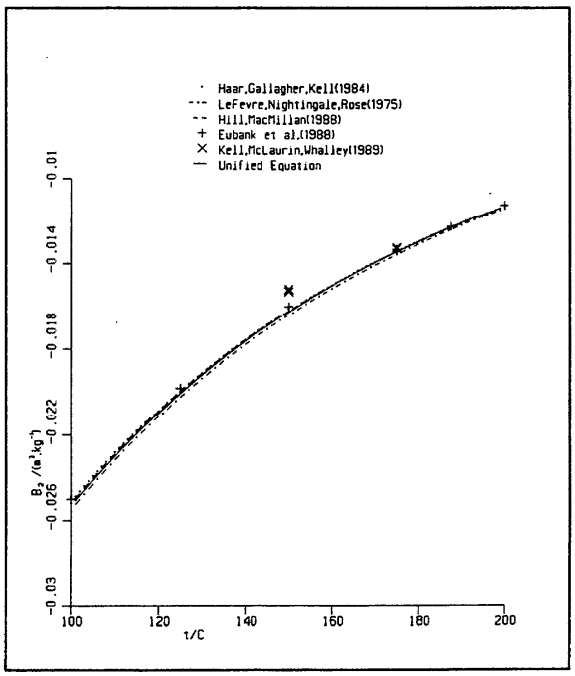

FIG. 123. Second virial coefficient: 100–200 °C.

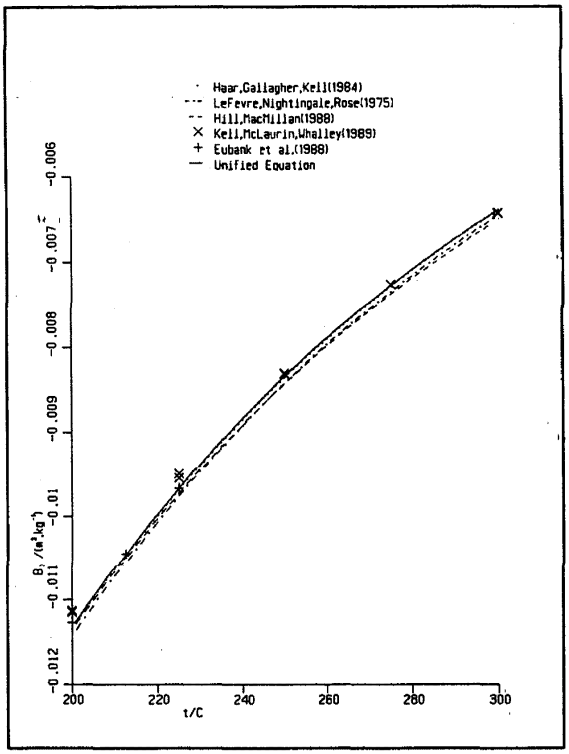

FIG. 124. Second virial coefficient: 200–300 °C.

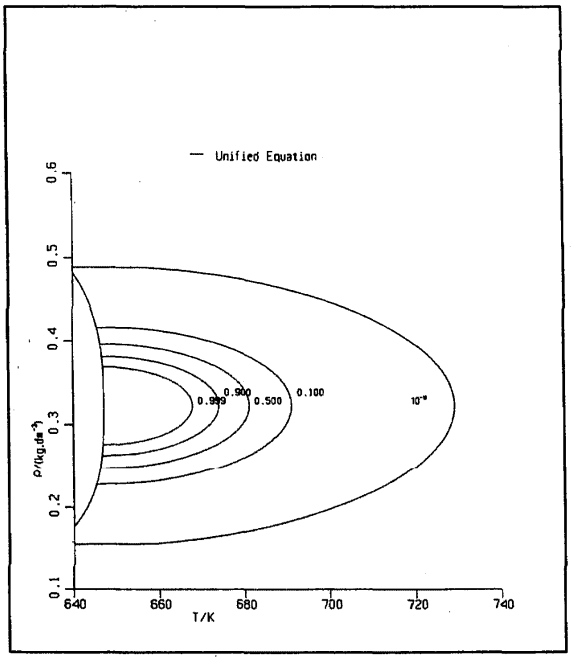

FIG. 126. Blending function F, critical region.

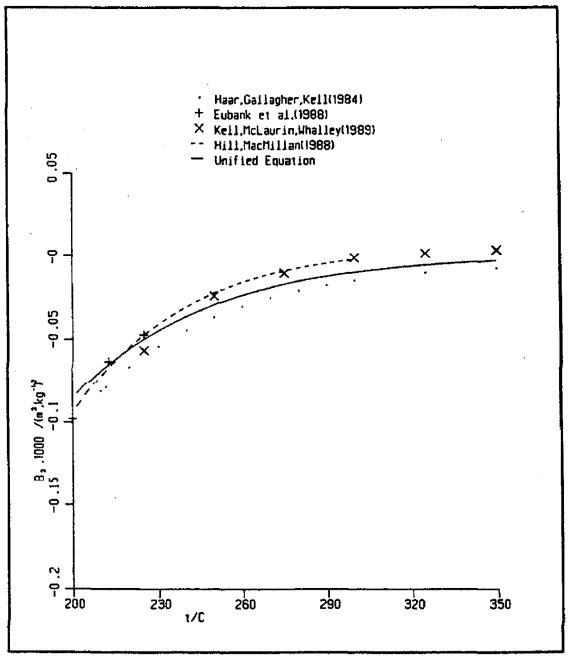

FIG. 125. Third virial coefficient: 200–350 °C.

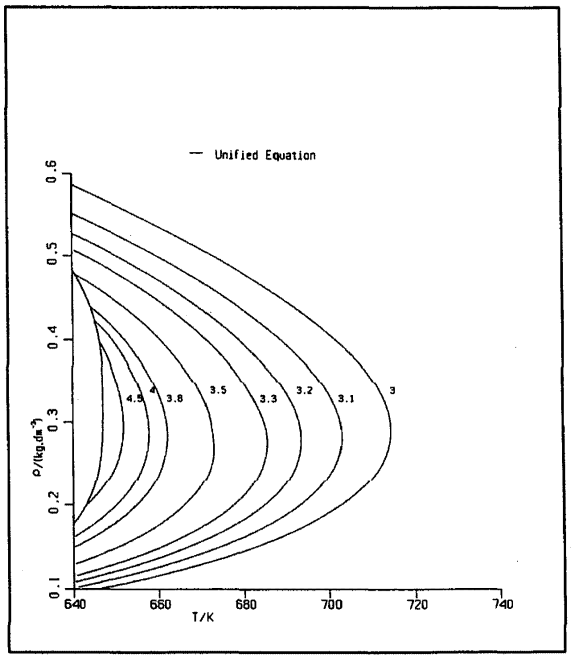

FIG. 127. Isochoric specific heat C_v, critical region.

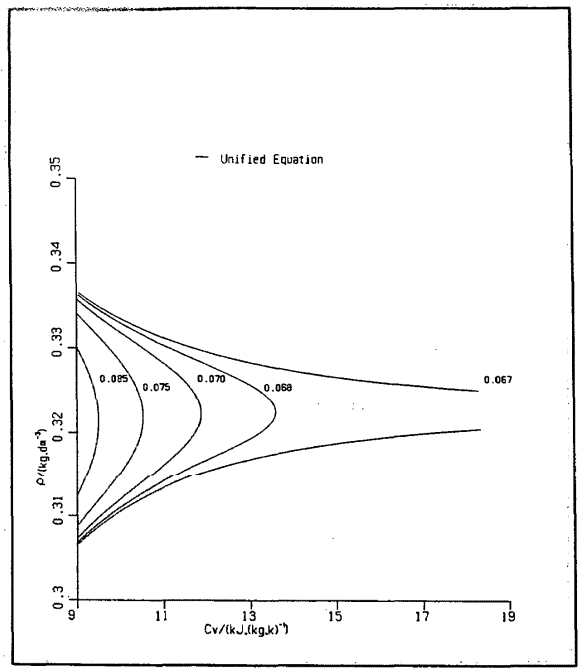

FIG. 128. Isochoric specific heat C_v, critical region.

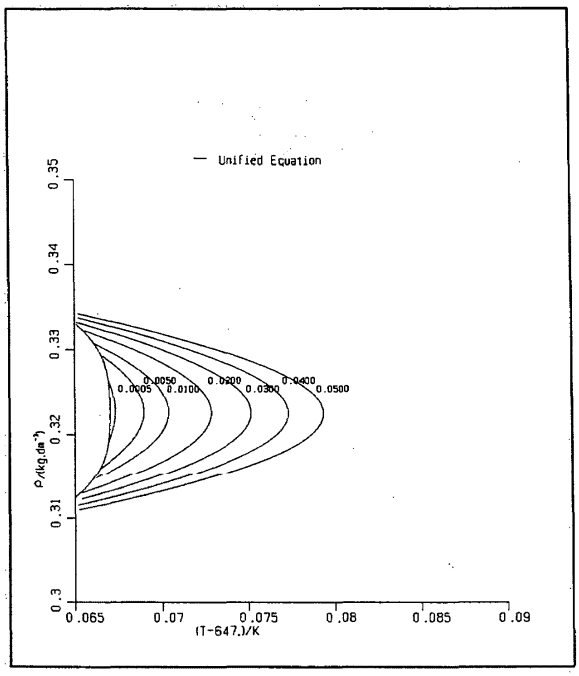

FIG. 130. Inverse isothermal compressibility $[\rho(\partial P/\partial \rho)]$, critical region.

point. At the critical temperature (647.067 K) C_v tends to infinity.

Figures 129 and 130 show corresponding contours in the critical region of the inverse of the isothermal compressibility while Figs. 131 and 132 display speed of sound contours. In all cases these presentations of second derivative quantities show a smooth transition from analytical far-field to singular critical region behavior.

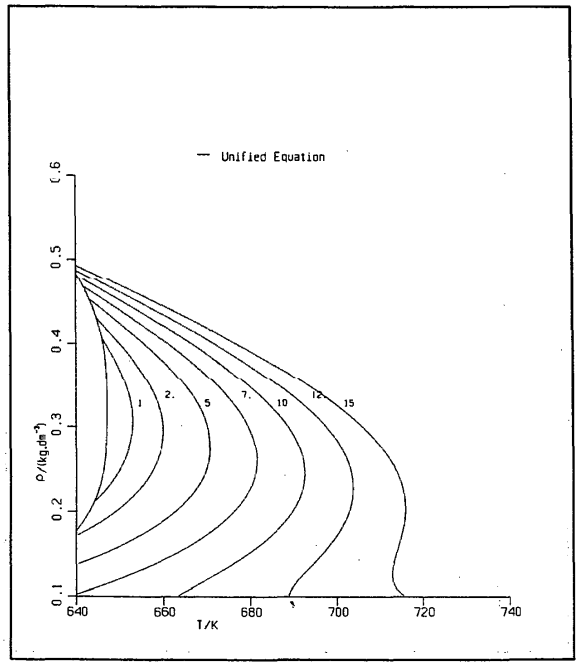

FIG. 129. Inverse isothermal compressibility $[\rho(\partial P/\partial \rho)]$, critical region.

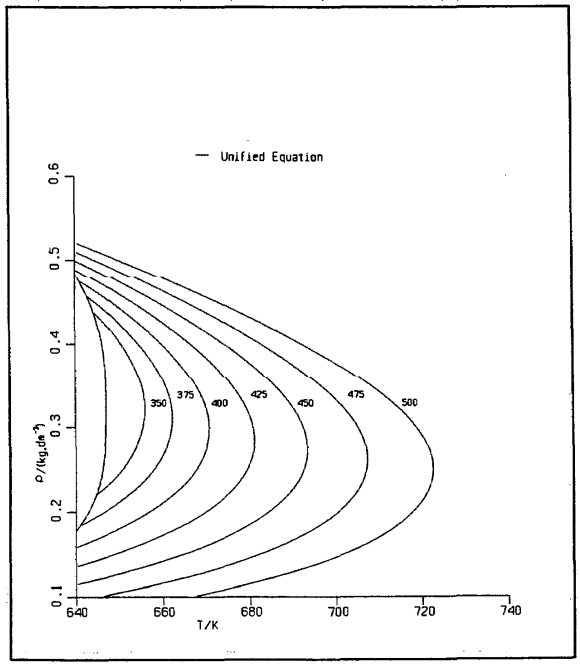

FIG. 131. Speed of sound, critical region.

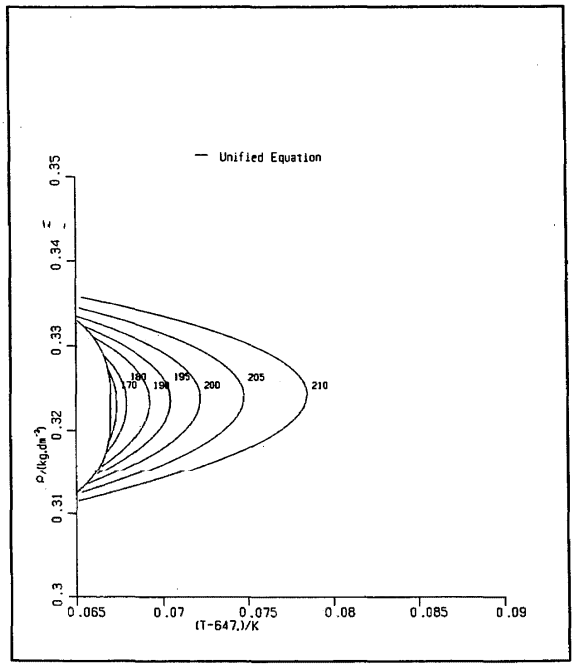

FIG. 132. Speed of sound, critical region.

7. Conclusions

(i) A unified equation of state has been formulated which fully incorporates the singular revised and extended scaling solution of Levelt-Sengers, Kamgar–Parsi, Balfour, and Sengers (valid in a limited region around the critical point and shown to provide a highly accurate representation of all thermodynamic data in that region) with a fully analytic far-field function.

(ii) The transition between far-field and near critical functions is smooth, as shown by the behavior of second-order derivatives of the Helmholtz function in the transition region.

(iii) The unified equation is continuous over all single-phase stable equilibrium states and has been shown to extend to metastable equilibrium (supercooled and supersaturated) states as well.

(iv) Within the data range available (up to about 1000 °C and 1 GPa), the unified equation appears to represent all experimental data on densities or pressure, speeds of sound, specific heats, and throttling and virial coefficients within the experimental uncertainties.

(v) From the range of states within which the unified equation was formulated and tested with abundant experimental data, the unified equation permits regular extrapolation of property estimations to a maximum pressure of about 25 GPa and a maximum temperature of 2000 °C; it does not provide a description of properties of dissociated mixtures of H_2O.

8. Acknowledgments

The author is grateful to the National Science and Engineering Research Council for financial support, and to R.D.C. MacMillan for the graphical comparisons. He would also like to express his appreciation for critical help and encouragement extending over a long period to the late George Kell, and to Lester Haar, Jan and Anneke Sengers, Wolfgang Wagner, Haruki Sato and the members of Working Group A of the International Association for the Properties of Steam.

9. References

Aleksandrov, A. A. and A. I. Kochetov, "The Experimental Determination of Ultrasonic Velocity in Water at Temperatures 266–423 K and at Pressures up to 100 MPa," Teploenergetika **26**, 65 (1979).

Aleksandrov, A. A. and A. I. Kochetov, "The Investigation of Sound Velocity in Water at High Pressures," in *Water and Steam*, edited by J. Straub and K. Scheffler (Pergamon, Oxford, 1980), p. 221.

Aleksandrov, A. A. and D. K. Larkin, "An Investigation of the Specific Volumes of Water at Near-Critical Temperatures and Pressures up to 1000 bar," Teploenergetika **21**, 80 (1974).

Aleksandrov, A. A. and D. K. Larkin, "An Experimental Determination of Ultrasonic Velocity in Water in a Wide Range of Temperature and Pressures," Teploenergetika **23**, 75 (1976).

Aleksandrov, A. A., V. S. Okhotin, and A. Z. Ershova, "Calculation of the Thermodynamic Properties of Water based on Data on the Velocity of Sound," Teploenergetika **28**, 74 (1981).

Aleksandrov, A. A., V. Okhotin, Z. Ershova, and A. Matveev, Izu. Vuzov. Energetika **7**, 120 (1981).

Angell, C. A., M. Oguni, and W. J. Sichina, "Heat Capacity of Water at Extremes of Supercooling and Superheating," J. Phys. Chem. **86**, 998 (1982).

Angus, S., B. Armstrong and K. M. de Reuck, "Carbon Dioxide—International Thermodynamic Table of the Fluid State—3," International Union of Pure and Applied Chemistry (Pergamon, Oxford, 1973).

Angus, S. and D. M. Newitt, "The Measurements of the Specific Enthalpy of Steam at Pressures of 60 to 1000 bar Temperatures of 400 to 700 °C," Phil. Trans. Roy. Soc. (London) **259A**, 107 (1966).

Baehr, H. D. and H. Schomacker, "Messungen der spezifischen isochoren Warmekapazitat in der Umgebung des kritishen Zustands von Wasser," Forsch. Ing.—Wes. **41**, 43 (1975).

Bridgeman, O. C. and E. W. Aldrich, "Vapour Pressure Tables for Water," Trans. ASME J. Heat Transfer **86**, 279 (1964).

Bridgeman, O. C. and E. W. Aldrich, "A Reappraisal of the Critical Constants for Water," ASME J. Heat Transfer **87**, 266 (1965).

Bridgeman, P. W., "Freezing Parameters and Compressions of Twenty-one Substances to 50,000 kg/cm^2," Proc. Am. Acad. Arts Sci. **74**, 399 (1942).

Chapela, G. A. and J. S. Rowlinson, "Accurate Representation of Thermodynamic Properties near the Critical Point," J. Chem. Soc. Faraday I **70**, 584 (1974).

Chukanov, V. N., "Properties of Metastable (Superheated) Water," Proc. 8th Symposium Thermo. Prop. Vol. II, 334 (1981).

Chukanov, V. N., and V. P. Skripov, "Specific Volumes of Severely Superheated Water," Teplo. Vys. Temp. **9**, 739 (1971).

Cooper, J. R., "Expressions for the Thermodynamic Properties of Water in the ideal-gas limit," Int. J. Thermophys. **3**, 35 (1982).

Davis, H. N. and J. H. Keenan, World. Eng. Cong. Rept. No. 455, Tokyo (1929).

Del Grosso, V. A. and C. W. Mader, "Speed of Sound in Pure Water," J. Acoust. Soc. Amer. **52**, 1442 (1972).

Egerton, A., and G. S. Callendar, "An Experimental Study of the Enthalpy of Steam," Phil. Trans. Roy. Soc. (London) **252**, 133 (1960).

Erokhin, H. F. and B. E. Kal'yanov, "Experimental Behavior of Ultrasonic Velocity and Some Other Quantities in the Super Critical Region of Water," Teploenergetika, **27**, 50 (1980).

Ertle, S., U. Grigull, and J. Straub, "Adiabatic and Isothermal Joule-Thomson Coefficients," in *Water and Steam*, edited by J. Straub and K. Scheffler, Pergamon, Oxford (1980), p. 191.

Eubank, P. T., L. L. Joffrion, M. R. Patel, and W. Warowny, "Experimental densities and Virial Coefficients for Steam from 348 to 498 K with correction by absorption effects," J. Chem. Thermodynamics, **20**, 1009 (1988).

Evstefeev, V. N., V. N. Chukanov, and V. P. Skripov, "Specific Volumes of Superheated Water," Teplo. Vys. Temp. **15**, 659 (1977).

Evstefeev, V. N., V. P. Skripov, and V. N. Chukanov, "Experimental Determination of the Speed of Ultrasound in Superheated Ordinary and Heavy Water," Teplo, Vys. Temp. **17**, 299 (1979).

Fine, R. A. and F. J. Millero, "Compressibility of Water as a Function of Temperature and Pressure," J. Chem. Phys. **59**, 5529 (1973).

Friedman, A. S. and L. Haar, "High Speed Computation of Ideal Gas Thermodynamic Functions," J. Chem. Phys. **22**, 2051–2058 (1954).

Gildseth, W., A. Habenschuss, and F. H. Spedding, "Precision Measurements of Densities and Thermal Dilation of Water Between 5 and 80 °C," J. Chem. Eng. Data **17**, 402 (1972).

Goff, J. and S. Gratch, "Low Pressure Properties of Water from − 160 to 212 °F," Trans. A.S.H.V.E. **51**, 125 (1945).

Grigor'ev, B. A., R. M. Murdaev, and Y. L. Rastorguev, "Experimental Investigation of the P-V-T Relation for Water," Teplo, Vys. Temp. **12**, 83 (1974).

Grindley, T., and J. E. Lind, Jr., "PVT Properties of Water and Mercury," J. Chem. Phys. **54**, 3983 (1971).

Guildner, L. A., D. P. Johnson, and F. E. Jones, "Vapor Pressure of Water at its Triple Point," Science **191**, 1267 (1976).

Haar, L., Report to IAPS WGI, Supplementary Information to the HGK Thermodynamic Surface, 1981. (Available from H. J. White, Secretary, International Association for the Properties of Steam, National Bureau of Standards, Washington, D. C.).

Haar, L., J. S. Gallagher, and G. S. Kell, NBS/NRC Steam Tables, Hemisphere, Washington, D.C. (1984).

Hanafusa, H., T. Tsuchida, M. Araki, H. Sato, M. Uematsu, and K. Wanatabe, *Volumetric Properties of Water in the Critical Region, High Temp–High Press*, Vol. 15, p. 311 (1983).

Hare, D. E., and C. M. Sorensen, "Densities of Supercooled H_2O and D_2O in 25 μ Glass Capillaries," J. Chem. Phys. **84**, 5085 (1986).

Havlicek, J. and L. Miskowsky, Hel. Phys. Acta. **9**, 161 (1936).

Hilbert, R. "PVT Values of Water and with 25 Weight Percent Sodium Chloride to 873 K and 4000 bar," Ph.D. thesis, Univ. Karlshrue, Federal Republic of Germany (1979).

Hill, P. G., "A Unified Equation of State for H_2O," Proc. 10th Int. Conf. Properties of Water and Steam, Moscow, Sept. 10–14, 1984, Mir Publishers, Moscow.

Hill, P. G., and R. D. C. MacMillan, "The Properties of Steam: Current Status," Trans. ASME J. Heat Trans. **110**, 763 (1988).

Holser, W. T. and G. C. Kennedy, Am. J. Sci. **256**, 744 (1958).

Holser, W. T. and G. C. Kennedy, Am. J. Sci. **257**, 71 (1959).

Holton, G., M. P. Hagelbert, S. Kao, and W. H. Johnson, Jr., "Ultrasonic-Velocity Measurements in Water at Pressures to 10,000 kg/cm^2," J. Acoust. Soc. Amer. **43**, 102 (1968).

Juza, J., V. Kmonicek and O. Sifner, 1966 Appendix to J. Juza. An Equation of State for Water and Steam, Acad., Naklad, Cesk. Acad. Ved. Prague, 131.

Juza, J., V. Kmonicek, O. Sifner, and K. Schovanec, "A Contribution to the Problem of Thermodynamic Similarity of H_2O and D_2O," Physica **32**, 362 (1966).

Keenan, J. H., F. G. Keyes, P. G. Hill, and J. G. Moore, *Steam Tables* (Wiley, New York, 1969).

Kell, G. S. and E. Whalley, "The PVT Properties of Water. I. Liquid Water in the Temperature Range 0–150 °C and at Pressures up to 1 kbar," Phil. Trans. Roy. Soc. (London) **258**, 565 (1965).

Kell, G. S., "Effects of Isotopic Composition, Temperature, Pressure, and Dissolved Gases on the Density of Liquid Water," J. Phys. Chem. Ref. Data **6**, 1109 (1977).

Kell, G. S., G. E. McLaurin, and E. Whalley, "The PVT Properties of Fluid Water in the Range 350 to 500 °C and along the Saturation Line from 150 to 350 °C," Phil. Trans. Roy. Soc. A (London) **315**, 235 (1985).

Kell, G. S. and E. Whalley, "Reanalysis of the Density of Liquid Water in the Range 0–150 °C and 0–1 kbar," J. Chem. Phys. **62**, 3496 (1975).

Kell, G. S., G. E. McLaurin, and E. Whalley, "The PVT Properties of Water: IV. Liquid Water in the Range 150–350 °C, from Saturation to 1 kbar," Phil. Trans. Roy. Soc. London, Ser. A **360**, 389 (1978).

Kell, G. S., "Effects of Isotopic Composition, Temperature, Pressure, and Dissolved Gases on the Density of Liquid Water," J. Phys. Chem. Ref. Data **6**, 1109 (1977).

Kell, G. S., G. E. McLaurin, and E. Whalley, "The PVT Properties of Fluid Water in the Range 350 to 500 °C and along the Saturation Line from 150 to 350 °C," Phil. Trans. Roy. Soc. A (London) **315**, 235 (1985).

Kell, G. S. and E. Whalley, "Reanalysis of the Density of Liquid Water in the Range 0–150 °C and 0–1 kbar," J. Chem. Phys. **62**, 3496 (1975).

Kell, G. S., G. E. McLaurin, and E. Whalley, "The PVT Properties of Water: IV. Liquid Water in the Range 150–350 °C, from Saturation to 1 kbar," Phil. Trans. Roy. Soc. London, Ser. A **360**, 389 (1978).

Kell, G. S., G. E. McLaurin, and E. Whalley, "PVT Properties of Water. VII. Vapour densities of light and heavy water from 150 to 500 °C," Proc. Roy. Soc. A (London) **425**, 49 (1989).

Kerimov, A. M., and M. K. Alieva, "Investigation of the Isochoric Specific Heat of Steam," Teploenergetika **22**, 58 (1985).

Kestin, J., V. J. Sengers, B. Kamgar-Parsi, and J. M. H. Levelt Sengers, "Thermophysical Properties of Fluid H_2O," J. Phys. Chem. Ref. Data **13**, 175 (1984).

Keyes, F. G. and L. B. Smith, Proc. Am. Acad. Arts Sci., **69**, 285 (1934).

Keyes, F. G., L. B. Smith and H. T. Gerry, Proc. Am. Acad. Arts Sci. **70**, 319 (1936).

Keyes, F. G., "The Second Virial Coefficient for Steam," Int. J. Heat Mass Trans. **5**, 137 (1962).

Keyes, F. G., J. Chem. Phys. **17**, 923 (1949).

Knoblauch, O., and A. Winkhau, Z. Ver. Deutsch. Ingenieurw. **59**, 376 (1915).

Knoblauch, O., and A. Winkhau, Z. Ver. Deutsch. Ingenieurw. **59**, 400 (1915).

Knoblauch, O., and A. Winkhau, Mitt. Forsch. Gebiete. Ingenieurw. **195**, I (1917).

Knoblauch, O. and W. Koch, Ver. Deutsch. Ingenieurw. **73**, 1733 (1928).

Koch, W., Forsch. Gebiete. Ingenieurw. **3**, 189 (1932).

Koster, H. and E. U. Frank, "The Specific Volume of Water to High Pressure, to 600 °C and 10 kbar," Ber. Buns. Physik. Chem. **73**, 716 (1969).

LeFevre, E. U., M. R. Nightingale, and J. W. Rose, "The Second Virial Coefficient of Ordinary Water Substance: A New Correlation," J. Mech. Eng. Sci. **17**, 243 (1975).

Levelt Sengers, J. M. H., J. Straub, K. Watanabe and P. G. Hill, "Assessment of Critical Parameter Values for H_2O and D_2O," J. Phys. Chem. Ref. Data **14**, 193 (1985).

Levelt Sengers, J. M. H., W. L. Greer and J. V. Sengers, "Scaled Equation of State Parameters for Gases in the Critical Region," J. Phys. Chem. Ref. Data **5**, 1 (1976).

Levelt Sengers, J. M. H., R. Kamgar-Parsi, F. W. Balfour, and J. V. Sengers, "Thermodynamic Properties of Steam in the Critical Region," J. Phys. Chem. Ref. Data **12**, 1 (1983).

Levelt Sengers, J. M. H., "How Close is Close to the Critical Point," in Perspectives in Statistical Physics, Edited by H. J. Raveche (North-Holland Publishing Company, Amsterdam, 1981).

Maier, S., and E. U. Frank, "The Density of Water from 200 to 850 °C and from 1000–6000 bar," Ber. Buns. Physik. Chem. **70**, 639 (1966).

Masui, R., S. Seino, O. Senda, and Y. Okamoto, "The Present State of the Absolute Measurement of Density of Water at National Research Laboratory of Metrology," Proc. 10th I.C.P.S., 158 (Mir Moscow,1984).

Murphy, T. A., J. V. Sengers, and J. M. H. Levelt Sengers, in Proc. 8th Int. Conf. Properties of Water and Steam, P. Bury, H. Peron, and B. Vodar eds. (Editions Europeenes Thermique et Industries, Paris, 1975), p. 603.

Novikov, I. I. and V. I. Avdonin, "Velocity of Sound in Saturated and Superheated Steam," Report to 7th International Conference Properties of Water and Steam, Tokyo, 1968. (ASME, New York, 1970).

Osborne, N. S., H. F. Stimson, and D. C. Ginnings, "Thermal Properties of Saturated Water and Steam," J. Res. Nat. Bur. Stand. **23**, 261 (1939).

Osborne, N. S., H. F. Stimson, and D. C. Ginnings, "Measurements of Heat Capacity of Vaporization of Water in the Range 0 to 100 °C," J. Res. Nat. Bur. Stand. **23**, 197 (1939).

Osborne, N. S., H. F. Stimson, and D. C. Ginnings, "Calorimetric Determination of the Thermodynamic Properties of Saturated Water in Both the Liquid and Gaseous States from 100 to 374 °C," J. Res. Nat. Bur. Stand. **18**, 389 (1937).

Osborne, N. S., H. G. Stimson, E. F. Fiock, and D. C. Ginnings, "The Pressure of Saturated Water Vapor in the Range 100 °C to 374 °C," J.

Res. Nat. Bur. Stand. **10**, 155 (1933).
Petitet, J. P., R: Tufeu and B. Le Neindre, "Determination of the Thermodynamic Properties of Water from Measurements of the Speed of Sound in the Temperature Range 251.15–293.15 K and the Pressure Range 0.1–350 MPa," Int. J. Thermophys. **4**, 35 (1983).
Petitet, J. P., L. Denielou, R. Tufeu, B. Le Neindre, "Velocity of Sound in Supercritical Water up to 700 °C and 300 MPa," Int. J. Thermophys., 7(5), 1065 (1986).
Philippi, R., "Experimental Bestimmung der spezifischen Warmekapazitat Cp," Fortschr-Ber. VOI Reihe 19, Nr. 13. Dusseldorf, Germany, 1987.
Pollak, R., Dissertation, Ruhr-University Bochum, paper submitted to 8th ICPS, Hijeres-Giens, France, 1974.
Pollak, R., in Proc. 8th Int. Conf. Properties of Water and Steam, P. Bury, H. Perdon and B. Vodar, eds. (Editions Europeenes Thermique et Industries, Paris, 1975), 821.
Rivkin, S. L. and T. C. Akhundov, Teploenergetika **9**, 57 (1962).
Rivkin, S. L. and T. C. Akhundov Teploenergetika **10**, 66 (1963).
Rivkin, S. L. and T. S. Akhundov, "Study of Specific Volumes of Water in the Region Close to the Critical Point," Teploenergetika **13**, 59 (1966).
Rogener, H. and P. Soll, "Contribution to Thermodynamic Measurement of the Isentropic Temperature—Pressure Coefficient of Water," Brennst.—Warme—Kraft, **32**, 472 (1980).
Sato, H., M. Uematsu, K. Watanabe, "Determination of the PVT—Surface of Water Based on Measured Values up to 1123 K and 1 kPa," JSME Bulletin **24**, 691 (1981).
Sato, H., M. Uematsu, K. Watanabe, A. Saul, and W. Wagner, 1975, "New International Skeleton Tables for the Thermodynamic Properties of Ordinary Water Substance" Background Report for the IAPS Skeleton Tables 1985 for the Thermodynamic Properties of Ordinary Water Substances. Issued by IAPS (now the International Association for the Properties of Water and Steam).
Sato, H., M. Uematsu, and K. Watanabe, "An Equation of State for Water in the High Density Region," Proceedings of the Eighth Symposium on Thermophysical Properties, ASME **11**, 287 (1982).
Saul, A. and W. Wagner, "International Equations for the Saturation Properties of Ordinary Water Substance," J. Phys. Chem. Ref. Data **16**, 893 (1987).
Sengers, J. V., J. M. H. Levelt Sengers, B. Kamgar-Parsi, "A Scaled Fundamental Equation for the Thermodynamic Properties of Steam near the Critical Point," Strojnicky Casopis **36**, 277 (1985).
Sengers, J. V. and J. T. R. Watson, "Improved International Formulations for the Viscosity and Thermal Conductivity of Water Substance," J. Phys. Chem. Ref. Data **15**, 1291 (1986).
Sengers, J. V. and B. Kamgar–Parsi, "Representative Equations for the Viscosity of Water Substance," J. Phys. Chem. Ref. Data **13**, 185 (1984).
Sengers, J. V., J. T. R. Watson, R. Basu, B. Kamgar–Parsi, and R. C. Hendricks, "Representative Equations for the Thermal Conductivity of Water Substance," J. Phys. Chem. Ref. Data **13**, 893 (1984).
Sirota, A. M., and B. K. Mal'tsev, "Experimental Investigation of the Heat Capacity of Water at 1—500 °C and to Pressures of 500 kbar/cm^2, Teploenergetika **6**, 7 (1959).
Sirota, A. M., and B. K. Mal'tsev, "Experimental Investigation of the Heat Capacity of Steam at 300–500 Atmospheres and 500–600 °C," Teploenergetika **7**, 67 (1960).
Sirota, A. M., and B. K. Maltsev, "Experimental Determination of the Specific Heat of Water in the Critical Region," Teploenergetika **9**, 52 (1962).
Sirota, A. M., and B. K. Mal'tsev, "Experimental Investigation of the Heat Capacity of Steam," Teploenergetika **9**, 70 (1962).
Sirota, A. M., and A. S. Grishkov, "Experimental Investigation of the Heat Capacity of Water at High Pressure," Teploenergetika **13**, 61 (1966).
Sirota, A. M., and T. L. Timrot, "Experimental Investigation of the Heat Capacity of Superheated Steam," Teploenergetika **3**, 16 (1956).
Sirota, A. M., B. K. Mal'tsev, and A. S. Grishkov, "Experimental Investigation of the Heat Capacity of Steam," Teploenergetika **10**, 57 (1963).
Sirota, A. M., A. S. Grishkov, and A. G. Tomishko, "Experimental Investigation of the Heat Capacity of Water Near the Melting Curve," Teploenergetika **17**, 60 (1970).
Sirota, A. M., B. K. Maltsev, P. E. Belyakova, "Tables of Reference Values for the Specific Heat Cp and the Enthalpy of Water and Steam," Teploenergetika **10**, 64 (1963).
Stasenko, V. A., L. P. Philipov, and L. A. Blagonravov, "Investigation of the Thermal Pressure Coefficient of Water," Proc. 10th I.C.P.S., 301 (Mir, Moscow, 1984).
Stimson, H. F., "Some Precise Measurements of the Vapor Pressure of Water in the Range from 25 to 100 °C," J. Res. Nat. Bur. Stand. **73a**, 493 (1969).
Straub, J., H. Rosner, "Classification of P-V-T data of Water and Steam," Report to IAPS WG 1 (1977).
Ter Minassian, L. P. Pruzan, and A. Soulard, "Thermodynamic Properties of Water under Pressure Up to 5 kbar and Between 28 and 128 °C. Estimations in the Supercooled Region Down to − 40 °C, J. Chem. Phys. **75**, 3064 (1981).
Trinh, E. and R. E. Apfel, "The Sound Velocity in Metastable Liquid Water under Atmospheric Pressure," J. Chem. Phys. **69**, 4245 (1978).
Vukalovich, M. P., V. N. Zubarev, and A. A. Alexandrov, Teploenergetika **8**, 79 (1961).
Vukalovich, M. P., V. N. Zubarev, and A. A. Alexandrov Teploenergetika **9**, 49 (1962).
Wagner, W. "A New Correlation Method for Thermodynamic Data Applied to the Vapor-Pressure Curve of Argon, Nitrogen, and Water," IUPAC Thermodynamic Tables Project Centre, Department of Chemical Engineering and Chemical Technology, Imperial College of Science and Technology, London SW7 2BY, England (1977).
Wagner, W., and A. Saul, "Correlation Equations for the Vapor Pressure and for the Orthobaric Densities of Water Substance," in Proceedings of the Tenth International Conference on the Properties of Steam, (Mir Moscow, 1984).
Wagner, W., and J. V. Sengers, "Draft Release on Saturation Properties of Ordinary Water Substance," IAPS Technical Report BN 1051 (1986).
Walsh, J. M., and M. H. Rice, "Dynamic Compression of Liquids from Measurements on Strong Shock Waves," J. Chem. Phys. **26**, 815 (1957).
Watanabe, H., and K. Iizuka, "The Thermal Expansion of Water Between 0 °C and 44 °C," Proc. 8th Symposium Thermo. Prop. Vol. II, 319 (1981).
Watson, J. T. R., R. Basu, and J. V. Sengers, "An Improved Representative Equation for the Dynamic Viscosity of Water Substance," J. Phys. Chem. Ref. Data **9**, 1255 (1980).
Woolley, H. W., "Thermodynamic Properties for H_2O in the Ideal Gas State in Water and Steam," J. Straub and K. Scheffler, eds. (Pergamon, Oxford, 1980), p. 166.
Woolley, H. W., "A Switch Function Applied to the Thermodynamic Properties of Steam Near the Critical Point," Int. J. Phys. **4**, 51 (1983).
Wormald, C. J., Thermodynamics of Vapors, Ph.D. Thesis, University of Reading, 1964.
Zheleznyi, B. V. "The Density of Supercooled Water," Russ. J. Phys. Chem. **43**, 1311 (1969).
Zubarev, V. N., P. G. Prusakov, and V. V. Barkovskij, "Experimental Determination of Specific Volumes of Steam at Temperatures of 673. 15–873.15 K and Pressures Up to 200 MPa," Teploenergetika **24**, 77 (1977).

Appendix A: The Ideal Gas Function

The ideal gas function is

$$\bar{\psi}_0 = \sum_{i=1}^{6} C_i(-\bar{T})^{2-i} + (C_7\bar{T} + C_8)\ln(-\bar{T}), \tag{3}$$

in which the coefficients C_i are:

$C_1 =$ 7.075 012 751 12	$C_5 = 0.003\,033\,815$
$C_2 = -8.342\,405\,699\,63$	$C_6 = 0.000\,390\,109$
$C_3 = -0.364\,601\,380$	$C_7 = 0.113\,592\,870$
$C_4 = -0.036\,897\,043$	$C_8 = 2.413\,178\,500$

With the above values of C_i, $\bar{\psi}_0$ has been shown to provide C_{p0} values within 0.04% of those of Woolley (1983) for $250 < T < 1500$ K.

The values of C_1 and C_2 have been adjusted to guarantee zero values of the energy and entropy at the triple point liquid state.

Appendix B: Coefficients A_{ijk}

		$A_1(I,J)$
I	J	
4	1	0.338 424 912 5D + 00
5	1	− 0.715 339 340 6D − 01
7	1	0.549 368 081 4D − 03
3	2	0.493 321 850 1D − 01
6	2	− 0.232 849 121 2D − 01
7	2	0.240 209 518 1D − 02
1	3	0.752 942 295 6D + 00

3	3	− 0.228 026 007 0D + 01
2	4	0.114 200 414 4D + 01
3	4	− 0.261 905 962 4D + 01
5	4	0.439 523 770 2D + 00
6	4	− 0.316 104 664 6D − 01
7	4	0.681 446 769 2D − 03
1	5	− 0.392 422 729 4D + 00
3	5	− 0.273 877 064 8D + 00
4	6	− 0.194 344 385 7D − 01
5	6	0.304 886 043 4D − 02
3	7	0.394 651 040 3D − 02

$A_2(I,J)$

I	J	
1	1	0.224 361 031 4D + 00
2	1	0.119 325 020 1D + 00
5	1	0.658 295 934 8D − 01
5	2	0.165 143 062 8D + 00
1	3	− 0.217 896 935 7D + 01
2	3	0.267 409 054 2D + 00
3	3	0.864 749 099 5D + 00
1	4	− 0.153 043 225 7D + 00
3	4	0.205 988 145 4D + 01
6	4	− 0.488 862 870 3D + 00
7	4	0.137 532 875 3D + 00
5	5	− 0.901 518 066 6D + 00
6	5	− 0.144 425 860 9D + 00
7	5	0.155 804 627 9D + 00
4	6	− 0.274 065 256 3D + 01
6	6	0.498 377 170 6D + 00
4	7	− 0.326 197 856 4D + 01
5	7	0.160 933 878 4D + 01
1	8	0.348 467 496 3D − 01
2	8	− 0.153 764 643 4D + 01
5	8	0.231 622 525 7D + 00
2	9	− 0.141 924 923 2D + 01
3	9	0.796 998 463 5D + 00
5	10	0.751 054 462 7D − 02
1	12	0.536 438 473 2D − 03

$A_3(I,J)$

I	J	
1	1	0.610 938 129 6D + 00
3	1	− 0.190 664 445 9D − 01
5	1	0.797 609 218 8D − 02
1	2	0.193 446 676 6D + 01
1	3	0.192 182 054 7D + 01
3	3	− 0.441 010 591 9D − 01
1	4	0.613 035 441 9D + 00
2	4	− 0.285 525 868 9D + 00
5	4	0.252 613 708 0D − 01
2	5	0.237 407 464 2D + 00
4	5	0.385 586 640 2D − 01
5	5	0.804 167 215 0D − 02

$A_4(I,J)$

I	J	
3	1	− 0.163 543 903 3D + 02
1	2	− 0.502 581 867 5D + 02
2	4	0.164 900 304 0D + 00
1	5	− 0.849 989 350 2D + 00
1	9	0.831 438 254 4D − 02
2	9	0.878 132 785 8D − 03
2	10	0.153 739 121 3D − 02
3	10	− 0.901 687 378 6D − 03
5	10	0.332 662 866 4D − 03

Appendix C: Dimensionless Variables and Derivatives

The principal variables are

Helmholtz Free Energy $\bar{\psi} = \frac{\psi}{RT}$,

Density $\bar{\rho} = \frac{\rho}{\rho_c}$ $\Delta\bar{\rho} = \bar{\rho} - 1$,

Temperature $\overline{T} = -\frac{T_c}{T}$ $\Delta\overline{T} = 1 + \overline{T}$,

Pressure $\overline{P} = \frac{P}{\rho_c RT} = \bar{\rho}^2 \frac{\partial\bar{\psi}}{\partial\bar{\rho}}$,

Entropy $\bar{s} = \frac{s}{R} = \overline{T}\frac{\partial\bar{\psi}}{\partial\overline{T}} - \bar{\psi}$,

Internal Energy $\bar{u} = \frac{u}{RT_c} = -\frac{\partial\bar{\psi}}{\partial\overline{T}}$,

Enthalpy $\bar{h} = \frac{h}{RT_c} = \bar{u} - \frac{\overline{P}}{\bar{\rho}\overline{T}}$.

The principal derivative quantities are

$$\overline{P} = \overline{P}_f + F(\overline{P}_n - \overline{P}_f) + \bar{\rho}^2 \frac{\partial F}{\partial\bar{\rho}}(\bar{\psi}_n - \bar{\psi}_f),$$

$$\left(\frac{\partial\overline{P}}{\partial\bar{\rho}}\right)_{\overline{T}} = \frac{\partial\overline{P}_f}{\partial\bar{\rho}} + F\left(\frac{\partial\overline{P}_n}{\partial\bar{\rho}} - \frac{\partial\overline{P}_f}{\partial\bar{\rho}}\right) + 2\frac{\partial F}{\partial\bar{\rho}}(\overline{P}_n - \overline{P}_f) + \left(2\bar{\rho}\frac{\partial F}{\partial\bar{\rho}} + \bar{\rho}^2\frac{\partial^2 F}{\partial\bar{\rho}^2}\right)(\bar{\psi}_n - \bar{\psi}_f),$$

$$\left(\frac{\partial\overline{P}}{\partial\overline{T}}\right)_{\bar{\rho}} = \frac{\partial\overline{P}_f}{\partial\overline{T}} + F\left(\frac{\partial\overline{P}_n}{\partial\overline{T}} - \frac{\partial\overline{P}_f}{\partial\overline{T}}\right) + \frac{\partial F}{\partial\overline{T}}(\overline{P}_n - \overline{P}_f) + \bar{\rho}^2\frac{\partial^2 F}{\partial\bar{\rho}\partial\overline{T}}(\bar{\psi}_n - \bar{\psi}_f) - \bar{\rho}^2\frac{\partial F}{\partial\bar{\rho}}(\bar{u}_n - \bar{u}_f),$$

$$\bar{u} = \bar{u}_f + F(\bar{u}_n - \bar{u}_f) - \frac{\partial F}{\partial\overline{T}}(\bar{\psi}_n - \bar{\psi}_f),$$

$$\bar{s} = \bar{s}_f + F(\bar{s}_n - \bar{s}_f) + \overline{T}\frac{\partial F}{\partial\overline{T}}(\bar{\psi}_n - \bar{\psi}_f),$$

$$\overline{C}_v = \overline{C}_{vf} + F(\overline{C}_{vn} - \overline{C}_{vf}) + 2\overline{T}^2\frac{\partial F}{\partial\overline{T}}(\bar{u}_n - \bar{u}_f) - \overline{T}^2\frac{\partial^2 F}{\partial\overline{T}^2}(\bar{\psi}_n - \bar{\psi}_f).$$

Also

$$\overline{C}_p = \frac{C_p}{R} = \overline{C}_v + \left[\overline{T}\left(\frac{\partial\overline{P}}{\partial\overline{T}}\right)_{\bar{\rho}} - \overline{P}\right]^2 \Bigg/ \left[\bar{\rho}^2\left(\frac{\partial\overline{P}}{\partial\bar{\rho}}\right)_{\overline{T}}\right],$$

and the dimensionless speed of sound is

$$\bar{a} = a/\sqrt{RT_c} = \sqrt{-\frac{\overline{C}_p}{\overline{C}_v}\frac{1}{\overline{T}}\left(\frac{\partial\overline{P}}{\partial\bar{\rho}}\right)_{\overline{T}}}.$$

Appendix D: The Derivatives of $\bar{\psi}_f$

Using the notation

$$\left(\frac{\partial\chi}{\partial\bar{\rho}}\right)_{\overline{T}} = \chi_\rho \quad \left(\frac{\partial^2\chi}{\partial\bar{\rho}^2}\right)_{\overline{T}} = \chi_{\rho\rho},$$

$$\left(\frac{\partial\chi}{\partial\overline{T}}\right)_{\bar{\rho}} = \chi_T \quad \text{etc.},$$

and given

$$\bar{\psi}_f = \bar{\psi}_o + \ln\bar{\rho} + W_1(\bar{\rho},\overline{T}) + E(\bar{\rho})W_2(\bar{\rho},\overline{T}) + G(\bar{\rho},\overline{T})W_3(\bar{\rho},\overline{T}) + H(\overline{T})W_4(\bar{\rho},\overline{T}),$$

we have

$$\overline{P}_f = \bar{\rho}^2\left(\frac{\partial\bar{\psi}_f}{\partial\bar{\rho}}\right)_{\overline{T}} = \bar{\rho} + \bar{\rho}^2[W_{1\rho} + E_\rho W_2 + EW_{2\rho} + G_\rho W_3 + GW_{3\rho} + HW_{4\rho}],$$

$$\left(\frac{\partial \bar{P}_f}{\partial \bar{\rho}}\right)_{\bar{T}} = 1 + 2\bar{\rho}[W_{1\rho} + E_\rho W_2 + EW_{2\rho} + G_\rho W_3 + GW_{3\rho} + HW_{4\rho}] + \bar{\rho}^2[W_{1\rho\rho} + E_{\rho\rho} W_2 + 2E_\rho W_{2\rho} + EW_{2\rho\rho} + G_{\rho\rho} W_3 + 2G_\rho W_{3\rho} + GW_{3\rho\rho} + HW_{4\rho\rho}],$$

$$\frac{\partial \bar{P}_f}{\partial \bar{T}} = \bar{\rho}^2[W_{1\rho T} + E_\rho W_{2T} + EW_{2\rho T} + G_{\rho T} W_3 + G_\rho W_{3T} + G_T W_{3\rho} + GW_{3\rho T} + H_T W_{4\rho} + HW_{4\rho T}],$$

$$\bar{u}_f = -\bar{\psi}_{oT} - W_{1T} - EW_{2T} - G_T W_3 - GW_{3T} - H_T W_4 - HW_{4T},$$

$$\bar{c}_{of} = -\bar{T}^2[\bar{\psi}_{oTT} + W_{1TT} + EW_{2TT} + G_{TT} W_3 + 2G_T W_{3T} + GW_{3TT} + H_{TT} W_4 + 2H_T W_{4T} + HW_{4TT}],$$

$$\bar{s}_f = -\bar{u}_f \bar{T} - \bar{\psi}_f.$$

The above W_k functions ($k = 1$ to 4) and their derivatives are

$$W_1 = \sum_{i=1}^{N_{R1}} \sum_{j=1}^{N_{T1}} A_1(i,j) R_1(i) T_1(j),$$

$$W_{1\rho} = \sum\sum A_1(i,j) R_{1\rho}(i) T_1(j),$$

$$W_{1\rho\rho} = \sum\sum A_1(i,j) R_{1\rho\rho}(i) T_1(j),$$

$$W_{1T} = \sum\sum A_1(i,j) R_1(i) T_{1T}(j),$$

$$W_{1TT} = \sum\sum A_1(i,j) R_1(i) T_{1TT}(j),$$

$$W_{1\rho T} = \sum\sum A_1(i,j) R_{1\rho}(i) T_{1T}(j),$$

$$W_2 = \sum_{i=1}^{N_{R2}} \sum_{j=1}^{N_{T2}} A_2(i,j) R_2(i) T_1(j),$$

$$W_{2\rho} = \sum\sum A_2(i,j) R_{2\rho}(i) T_1(j),$$

$$W_{2\rho\rho} = \sum\sum A_2(i,j) R_{2\rho\rho}(i) T_1(j),$$

$$W_{2T} = \sum\sum A_2(i,j) R_2(i) T_{1T}(j),$$

$$W_{2TT} = \sum\sum A_2(i,j) R_2(i) T_{1TT}(j),$$

$$W_{2\rho T} = \sum\sum A_1(i,j) R_{2\rho}(i) T_{1T}(j),$$

$$W_3 = \sum_{i=1}^{N_{R3}} \sum_{j=1}^{N_{T3}} A_3(i,j) R_3(i) T_2(j),$$

$$W_{3\rho} = \sum\sum A_3(i,j) R_{3\rho}(i) T_2(j),$$

$$W_{3\rho\rho} = \sum\sum A_3(i,j) R_{3\rho\rho}(i) T_2(j),$$

$$W_{3T} = \sum\sum A_3(i,j) R_3(i) T_{2T}(j),$$

$$W_{3TT} = \sum\sum A_3(i,j) R_3(i) T_{2TT}(j),$$

$$W_{3\rho T} = \sum\sum A_3(i,j) R_{3\rho}(i) T_{2T}(j),$$

$$W_4 = \sum_{i=1}^{N_{R4}} \sum_{j=1}^{N_{T4}} A_4(i,j) R_1(i) T_1(j),$$

$$W_{4\rho} = \sum\sum A_4(i,j) R_{1\rho}(i) T_1(j),$$

$$W_{4\rho\rho} = \sum\sum A_4(i,j) R_{1\rho\rho}(i) T_1(j),$$

$$W_{4T} = \sum\sum A_4(i,j) R_1(i) T_{1T}(j),$$

$$W_{4TT} = \sum\sum A_4(i,j) R_1(i) T_{1TT}(j),$$

$$W_{4\rho T} = \sum\sum A_4(i,j) R_{1\rho}(i) T_{1T}(j).$$

In the above expressions

$$R_1(i) = (1-E)(\bar{\rho})^{i-2},$$

$$R_{1\rho}(i) = (1-E)(i-2)(\bar{\rho})^{i-3} - E_\rho(\bar{\rho})^{i-2},$$

$$R_{1\rho\rho}(i) = (1-E)(i-2)(i-3)(\bar{\rho})^{i-4} - 2E_\rho(i-2)(\bar{\rho})^{i-3} - E_{\rho\rho}(\bar{\rho})^{i-2},$$

except that

$$R_1(2) = (1-E)\ln\bar{\rho} - \bar{\rho}^2 \ln\bar{\rho} + \frac{\bar{\rho}^2}{2}$$

$$R_{1\rho}(2) = (1-E)/\bar{\rho} - E_\rho \ln\bar{\rho} - 2\bar{\rho}\ln\bar{\rho}$$

$$R_{1\rho\rho}(2) = -(1-E)/\bar{\rho}^2 - 2E_\rho/\bar{\rho} - E_{\rho\rho}\ln\bar{\rho} - 2\ln\bar{\rho} - 2,$$

and

$$R_2(i) = (\bar{\rho})^i,$$

$$R_{2\rho}(i) = i(\bar{\rho})^{i-1},$$

$$R_{2\rho\rho}(i) = i(i-1)(\bar{\rho})^{i-2},$$

$$R_3(i) = (\bar{\rho})^{i+1},$$

$$R_{3\rho}(i) = (i+1)(\bar{\rho})^i,$$

$$R_{3\rho\rho}(i) = (i+1)(i)(\bar{\rho})^{i-1},$$

and

$$T_1(j) = (\bar{T})^{j-1},$$

$$T_{1T}(j) = (j-1)(\bar{T})^{j-2},$$

$$T_{1TT}(j) = (j-1)(j-2)(\bar{T})^{j-3},$$

$$T_2(j) = (\bar{T})^{j+1},$$

$$T_{2T}(j) = (j+i)(\bar{T})^j,$$

$$T_{2TT}(j) = (j+1)(j)(\bar{T})^{j-1}.$$

The function $\bar{\psi}_0(\bar{T})$ given in Appendix A is given by

$$\bar{\psi}_o(\bar{T}) = \sum_{i=1}^{6} C_i(-\bar{T})^{2-i} + (C_7\bar{T} + C_8)\ln(-\bar{T}),$$

and its derivatives are

$$\bar{\psi}_{oT} = -\sum_{i=1}^{6} C_i(2-i)(-\bar{T})^{1-i} + C_7[\ln(-\bar{T}) + 1] + C_8/\bar{T},$$

$$\bar{\psi}_{oTT} = \sum_{i=1}^{6} C_i(2-i)(1-i)(-\bar{T})^{-i} + C_7/\bar{T} - C_8/\bar{T}^2.$$

The functions E, G, and H and their derivatives are given in Appendix E.

Appendix E: The Functions E, F, G, H and Their Derivatives

(i) The Function $E(\bar{\rho})$

$$E = e^{-\bar{\rho}^2}$$

$$E_\rho = -2\bar{\rho}E$$

$$E_{\rho\rho} = -2E - 2\bar{\rho}E_\rho.$$

(ii) The Function $F(\bar{\rho},\bar{T})$

With

$$F = 1 - \exp(-1/Z)$$

and

$$Z = \exp[(\zeta/\delta)^4] - 1,$$

in which

$$\zeta = \sqrt{(\Delta\bar{\rho}/\Delta\bar{\rho}_0)^2 + (\Delta\bar{T}/\Delta\bar{T}_0)^2}$$

we have (defining $F_\zeta = \partial F/\partial\zeta$, $F_{\zeta\zeta} = \partial^2 F/\partial\zeta^2$),

$$F_\zeta = -\frac{4}{\delta}\exp(-1/Z)(1/Z + 1/Z^2)[\ln(1+Z)]^{3/4},$$

UNIFIED EQUATION OF STATE FOR H_2O

$$F_{\zeta\zeta} = -\frac{12}{\delta^2}\exp(-1/Z)(1/Z + 1/Z^2)[\ln(1+Z)]^{1/2} \times [1 + \tfrac{4}{3}(1/Z^2 - 1/Z - 1)\ln(1+Z)],$$

and (with $\zeta_\rho = \partial\zeta/\partial\bar{\rho}$, $\zeta_{\rho\rho} = \partial^2\zeta/\partial\bar{\rho}^2$ etc.)

$$\zeta_\rho = \Delta\bar{\rho}/(\zeta\Delta\bar{\rho}_0^2)$$

$$\zeta_T = \Delta\bar{T}/(\zeta\Delta\bar{T}_0^2)$$

$$\zeta_{\rho\rho} = [1/\zeta - (\Delta\bar{\rho}/\Delta\bar{\rho}_0)^2/\zeta^3]/\Delta\bar{\rho}_0^2$$

$$\zeta_{TT} = [1/\zeta - (\Delta\bar{T}/\Delta\bar{T}_0)^2/\zeta^3]/\Delta\bar{T}_0^2$$

$$\zeta_{\rho T} = -\Delta\bar{\rho}\Delta\bar{T}/(\zeta^3\Delta\bar{\rho}_0^2\Delta\bar{T}_0^2),$$

which may be used in evaluating

$$F_\rho = F_\zeta\zeta_\rho$$

$$F_{\rho\rho} = F_{\zeta\zeta}(\zeta_\rho)^2 + F_\zeta\zeta_{\rho\rho}$$

$$F_T = F_\zeta\zeta_T$$

$$F_{TT} = F_{\zeta\zeta}(\zeta_T)^2 + F_\zeta\zeta_{TT}$$

$$F_{\rho T} = F_{\zeta\zeta}\zeta_\rho\zeta_T + F_\zeta\zeta_{\rho T}.$$

(iii) The Function $G(\bar{\rho},\bar{T})$

$$G = \exp(-\alpha\Delta\bar{T} - \beta\Delta\bar{\rho} - \gamma\Delta\bar{T}^2 - \delta\Delta\bar{\rho}^2)$$

$$G_\rho = G(-\beta - 2\delta\Delta\bar{\rho})$$

$$G_{\rho\rho} = G_\rho(-\beta - 2\delta\Delta\bar{\rho}) - 2\delta G$$

$$G_T = G(-\alpha - 2\gamma\Delta\bar{T})$$

$$G_{TT} = G_T(-\alpha - 2\gamma\Delta\bar{T}) - 2\gamma G$$

$$G_{\rho T} = G_T(-\beta - 2\delta\Delta\bar{\rho}).$$

(iv) The Function $H(\bar{T})$

$$H = \exp[-\nu(\bar{T} + 3)]$$

$$H_T = -\nu H$$

$$H_{TT} = \nu^2 H.$$